Engineering *Brome mosaic virus* as a potential drug delivery nanoparticle for prostate cancer

by

Nadine Lee

Thesis presented in partial fulfilment of the requirements for the degree of Master of Science in the Faculty of Science at Stellenbosch University

Supervisor: Prof. Johan T. Burger

Co-supervisor: Dr. Hans J. Maree

March 2017

Declaration

By submitting this thesis electronically, I declare that the entirety of the work contained therein is my own, original work, that I am the sole author thereof (save to the extent explicitly otherwise stated), that reproduction and publication thereof by Stellenbosch University will not infringe any third party rights and that I have not previously in its entirety or in part submitted it for obtaining any qualification.

March 2017

Abstract

Cancer is a leading cause of annual mortality worldwide. Prostate cancer is the second most prevalent type of cancer after breast cancer. The conventional treatment options that are currently available are not optimal due to their non-specificity as well as treatment often failing. Recent advances have turned to nanotechnology as the future of cancer therapy, and viral nanoparticles (VNPs) in particular are promising delivery vehicles. VNPs provide a protein scaffold that is relatively easy to modify while being biodegradable. Plant viruses specifically can be purified with ease at high concentrations and are safe for use in humans. *Brome mosaic virus* (BMV) is an icosahedral virus selected for this study due to its stability under a range of experimental conditions, such as pH and temperature, and its robustness in chemical conjugation experiments. BMV was also selected for the availability of modifiable amino acids on its exterior surface.

The goal of this project was to engineer BMV as a potential delivery nanoparticle for prostate cancer treatments. Wild type BMV was purified from *Nicotiana benthamiana* and particles quantified using transmission electron microscopy as well as dot blots. The virus particles were modified by conjugation of two fluorescent molecules, Alexa Fluor-647 and Cy5, to the glutamic acid residues on the exterior surface of the BMV capsid. Two peptides, PKRGFQD-C and SNTRVAP-C, were conjugated to the solvent-exposed lysine residues using three SM(PEG)$_n$ crosslinkers of different lengths. These peptides respectively target the receptors α-2-macroglobulin and GRP78, which are found on the cell surface of androgen-independent prostate cells. The SM(PEG)$_{24}$ crosslinker could successfully conjugate the peptides. When the fluorescent labeling was performed first, the peptide conjugation was unsuccessful. As an alternative, the fluorescent molecule and peptides were both conjugated to the lysine residues. The VNPs were assessed in normal and cancerous prostate cell lines for non-specific and targeted uptake. This was assessed using fluorescence microscopy and flow cytometry.

The uptake of the VNPs was 75% for PKRGFQD-C and 95% for SNTRVAP-C in the PC3 cell line, which is indicative of late-stage androgen-independent cancer. The uptake in VCaP (early stage androgen-dependent cancer) was lower than for PNT2 (normal prostate cells). We consider these results positive as the VNPs will most likely target the androgen-independent cells. This study demonstrated that BMV, as a candidate VNP, can successfully

be modified with a fluorescent molecule and targeting peptide in order to specifically target prostate cancer cells.

Opsomming

Kanker is 'n beduidende oorsaak van die jaarlikse sterftesyfer wêreldwyd. Prostaatkanker is die tweede mees algemene vorm van kanker, na borskanker. Die konvensionele behandeling opsies wat tans beskikbaar is, is nie optimaal weens hul nie-spesifisiteit en die behandelings wat dikwels oneffektief is. Onlangse vooruitgang kyk na nanotegnologie as die toekoms van kankerterapie, en virale nanopartikels (VNPs) word gesien as ‘n belowende afleweringsmiddel. VNPs bied 'n proteïensteier wat relatief maklik is om te modifiseer terwyl dit ook bio-afbreekbaar is. Plantvirusse spesifiek kan met gemak gesuiwer word teen 'n hoë konsentrasie en is veilig vir menslike gebruik. *Brome mosaic virus* (BMV) is 'n twintigvlak-virus wat gekies is vir hierdie studie as gevolg van sy stabiliteit onder 'n verskeidenheid van eksperimentele toestande, soos pH en temperatuur, en sy stabiliteit in chemiese konjugasie eksperimente. BMV is ook gekies vir die beskikbaarheid van veranderbare aminosure op sy buitenste oppervlakte.

Die doel van hierdie projek was om BMV te modifiseer as 'n potensiële afleweringsnanopartikel vir prostaatkankerbehandelings. Wilde tipe BMV is gesuiwer van *Nicotiana benthamiana* en die partikels is gekwantifiseer met behulp van transmissie-elektronmikroskopie asook immunoklad-tegnieke. Die virusdeeltjies is gewysig deur konjugasie van twee fluoresserende molekules, Alexa Fluor-647 en Cy5, aan die glutamiensuur aminosuur op die buitenste oppervlak van die BMV kapsied. Twee peptiede, PKRGFQD-C en SNTRVAP-C, is gekonjugeer aan die lisien aminosure met behulp van drie koppelstukke van verskillende lengtes. Hierdie peptiede teiken onderskeidelik die reseptore α-2-macroglobulin en GRP78 wat gevind word op die seloppervlak van androgeen-onafhanklike prostaatselle. Die SM(PEG)$_{24}$ koppelstuk het die peptiedes sukkesvol gekonjugeer. Alternatiewelik is beide die fluoresserende molekule en peptiede ook gekonjugeer aan die lisien aminosure. Wanneer die fluoresserende aanhegting eerste uitgevoer was, was die peptied konjugasie onsuksesvol. Beide die fluoresserende molekule en peptiede is suksesvol gekonjugeer aan die lisien aminosure. Die VNPs is getoets in normale en kanker prostaat sellyne vir nie-spesifieke en geteikende opname met behulp van fluoresserende mikroskopie en vloeisitometrie.

Die opname van die VNPs was 75% vir PKRGFQD-C en 95% vir SNTRVAP-C in die PC3 sellyn, wat 'n voorbeeld van 'n laat-stadium androgeen-onafhanklike kanker is. Die opname in VCaP, 'n voorbeeld van die vroeë stadium androgeen-afhanklike kanker, was minder

beduidend as vir PNT2, wat normale prostaat selle is. Ons is van mening dat hierdie resultate positief is, want die VNPs sal waarskynlik die androgeen-onafhanklike selle teiken. Hierdie studie het getoon dat BMV, as 'n kandidaat VNP, suksesvol gemodifiseer kan word met 'n fluoresserende molekule en teikenpeptied om spesifiek prostaatkankerselle te teiken.

Acknowledgements

I would like to acknowledge the following people and institutions for their contributions to this study:

- My supervisor Prof. J.T. Burger and co-supervisor Dr. H.J. Maree for the opportunity to perform this project and their supervision and guidance.
- Elré Taai and Luan Africa for their technical assistance for the duration of this project.
- The NRF and the Genetics Department at Stellenbosch for funding.
- Dr. Angelique Coetzer and Madelaine Frazenberg at CAF for their technical assistance with the STEM.
- Lize Engelbrecht, Rozanne Adams and Dumisile Lumkwana at CAF for their technical assistance with the fluorescence microscopy and flow cytometry.
- Mohamed Jaffer at UCT for the TEM images he generated.
- Frank Poole at DAFF for the BMV infected source material.
- Prof. Amanda Swart and Dr. Karl Storbeck at the Biochemistry Department, Stellenbosch for the prostate cell lines.
- Prof. Bellstedt at the Biochemistry Department, Stellenbosch for allowing the use of their ultracentrifuge.
- Prof. Ed Rybicki and Dr. Ann Meyers at UCT for allowing the use of their ultracentrifuge and the purified BMV.
- Dr. Nicole Steinmetz at Case Western University, USA for allowing us the collaboration opportunity.
- My family for their support throughout this study and my father for taking the time to read through my thesis.
- And lastly my husband, Zander, for his loving support and understanding throughout the course of this study.

Table of contents

List of abbreviations

x *g*	relative centrifugal force
Å	angstrom
AMV	*Avian Myeloblastosis Virus*
AP	Alkaline phosphatase
BCIP	5-bromo-4-chloro-3'-indolyphosphate p-toluidine salt
BF	Bright field
BMV	*Brome mosaic virus*
bp	base pair
BRU	Biopharming Research Unit
BSA	Bovine serum albumin
CAF	Central Analytical Facility
cBMV	cysteine-*Brome mosaic virus*
CCMV	*Cowpea chlorotic mottle virus*
cDNA	Complementary DNA
CPMV	*Cowpea mosaic virus*
CP	Coat protein
CTAB	Cetyltrimethylammonium bromide
CuAAC	Copper(I)-catalyzed alkyne-azide cycloaddition
Cy5	Cyanine 5
DAFF	The Department of Agriculture, Forestry and Fisheries
DAPI	4',6-diamidino-2-phenylindole
DMEM	Dulbecco's Modified Eagle Medium
DMSO	Dimethyl sulfoxide

DNA	Deoxyribonucleic acid
dNTP	Deoxynucleotide
DPBS	Dulbecco's Phosphate Buffered Saline
DTT	Dithiothreitol
EDC	1-Ethyl-3-(3-dimethylaminopropyl)carbodiimide
EDTA	Ethylenediaminetetraacetic acid
eq	equivalents
EMU	Electron Microscope Unit
EPR	Enhanced Permeability and Retention
EtBr	Ethidium Bromide
FACS	Fluorescence-activated cell sorting
FBS	Fetal bovine serum
FDA	Food and Drug Administration
FE-SEM	Field Emission Scanning Electron Microscope
GES	Guanidinium isothiocyanate-EDTA-sarkosyl
Glu	Glutamic acid
HCl	Hydrogen chloride
HCRSV	*Hibiscus chlorotic ringspot virus*
HEPES	4-(2-hydroxyethyl)-1-piperazineethanesulfonic acid
HOBt	Hydroxybenzotriazole
IDT	Integrated DNA Technologies
IgG	Immunoglobulin G
LSM	Laser Scanning Microscope
M	molar
m/z	mass to charge ratio

MALDI-TOF MS	Matrix-Assisted Laser Desorption/Ionization Time-of-Flight Mass Spectrometry
MDR	Multidrug resistance
MW	molecular weight
NBT	Nitro-blue tetrazolium chloride
ODF	Orientated dark field
pA	picoampere
PBS	Phosphate buffered saline
PBS-T	Phosphate buffered saline-Tween
PCR	Polymerase chain reaction
PEG	Polyethylene glycol
PVP	Polyvinylpyrrolidone
PVX	*Potato virus X*
RCNMV	*Red clover necrotic mottle virus*
RNA	Ribonucleic acid
RO	Reverse osmosis
rpm	revolutions per minute
RPMI	Roswell Park Memorial Institute
RT	Reverse transcriptase
RT-PCR	Reverse transcriptase polymerase chain reaction
SDS-PAGE	Sodium dodecyl sulfate polyacrylamide gel electrophoresis
SEM	Scanning electron microscope
$SM(PEG)_n$	Succinimidyl-[(N-maleimidopropionamido)-diethyleneglycol] ester
STEM	Scanning transmission electron microscope
TAE	Tris base-acetic acid-EDTA

TEM	Transmission electron microscope
TFAA	Trifluoroacetic anhydride
TMV	*Tobacco mosaic virus*
U	enzyme unit
UCT	University of Cape Town
UV	Ultraviolet
UWC	University of the Western Cape
v/v	volume per volume (1 ml in 100 ml)
VEGF	Vascular endothelial growth factor
VNP	Viral nanoparticle
w/v	weight per volume (1 g in 100 ml)
WGA	Wheat germ agglutinin

List of figures

List of tables

Chapter 1

Introduction

1.1. General introduction

Cancer is a complex disease diagnosed in millions of people each year and it is a major contributor to mortality worldwide. It is comprised of more than 100 distinct diseases, each with different risk factors and epidemiology. It can originate in most cells and tissues and can be characterized by the uncontrolled proliferation of cells (Stratton et al., 2009). It develops through a multistep carcinogenesis process which utilizes multiple cellular physiological systems. The disease might start as a localized tumor, but it is prone to metastasis in which it quickly spreads throughout the body, which also complicates the treatment process (Reichert, 2008; Stratton et al., 2009; Zou, 2005).

The latest statistics from the GLOBOCAN 2012 project, which is run by the World Health Organization's International Agency for Research on Cancer, indicates that in 2012, 14 million new cases of cancer were diagnosed worldwide. The number of cancer-related deaths were estimated at 8 million people and 32.6 million people were still living with cancer after 5 years of being diagnosed, indicating the prevalence of the disease. The cancer types with the highest incidence among men are lung cancer, with an incidence of 34.2 per 100 000, and prostate cancer, with an incidence of 31.1 per 100 000. Breast cancer had the highest incidence of all cancer types and in women the incidence was 43.3 per 100 000. The second highest cancer type among women was colorectal cancer with an incidence of 14.3 per 100 000 (Forman and Ferlay, 2014).

Prostate cancer has the fourth highest incidence[1] of all cancers, with an incidence of 31.1 per 100 000, but the mortality for prostate cancer ranks only eighth with 7.8 per 100 000. The prevalence of prostate cancer, however, is a lot higher, ranking second after breast cancer with 3.8 million cases (Figure 1.1) (Forman and Ferlay, 2014). These statistics suggest that prostate cancer is a major type of cancer that burdens a significant portion of society and that research into treatment is critical.

[1] Incidence refers to the number of new cases diagnosed whereas prevalence refers to the number of cancer cases after 5 years from initial diagnosis.

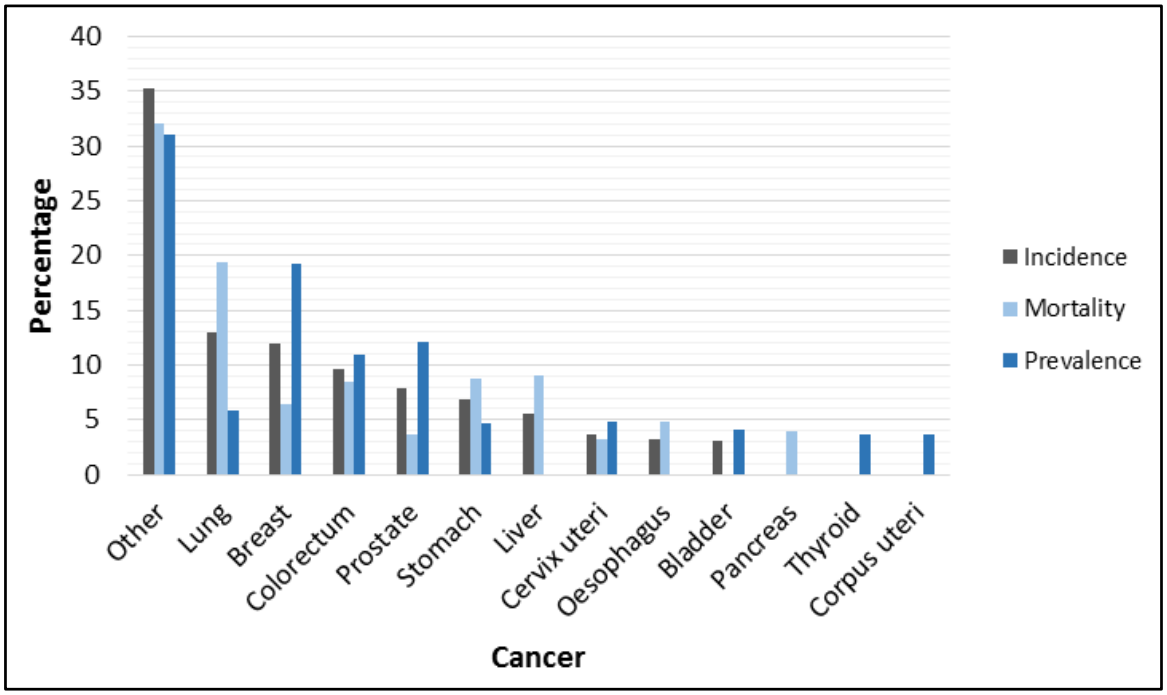

Figure 1.1: Estimated percentage of incidence, mortality and prevalence of cancer in men and women for major sites of cancer in 2012 (Adapted from Ferlay et al., (2013))

The treatment options that are currently available for cancer include chemotherapy, surgical removal of the tumor and radiation (Singhal et al., 2010). However, despite many research efforts that have gone into improving these treatments, it still holds a great number of limitations. Challenges that are frequently encountered include the non-specific distribution of the chemotherapeutic agents throughout the body; the build-up of cytotoxicity due to the high concentration of agents in the body, mainly attributed to the large dosages of chemotherapy needed due to its untargeted systemic mechanism (Destito et al., 2009); difficulty in monitoring the outcome of the response to treatment options; the development of multidrug resistance; residual cells that remain after surgical removal and the inability of therapeutics to reach the tumor site (Das et al., 2009; Hull et al., 2014; Parveen and Sahoo, 2008, 2006). These factors signal the need for a more refined approach to the treatment of cancer.

1.2. Aims and objectives

The aim of this study was to modify an icosahedral plant virus, *Brome mosaic virus*, for targeted delivery to prostate cancer cell lines and fluorescence-based detection. The following objectives were set out to achieve the proposed aim:

- To propagate BMV in a suitable plant host
- To purify BMV from the plant material

- To modify BMV in order to detect it via fluorescence
- To modify the surface of the viruses with a targeting peptide to target prostate cancer cell lines
- To test the efficiency of these modifications *in vitro*

1.3. Chapter layout

Chapter 1: Introduction

This chapter gives a general introduction and aims and objectives of the study as well as outlines the chapters in the thesis. Research outputs from this study are also highlighted here.

Chapter 2: Literature review

The literature review gives a thorough summary of the literature on cancer and drug delivery nanoparticles.

Chapter 3: Materials and methods

The methods that were used in this study are outlined here, as well as the materials and equipment used.

Chapter 4: Results and discussion

This chapter presents all the results of the study as well as an interpretation of the results.

Chapter 5: Conclusion

The last chapter gives concluding remarks on all the findings as well as future prospects of the research.

1.4. Research outputs

The following conference presentations and posters resulted from this research project.

1.4.1. Conference proceeding

Lee, N., Taai, E., Africa, L.D., Steinmetz, N.F., Rybicki, E.P., Burger, J.T., Maree, H.J. Engineering of *Brome mosaic virus* as a drug delivery nanoparticle to prostate cancer cells. Presentation of preliminary research presented at the 2nd SA Biomedical Engineering Conference, Stellenbosch, South Africa, 22-24 March 2016.

1.4.2. Posters

Lee, N., Africa, L. D., Taai, E., Steinmetz, N. F., Rybicki, E. P., Burger, J. T., Maree, H. J. Engineering of *Brome mosaic virus* as a potential drug delivery nanoparticle to prostate cancer cells. Poster of first preliminary research presented at Virology Africa, Cape Town, South Africa, 30 November – 3 December 2015.

Lee, N., Africa, L. D., Taai, E., Steinmetz, N. F., Rybicki, E. P., Burger, J. T., Maree, H. J. Engineering of *Brome mosaic virus* as a potential drug delivery nanoparticle to prostate cancer cells. Poster of additional preliminary research presented at the DST-NRF Nanotechnology Symposium, Pretoria, South Africa, 27 – 28 June 2016.

Chapter 2

Literature review

2.1. Cancer

Cancer is a complex disease that may be caused by a wide variety of factors. The most common known factor is carcinogens, such as tobacco smoke and ultraviolet (UV) radiation (Bouwman and Jonkers, 2014). These act as mutagens that cause DNA mutations, which transform normal human cells into cancerous cells through a multistep process. These mutations contribute to the formation of oncogenes, which gain a function that is beneficial to the growth of the tumor, and tumor suppressor genes, which lose a function important for the control of tumors (Hanahan and Weinberg, 2000). These carcinogens also cause DNA damage and the already defective DNA repair signaling pathways aggravate the accumulation of DNA damage over time (Bouwman and Jonkers, 2014).

The cancer genome project was initialized to identify the important genes that are susceptible to mutations and thus far 30 tumor suppressive and 100 oncogenes have been identified (Futreal *et al*., 2001). In another census, a total of 291 genes were identified that are involved with oncogenesis (Futreal *et al*., 2004). Oncogenes and tumor suppressor genes also contribute to the metabolism of cancer cells by increasing the survival of the tumors by enhancing the metabolic pathways. A number of metabolic genes were identified that are overexpressed in cancer cells and 16 genes were identified that are specifically contributing to tumorigenesis (Scalbert and Romieu, 2014).

Cancer is also considered a heritable disease, as has been shown by numerous genome-wide association studies that identified a number of alleles that increase the susceptibility to cancer. This is also apparent from cancer types that are more prevalent in families. Some cancers can also be more heritable than others, as more alleles are associated with some cancer types. These identified alleles allow for initial diagnoses of susceptibility to a certain cancer type, providing patients with a potential preventative option (Chanock, 2014).

2.1.1. Complexity of the disease

The complexity of the disease is largely due to the vast number of types and subtypes of cancer among different populations as a result of the different environments of these regions in the world (Hudson, 2014). In 2007 the International Cancer Genome Consortium was

founded and they have discovered 50 different tumor types and subtypes within the 25,000 cancer genomes that were studied (Hudson *et al*., 2010). This is due to the number of mutations that are present in a single tumor (Hudson, 2014) and that each tumor mass can present with multiple tumor populations, each with its own unique mutation profile mass (Samuel and Hudson, 2013). These tumors also continue to mutate and therefore can develop drug resistance over time, which makes this disease even more difficult to treat and leads to treatment plans failing after some time (Hudson, 2014).

Figure 2.1 outlines the main characteristics that are considered to contribute to the progression of the disease. In this study our focus will be on the characteristics that contribute to the development of the tumor microenvironment (Figure 2.2). The tumor microenvironment is a key factor that complicates the treatment process. An important characteristic of the microenvironment is the ability of the tumor to form its own blood vessels through a process known as angiogenesis. This is initialized once the tumor growth increases and it is no longer supplied by the blood vessels. It leads to a hypoxic state in the tumors, which prompts an increase in the release of vascular endothelial growth factor (VEGF). This is essential for angiogenesis and thereby the tumors are able to create their own blood supply, allowing their independent survival (Weis and Cheresh, 2011).

This microenvironment is also associated with inflammation. Inflammation has been shown to be associated with the progression of the disease by contributing to angiogenesis, metastasis, cancer cell division and also lowered response to treatment (Colotta *et al*., 2009). Inflammation leads to genetic and epigenetic instability, mediated by the reactive oxygen species (ROS) that cause DNA damage. Inflammation may also promote the growth of the tumor by providing growth factors that may support angiogenesis. The environment created by inflammation may also be immunosuppressive, thereby allowing the cancer cells to evade the immune system (Grivennikov *et al*., 2010). This is in large contributed by the loss or mutation of cell receptors on the surface of tumors (Schreiber *et al*., 2011) which may lead to the upregulation of receptors that signal the downregulation of the immune response (Trinchieri, 2014).

The tumor microenvironment ultimately leads to a decrease in the effectiveness of the different treatments available. The vascular bed becomes hyperpermeable to macromolecules and the inflow of extravasated proteinaceous fluid leads to an increase in the interstitial pressure inside the cancer cells, which prevents transcapillary transport and in turn limits the uptake of therapeutic molecules. It also leads to poor blood flow in tumors

and many tumors have varying areas of high or low blood flow. This heterogeneous region of blood flow complicates therapy, as it has been shown that hypoxic regions are less responsive to radiotherapy, and chemotherapy requires good blood flow to reach the site of the tumor. It has also been shown that oxygen deprivation is associated with increased metastasis (Langley, 2014).

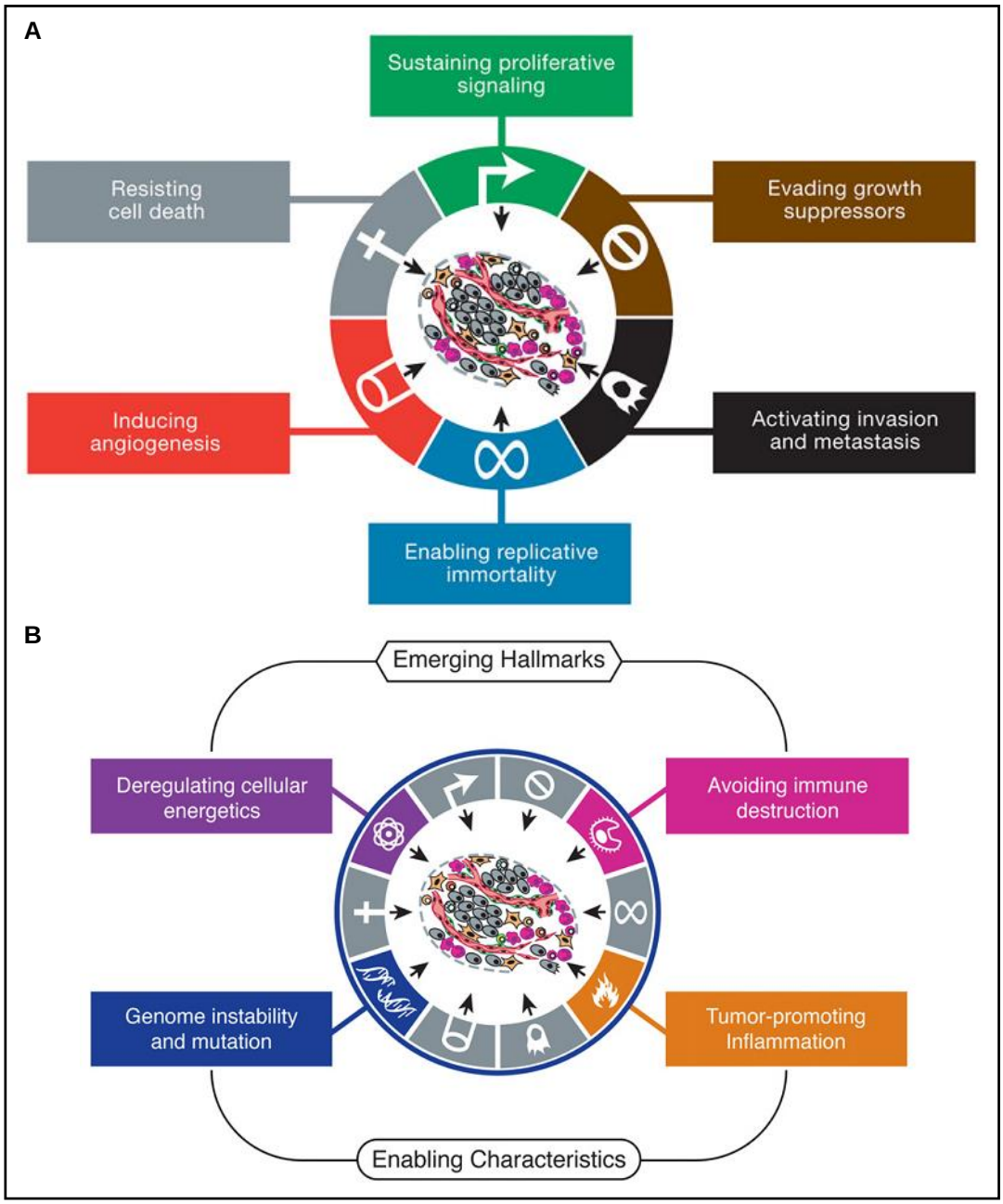

Figure 2.1: Characteristics of cancer that enable its progression. **(A)** Six validated and accepted characteristics (Hanahan and Weinberg, 2000), **(B)** Two emerging hallmarks that are currently under study and two characteristics that enables the progression of the disease (Hanahan and Weinberg, 2011)

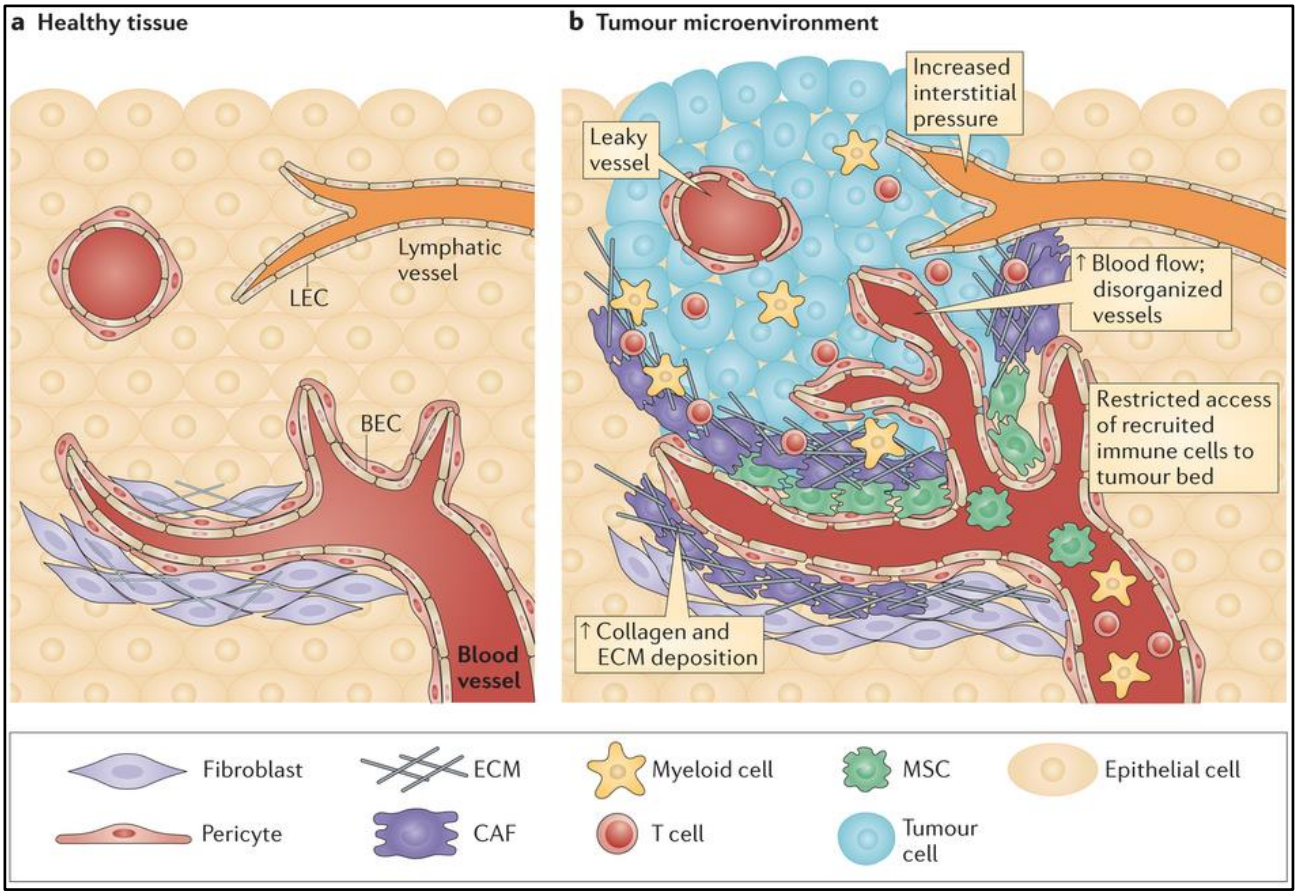

Figure 2.2: The tumor microenvironment. Blood endothelial cells (BEC) and lymphatic endothelial cells (LEC) are indicated in the healthy cells (Turley *et al.*, 2015)

A critical factor that makes the disease so devastating is its ability to metastasize. In this process some cancer cells will break off and adopt new metamorphic features as well as gene expression profiles. They will then migrate to other sites in the body where they will invade and proliferate (Thiery *et al*., 2009).

2.1.2. Prostate cancer

Prostate cancer can be classified according to three stages of androgen dependence, of which two are illustrated in Figure 2.3. Firstly, early prostate cancer cells are classified as androgen dependent, because they rely on the androgen receptor for growth. It requires 5α-dihydrotestosterone to bind to the androgen receptor, thereby dissociating it from the heat-shock protein bound to the inactive state. The androgen receptor then translocates to the nucleus where it activates the appropriate genes for growth (Debes and Tindall, 2004). Prostate cells that respond to androgen but do not require it for growth are termed androgen sensitive. This allows for an alternative treatment option by using hormonal treatment for the prevention of tumor growth (Paul and Breul, 2000; Rambeaud, 1999; Sciarra *et al*., 1999). Lastly, late stage prostate cancer can be defined as androgen-independent. This type of

cancer cell does not require the androgen receptor for growth and may rely on other pathways. In many cases the androgen receptor is mutated or amplified and may respond to different ligands, other than dihydrotestosterone (Debes and Tindall, 2004). Androgen-independence usually occurs when the disease recurs after treatment was initially successful (Lara and Meyers, 1999; Laufer *et al*., 2000), many times accompanied by changes in the androgen receptor, either through mutation, amplification or loss *(Culig et al*., 1998; Henshall *et al*., 2001; Kinoshita *et al*., 2000; Wang and Uchida, 1997).

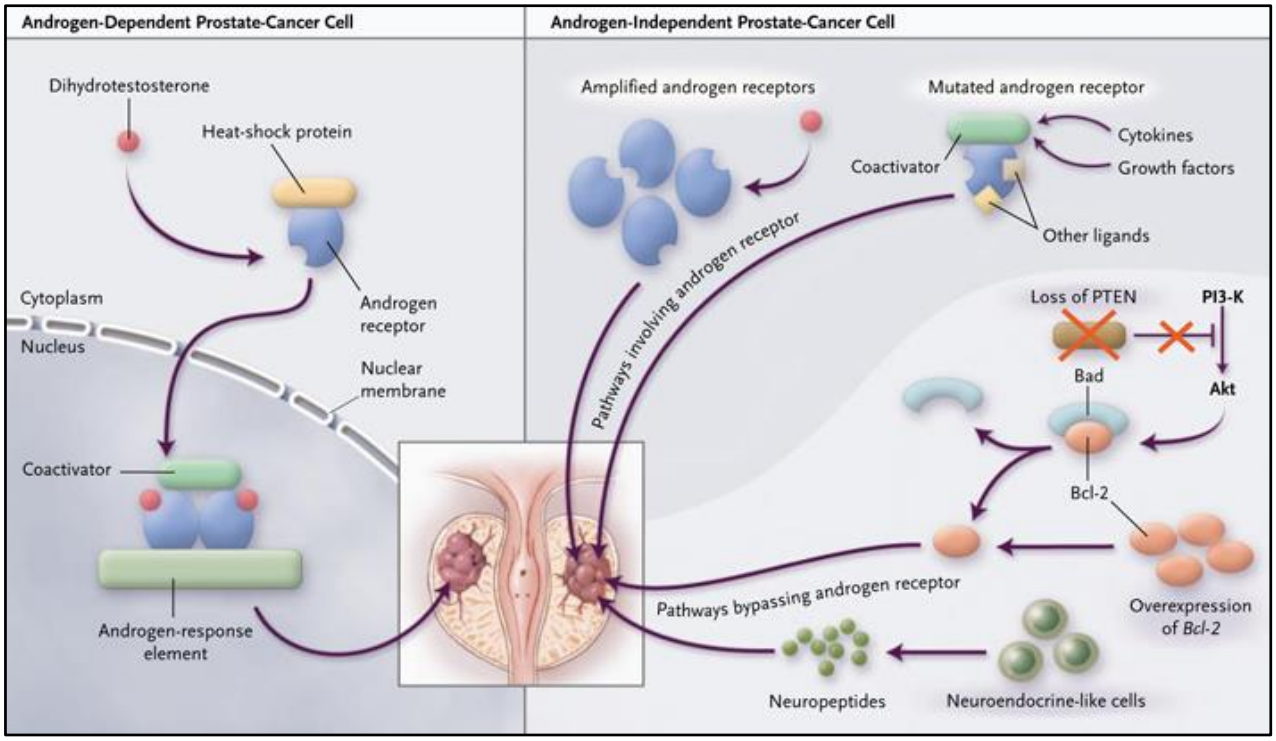

Figure 2.3: Androgen-dependent and androgen-independent prostate cancer models (Debes and Tindall, 2004)

2.2. Nanotechnology

A new field that hopes to improve the treatment and diagnosis of cancer is nanotechnology. A nanomaterial can be defined as a material with at least one dimension that is less than 100 nm and exhibits unique properties due to its nanometer size range and its shape. Nanotechnology can therefore be defined as the 'intentional design, characterization, production, and application of materials, structures, devices, and systems by controlling their size and shape in the nanoscale range (1 to 100 nm)' (COMA, 2007). Nanomedicine is a subset of nanotechnology and this can be defined as the 'monitoring, repair, construction and control of human biological systems at the molecular level, using engineered nanodevices and nanostructures' (Freitas, 1999).

2.2.1. Advantages of nanoparticles

These nanomaterials offer an advantage to conventional cancer treatment as they can interact with molecules on the surface of cells as well as inside cells (Destito *et al*., 2009). This is an advantage as it can limit the therapeutics to the site of the cancer cells, thereby reducing harmful effects to the surrounding healthy cells (Misra *et al*., 2010). Certain properties of nanotherapeutics allow them to do this: i) the nanoparticles can be designed to carry therapeutic drugs to the cells; ii) the nanoparticles can be modified with targeting ligands to increase their affinity for cancer cells; iii) multiple drug molecules can be loaded onto the nanoparticles to elicit a combinatorial therapeutic effect and iv) nanoparticles can bypass drug resistance mechanisms (Acharya *et al*., 2009).

Inherent properties of these nanoparticles that make them suitable for cancer therapy are their size, payload density, duration of effect and surface properties that allows for targeting. The small size allow the nanoparticles to enter the tumors while avoiding extravasation by the tumor vasculature through the Enhanced Permeability and Retention (EPR) effect. The nanoparticles can carry a large number of molecules on their surface, meaning that ultimately a very high concentration of drug molecules can be loaded on a single particle (Heidel and Davis, 2011). Many factors, such as the size, surface modifications and particle composition, lead to an increase in the duration that these particles are able to circulate in the body before being cleared (Alexis *et al*., 2008; Li and Huang, 2008). This allows for an increased dosage of drugs at the cancer cells, leading to more efficient treatment. The last property is the ability to modify the surface of the particles in order to improve their movement to the cancer cells, either by modifying the surface charge for improved circulation or by incorporating a targeting ligand to improve its specificity for the target cell. This has been found to enhance endocytosis of these particles by cancer cells, thereby limiting treatment to cancer cells only.

This also has an advantage for multidrug resistance (MDR), which normally severely limits the intake and effect of conventional cancer drugs. The microenvironment of cancer cells, namely the high interstitial pressure, reduced microvascular pressure and poor vascular regions, reduces the ability of drugs reaching the tumor cells. The cancer cells also elicit many cellular pathways in order to degrade the cancer drugs. As nanoparticles enter the cancer cells by endocytosis, they are able to avoid the MDR mechanisms that are elicited at the microenvironment. The drug molecules bound to the nanoparticle will also not be degraded as fast as freely circulating molecules (Heidel and Davis, 2011). These

advantages suggest that nanoparticles can be utilized for more specific and efficient treatment of cancer.

2.2.2. Types of nanoparticles

Currently a wide variety of particles are being studied for their functionality as nanoparticles. This ranges from synthetic molecules to various biological molecules and relies on different distinguishing features depending on the application of the nanoparticle (Figure 2.4). The key properties that determine the use of the nanoparticle is its size, the surface properties and charge, the shape of the particle as well as its composition, which relates to it being an organic or inorganic particle (van Kan-Davelaar *et al*., 2014).

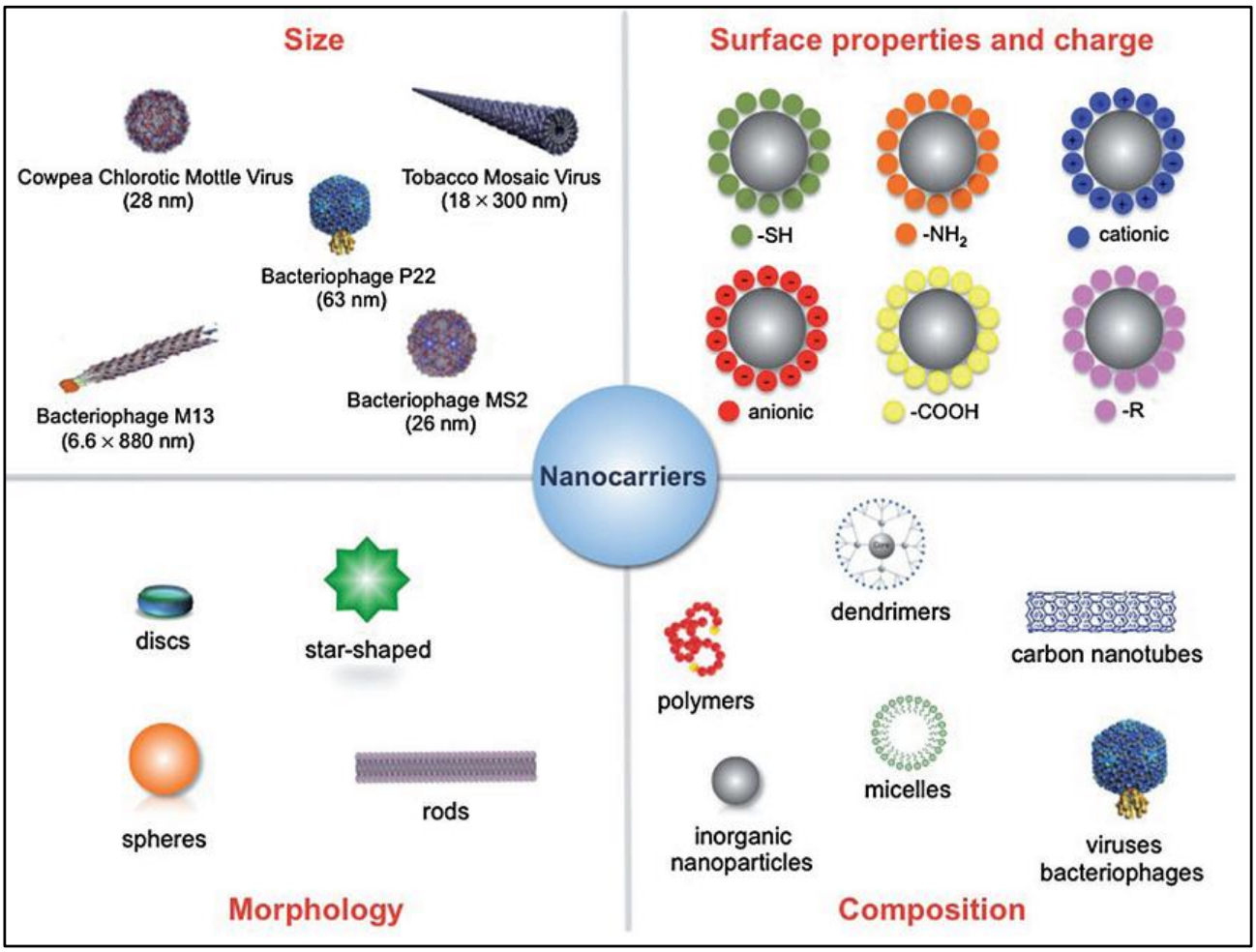

Figure 2.4: Different types of nanoparticles based on distinguishing properties (van Kan-Davelaar *et al*., 2014)

Although inorganic nanoparticles have been well studied and three have been approved for phase I clinical trials (Table 2.1), there are some challenges that accompany them. The heavy metals may cause toxicity in the body and they have increased difficulty of

bioelimination after the therapeutics have been delivered (Destito *et al*., 2009). This prompts an even more refined strategy for the delivery of cancer therapeutics.

Table 2.1: Inorganic nanoparticles in clinical trials (Bregoli *et al*., 2016)

Product name and manufacturer	Type of particle	Cancer targeted
Aurimune (CYT-6091) / CytImmune Sciences	PEGylated gold nanoparticle for TNF-α delivery	Solid tumors
Auroshell, Aurolase / Nanospectra Biosciences, Inc.	Gold-coated silica nanoparticles for photothermal therapy	Head, neck and lung cancer
BTXR3 / Nanobiotix	Hafnium oxide nanoparticles for radiotherapy	Squamous cell carcinoma of the oral cavity and adult soft tissue sarcoma

2.2.2.1. Organic nanoparticles

Many organic nanoparticles have been successful in their applications, ranging from phase I-III clinical trials and some even received approval from the Food and Drug Administration (FDA). The most successful nanoparticles are liposomes, albumin-based nanoparticles, micelles and polymeric nanoparticles (Bregoli *et al*., 2016). This indicates that substantial research is done on nanoparticles as the future of cancer treatment and diagnostics. Although these organic nanoparticles are very successful in their applications, viral nanoparticles surpass them in terms of their inherent properties that make them ideal nanocarriers.

2.3. Viral nanoparticles

Viruses are evolved to invade a host and deliver genomic cargo into cells (van Kan-Davelaar *et al*., 2014; Yildiz *et al*., 2011), which means that they are inherently equipped to function as a delivery vehicle. Viruses have been extensively studied and characterized on their biological, genetic and physical properties. This knowledge enables the manipulation of virus particles to suit specific experimental needs (Strable and Finn, 2009).

There are many advantages that make viruses more ideal than other biological nanoparticles, namely i) their wide size range and the characterization of their structures at atomic resolution; ii) their monodisperse size and composition of their structures; iii) the wide variety of shapes available, each with distinct properties; iv) their constrained interior cavity which allows for packaging of molecules on the inside of the particles as well; v) their composition may be manipulated by changing the viral genome; vi) their ability of self-

assembly and polyvalence, which contributes to the stability of the particles; vii) they can be produced in large quantities, with relative ease; viii) they are stable at a wide range of experimental conditions, such as pH, temperature and chemical modification; and ix) they have large surface areas, which allows the conjugation of a large number of molecules per particle (Strable and Finn, 2009; van Kan-Davelaar *et al*., 2014) .

Because of extensive studies done on viruses, amino acids on the protein capsid of the virus can be identified and modified for bioconjugation. The extensive knowledge of the viral capsid structure also allows the design of ligands in order to improve the targeting abilities of the viral particles. Viruses also have a significant advantage over other nanoparticles due to the multiple uniformly distributed sites onto which ligands can be introduced (Destito *et al*., 2009).

Viruses have been used for vaccines and gene-therapy for many years and some of these vaccines are currently used in the clinic, namely the *Human papillomavirus* (HPV) vaccine Gardasil[2] (Merck & Co Inc.). Gene therapies based on the *Adenovirus*, *Adeno-associated virus*, and *Lentivirus* are currently in clinical trials (Wen *et al*., 2012b). Viruses derived from plants and bacteria are considered the ideal nanoparticles as they are biocompatible, biodegradable, non-infectious to mammals, they can be produced in large quantities from their respective hosts and they are available in many shapes and sizes (van Kan-Davelaar *et al*., 2014; Yildiz *et al*., 2011). Viral nanoparticles (VNPs) can also be easily modified, either genetically or chemically, and they present with well-ordered, multivalent functional groups on their internal and external surfaces (Wen and Steinmetz, 2014).

Some of the VNPs currently in development are *Brome mosaic virus* (BMV), *Cowpea chlorotic mottle virus* (CCMV), *Cowpea mosaic virus* (CPMV), *Hibiscus chlorotic ringspot virus* (HCRSV), *Red clover necrotic mottle virus* (RCNMV), *Potato virus X* (PVX), *Tobacco mosaic virus* (TMV), and bacteriophages MS2, Qβ and M13 (Figure 2.5) (Steinmetz, 2010).

An icosahedral plant virus that has been extensively studied for its use in nanotherapy is CPMV (Destito et al., 2009). CPMV is a member of the family *Comoviridae* with a two-part single stranded RNA genome and a non-enveloped viral capsid. The coat proteins of the capsid consists of 60 copies of the 23 kDa small subunit and the 41 kDa large subunit which fuses to form an icosahedral capsid that surrounds the RNA (Manchester and Steinmetz, 2009). The icosahedral structure allows for polyvalent display of peptides on the capsid

[2] The vaccine contains recombinant VLPs that are assembled from the L1 proteins from the capsid protein of HPV and not the whole virus.

protein because of its symmetric nature. The crystal structure of CPMV is available at 2.8 Å resolution, which allows for designing molecules to be attached to its surface (Chatterji *et al*., 2004). The capsid diameter is 30 nm with a thickness of 1.2 nm. CPMV can be purified in large quantities from infected leaves and the particles are stable in a wide range of pH and temperature (Manchester and Steinmetz, 2009) and permissive to genetic and chemical modifications (Chatterji *et al*., 2004), making it a suitable candidate for nanoparticle applications.

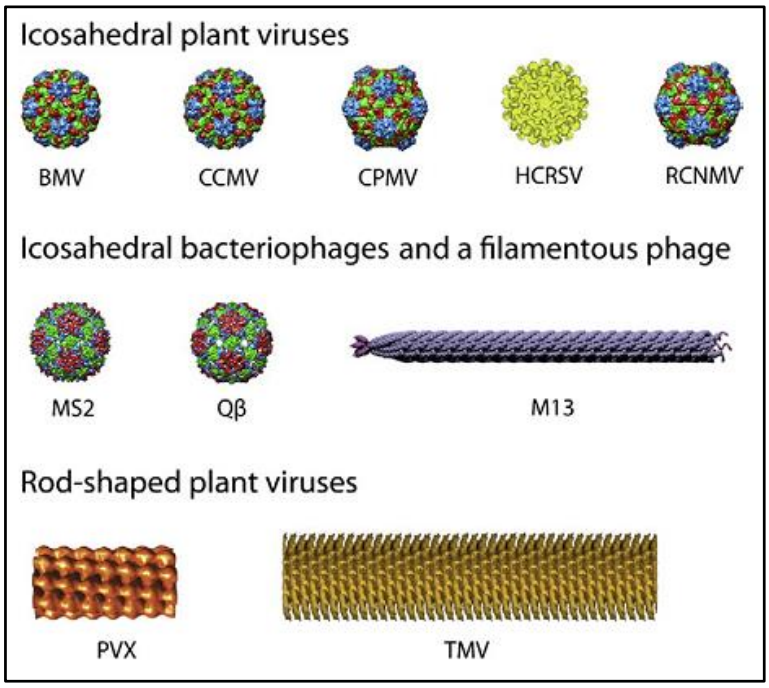

Figure 2.5: VNPs currently in development (Steinmetz, 2010)

Not only has CPMV extensively been studied for its exterior surface modification, but modification of its interior has also been successful. It has been found that CPMV has a natural affinity for vimentin which is expressed on the cell-surface of HeLa (cervical cancer), HT-29 (colon cancer) and PC3 (prostate cancer) cells to promote internalization of the particles. This means that efforts can also be focused on interior modification of CPMV (Wen *et al*., 2012a). In a study by Wen *et al*., (2012) they demonstrated that the reactive cysteine residues on the interior of CPMV can be utilized to attach fluorescent dye molecules. They also produced a CPMV devoid of any RNA, which they found to increase the affinity for dye molecules.

2.4. *Brome mosaic virus*

Another plant virus with great potential as a VNP is BMV. BMV is a T=3 icosahedral shaped virus from the family *Bromoviridae* and genus *Bromovirus* (Fauquet *et al*., 2005). It has a diameter of 28 nm at a pH below 6 (Lucas *et al.*, 2001). It has a molecular weight of 4.6 x 10^6 Da and a coat protein size of 20 kDa (Bockstahler and Kaesberg, 1962). The coat protein consists of 189 amino acids and a highly positively charged amino-terminus (Lucas *et al*., 2002).The crystal structure has been resolved at 3.4 Å resolution (Lucas *et al*., 2002). The virus is comprised of 180 subunits in its coat protein which assumes an equal number of either A, B or C conformation (Figure 2.6). It has a multipartite single-stranded RNA genome, consisting of RNA1 (3.2 kb), RNA2 (2.8 kb), RNA3 (2.1 kb) and a small RNA4 (800 bp) that encodes only for the coat protein and is found packaged together with RNA3 (Ahlquist *et al*., 1990).

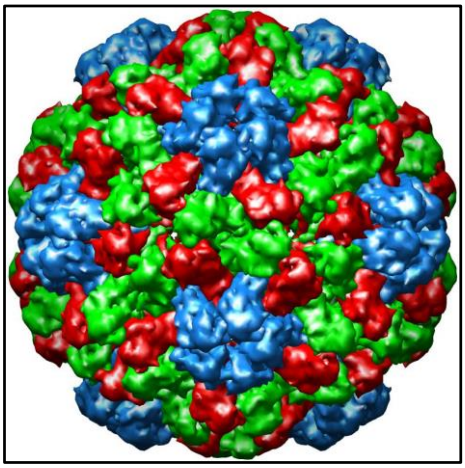

Figure 2.6: Structure of BMV representing the T=3 organization of the 180 coat proteins

BMV has been studied extensively for its ability to disassemble and reassemble into empty capsids. This has been utilized to encapsulate a number of synthetic molecules, such as gold nanoparticles, iron oxide cores and quantum dots, and fluorescent molecules (Daniel *et al*., 2010; Dixit *et al*., 2006; Huang *et al*., 2011, 2007; Jung *et al*., 2011; Sun *et al*., 2007). Thus far BMV has not been thoroughly explored for its use in bioconjugation. Yildiz *et al*. (2012) demonstrated the ability of cysteine-BMV (cBMV) mutants to conjugate OregonGreen 488 to the introduced cysteine residues using thiol-maleimide chemistry. cBMV was also successfully conjugated with PEG2000, Transferrin, Doxorubicin and R5-peptides. OregonGreen 488 was also successfully conjugated to the lysine residues of cBMV and PEG2000 to the cysteine residues (Wen *et al*., 2012a). Thus far native BMV has not been used with bioconjugation chemistries other than the addition of a fluorophore to

the lysine residues. This study will be a novel approach, since it is the first time that native BMV will be modified as a VNP with a targeting peptide.

2.5. Production of VNPs

VNPs can be produced from their natural hosts in gram quantities. The purified VNPs can then be modified for the desired application by means of three different methods, namely genetic engineering, chemical bioconjugation and self-assembly (Figure 2.7).

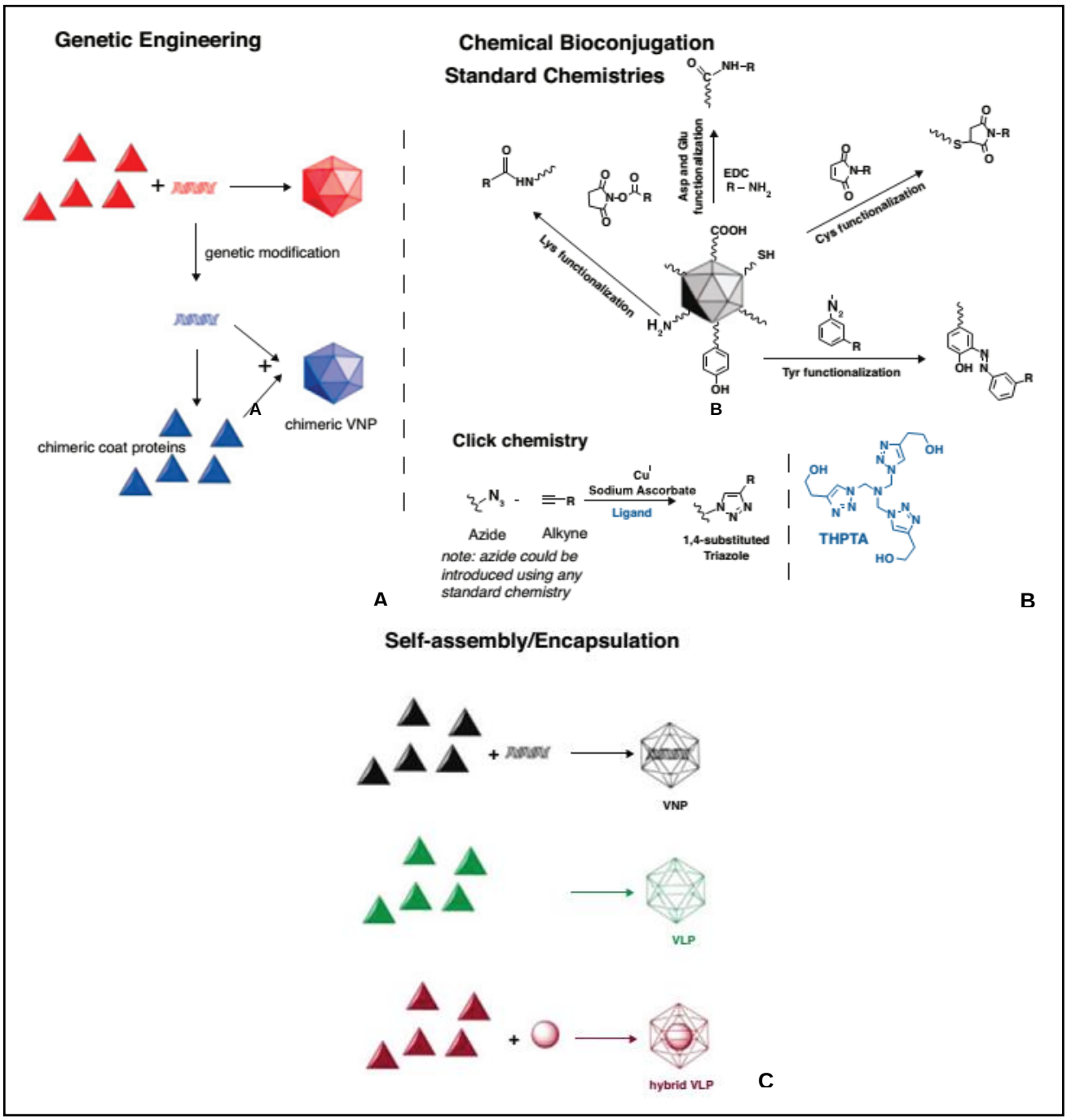

Figure 2.7: Different methods for production of VNPs. **(A)** Genetic engineering, **(B)** Chemical bioconjugation, **(C)** Self-assembly. Adapted from Yildiz *et al*. (2011).

In genetic engineering amino acids can be inserted into the virus genome that can serve as targets during chemical modification (Yildiz *et al.*, 2011). This is commonly used to add cysteine residues to CPMV (Wang *et al*., 2002). Peptides can also be inserted as well as peptide-based affinity tags (Yildiz *et al*., 2011). In chemical conjugation specific bioconjugation methods are used to functionalize the amino acids on the virus capsid to introduce molecules of choice. Encapsulation makes use of the ability of viruses to swell and encapsulate a molecule or to disassemble and reassemble around the molecule of choice. These two methods are used to introduce a variety of molecules (Figure 2.8) that can be used in a variety of applications (Yildiz *et al*., 2011).

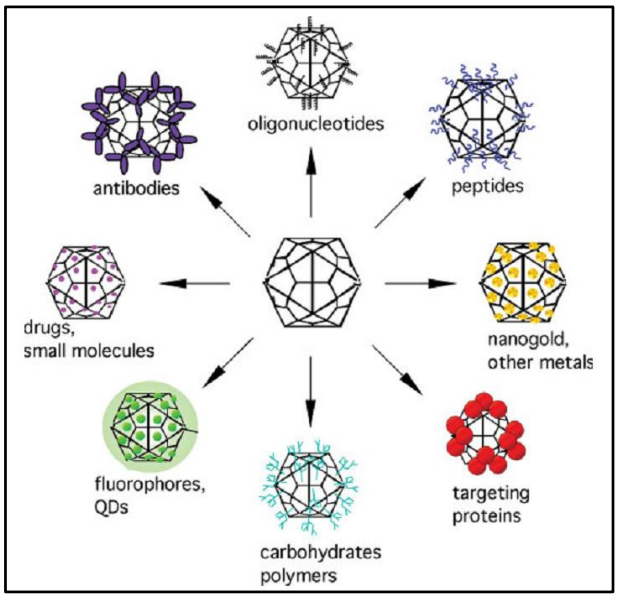

Figure 2.8: Variety of molecules that can be conjugated or encapsulated into VNPs for different applications (Singh *et al*., 2006).

2.5.1. Targeting mechanism

VNPs can be internalized into cells by two different mechanisms, passive targeting and active targeting (Figure 2.9). Passive targeting refers to the accumulation of nanoparticles to the desired site by making use of the unique properties of the nanoparticles, such as their size, and the microenvironment of the tumor site. Nanoparticles are able to use the vascularized areas of the tumor site and the higher metabolic rate of cancer cells to rapidly accumulate on the inside of the tumor. This is also known as the enhanced permeability and retention (EPR) effect in which the tumor vasculature is composed of various gaps along the endothelium. This allows the internalization of macromolecules up to 400 nm in diameter. Active targeting makes use of a ligand attached to the nanoparticle that is specific to a receptor presented on the cancer cells. It is therefore important that the receptor is only

expressed on the tumor and not on healthy cells as this will decrease the targeting ability of the particles. Upon binding to the tumor receptor, the nanoparticle can be internalized by endocytosis. This method of targeting further increases the effectiveness of treatment and also lowers the toxicity to healthy cells (Bamrungsap *et al.*, 2012; Misra *et al*., 2010)

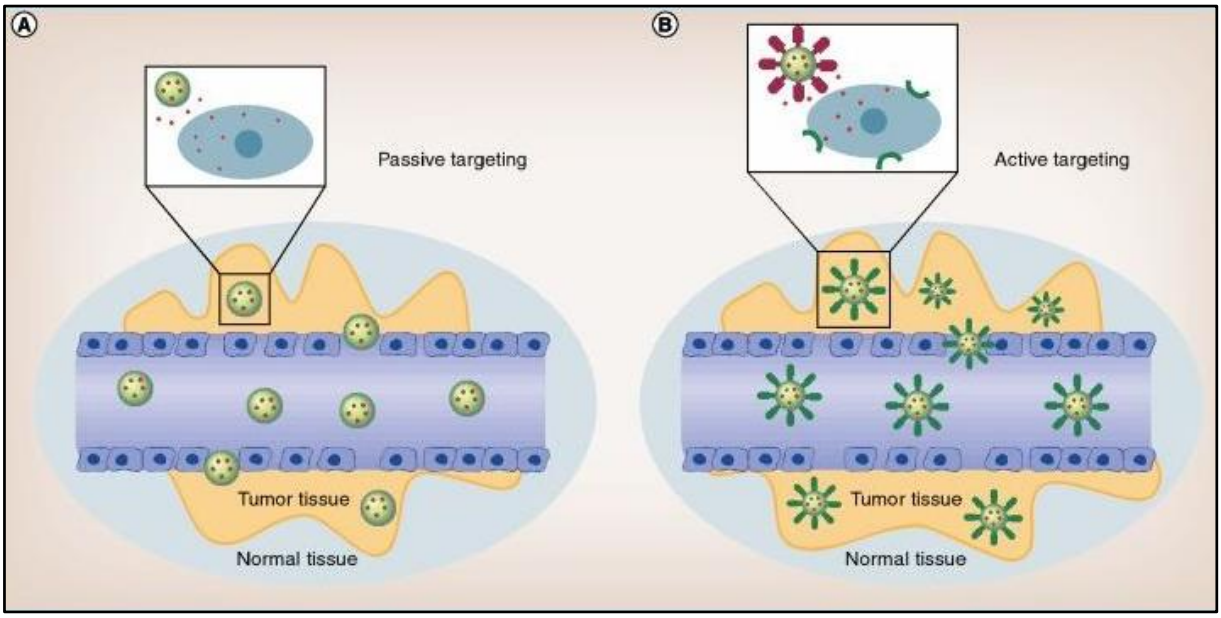

Figure 2.9: Passive and active targeting of nanoparticles to cancer cells. **(A)** Passive targeting, **(B)** Active targeting (Bamrungsap *et al*., 2012)

2.5.2. Conjugation of a fluorescent molecule

A fluorescent molecule is added to the VNP in order to track its movement *in vitro*. This can also be used as an imaging agent *in vivo*, but for this study it will be used to validate the internalization of the VNPs *in vitro*.

BMV has 8 solvent exposed glutamic acid residues per coat protein, as determined by VIPERdb (Carrillo-Tripp *et al*., 2009): Glu76 and Glu160 in the A subunit and Glu55, Glu76 and Glu160 in both the B and C subunits. The reactivity of these amino acids is unknown as it has never been used for bioconjugation. The reason for choosing the glutamic acids is that they are readily available on the exterior of the coat protein of BMV. Additionally, the glutamic acids can easily be modified using the 1-Ethyl-3-(3-dimethylaminopropyl)carbodiimide (EDC) coupling reaction and the copper(I)-catalyzed alkyne-azide cycloaddition (CuAAC), also known as “click” chemistry.

The EDC coupling is used to conjugate an alkyne to the carboxylate group of the glutamic acids by means of an EDC activated propargylamine. The alkyne is then functionalized using

the CuAAC reaction to attach a fluorescent molecule containing a terminal azide (Bruckman and Steinmetz, 2014) (Figure 2.10).

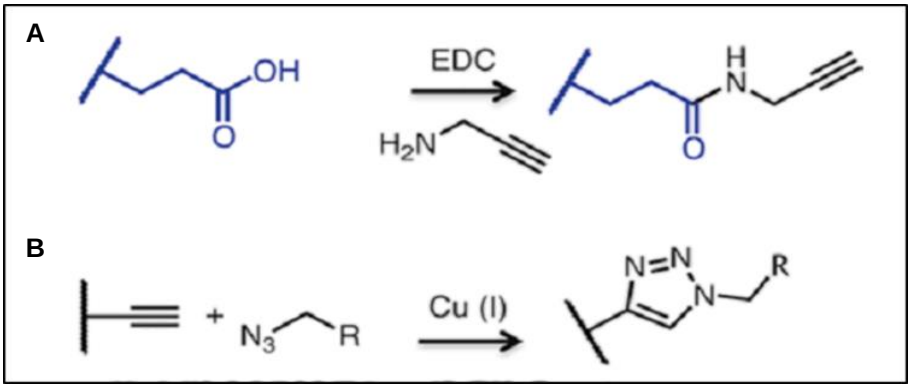

Figure 2.10: Conjugation of a fluorophore to the glutamic acids on the exterior coat protein of BMV. **(A)** EDC reaction to attach an alkyne to the glutamic acids, **(B)** CuAAC reaction to functionalize the alkyne with an azide-containing fluorophore (Bruckman and Steinmetz, 2014)

2.5.3. Conjugation of a targeting peptide

Finally a targeting peptide is required for the VNPs to target the cancer cells. Mandelin *et al*. (2015) identified two novel peptides, PKRGFQD and SNTRVAP, which are specific for the receptors on androgen-independent prostate cancer. PKRGFQD has been shown to specifically target the α-2-macroglobulin receptor and SNTRVAP for the 78-kDa glucose-regulated protein (GRP78) receptor. These receptors are specifically upregulated in androgen-independent cell lines.

Androgen deprivation is one of the main treatment options currently used for metastatic prostate cancer, but the limitation is that many metastatic cancers develop androgen-independence. This makes this treatment ineffective and the tumors give rise to osteoblastic bone and soft tissue metastasis, which ultimately can be fatal (Mandelin *et al*., 2015). Therefore the targeting peptides will aid in the delivery of nanoparticles to androgen-independent cancer cells to improve the treatment thereof. The peptides have not been studied for their use as targeting ligands for nanoparticles and therefore this will be a novel approach in this study.

BMV has previously been shown to have 180 reactive lysine residues (Wen *et al*., 2012a) that can be used to successfully conjugate molecules using NHS ester chemistry. An amine-to-sulfhydryl crosslinker with soluble polyethylene glycol (PEG) spacer arms can be used to achieve this. The NHS group on the one end of the crosslinker will conjugate to the amine

group on the lysine to create an amide bond with the release of a free NHS compound (Figure 2.11) (Thermo Scientific, 2012).

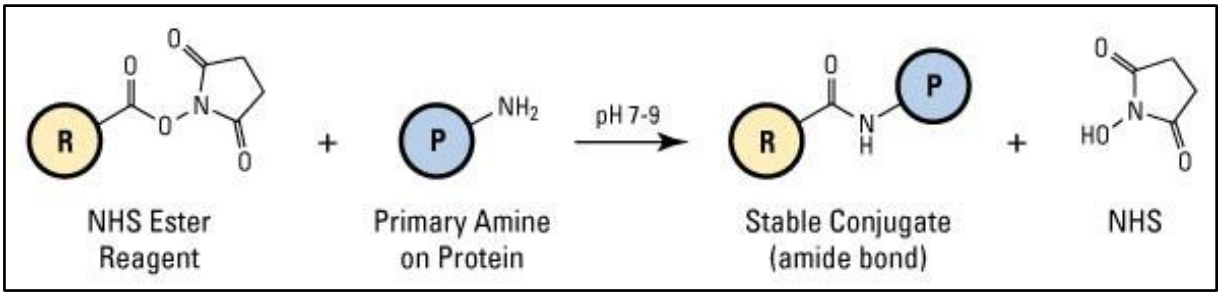

Figure 2.11: NHS ester reaction representing the conjugation of the amine on the crosslinker to the amine of the lysine on the BMV coat protein. The NHS ester reagent represents the free amine on the crosslinker and the primary amine of protein represents the free amine group on the lysine residue (Thermo Scientific, 2012)

The peptides were synthesized with a terminal cysteine that will be conjugated to the maleimide group on the crosslinker using maleimide chemistries. In this reaction the sulfhydryl on the cysteine will conjugate to the maleimide group on the crosslinker to create a thioether bond (Figure 2.12) (Thermo Scientific, 2012).

Crosslinkers of different lengths will be utilized to assess the efficiency of conjugation with the varying distance that the peptide is conjugated to the lysine on the coat protein. The principle is that certain crosslinkers might not create sufficient space for the peptide to bind as there might be interference from surrounding amino acids in the coat protein.

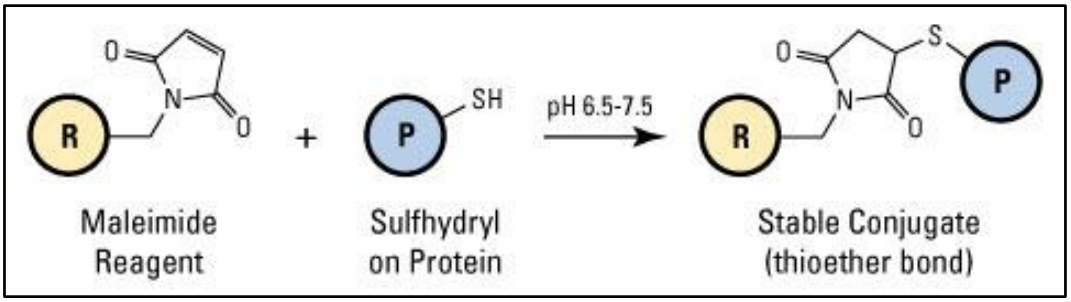

Figure 2.12: Maleimide reaction representing the conjugation of the sulfhydryl on the peptide to the maleimide on the crosslinker (Thermo Scientific, 2012)

2.6. Conclusion

Cancer is a devastating disease that affects the lives of millions of people each year. The current treatment options that are available are not optimal and there is a need for a more refined treatment. Nanomedicine offers the opportunity for a treatment that can be tailored and that can specifically target cancer cells, without leading to damage to healthy cells, as

is the case with conventional treatments. Various nanoparticles have been developed, both organic and inorganic nanoparticles, but currently viruses are considered the ideal nanocarrier.

VNPs can be tailored for any specific application and the many shapes and sizes of viruses that are available makes them suitable for a desired application. *Brome mosaic virus* is an icosahedral virus that has been extensively studied for its reassembling ability to encapsulate molecules, but not for bioconjugation. This study will be novel in its regard to bioconjugate native BMV for the targeting of prostate cancer.

Chapter 3

Materials and methods

3.1. Diagnostics

Plant material infected with *Brome mosaic virus* (BMV) was received from the Department of Agriculture, Forestry and Fisheries (DAFF). The presence of BMV in this plant material was confirmed by means of reverse transcriptase polymerase chain reaction (RT-PCR) and a dot blot.

3.1.1. RT-PCR

Primers were designed for the coat protein gene located on RNA 3 (Accession number X58459.1) using the Oligo Explorer (v 1.1.2) software (Kuulasma, 2000). The characteristics of the primers are summarized in Table 3.1.

Table 3.1: Primers used for diagnostics of BMV

Primer	Sequence	Tm (°C)	Amplicon size
BMV_CP_F	5'-CAGGAACTGGTAAGATGACTC-3'	52.3	521 bp
BMV_CP_R	5'-CCTTACGTGCTCAACTTCTAG-3'	52.8	

3.1.1.1. Crude extraction of viral RNA

Initially, an optimized one-step RT-PCR was used to screen for BMV. First, 0.3 g of leaf tissue was ground in 2 ml extraction buffer (2 % [w/v] PVP-40, 0.2 % [w/v] bovine serum albumin [BSA], 0.05 % [v/v] Tween20, 1 % [w/v] $Na_2S_2O_5$, in carbonate buffer [0.159 % (w/v) Na_2CO_3, 0.293 % (w/v) $NaHCO_3$], pH 9.6). Of this homogenate, 8 µl was added to 50 µl GES buffer (0.1 M glycine NaOH [pH 9], 0.05 M NaCl, 0.001 M EDTA, 0.5 % [v/v] Triton X-100) and incubated at 95 °C for 10 minutes. It was then incubated on ice for 5 minutes, after which 2 µl of the reaction was used in the RT-PCR.

3.1.1.2. One-step RT-PCR

The RT-PCR reaction mix contained 1 x KAPA *Taq* Buffer A (KAPA Biosystems), 0.625 µM each of forward and reverse primer (IDT), 0.2 mM dNTP mix (Fermentas), 5 mM dithiothreitol (DTT), 10 U *Avian Myeloblastosis Virus* (AMV) reverse transcriptase (RT) (Fermentas), 1 U

KAPA *Taq* (KAPA Biosystems), 2.5 µl 5 x Cresol loading dye (30 % [w/v] sucrose; 125 mg cresol red dye) and was diluted to a final volume of 25 µl using Milli-Q® water.

The reaction was performed using the 2720 thermal cycler (Applied Biosystems) and cycling conditions included an initial step at 48 °C for 30 minutes, followed by 35 cycles of 94 °C for 30 seconds, annealing at 55 °C for 30 seconds and elongation at 72 °C for 30 seconds. The final extension was at 72 °C for 7 minutes.

The PCR products were resolved on a 1.5 % (w/v) TAE-agarose gel (2 M Tris, 1 M glacial acetic acid, 0.05 M Na_2EDTA, pH 8), stained with ethidium bromide (EtBr), at 110 V for 40 minutes. The gel was visualized using a Bio-Rad Gel Doc™ XR+ Molecular Imager®.

3.1.1.3. RNA extraction

RNA was extracted for a two-step RT-PCR using an adapted Cetyltrimethylammonium bromide (CTAB) extraction protocol (2 % [w/v] CTAB, 2.5 % [w/v] PVP-40, 100 mM Tris-HCL [pH 8], 2 M NaCl, 25 mM EDTA [pH 8] and 3 % [v/v] β-mercaptoethanol) (White *et al*., 2008). The extracted RNA was quantified on a NanoDrop™ 2000 spectrophotometer (Thermo Scientific).

3.1.1.4. Two-step RT-PCR

The extracted RNA was subjected to cDNA synthesis by mixing 250 ng of RNA, 0.25 µl of the reverse primer (IDT) to a final volume of 10 µl with Milli-Q® water. The mix was incubated at 65 °C for 5 minutes and subsequently on ice for 2 minutes. The reaction mix contained 5x AMV-RT buffer (Fermentas), 10 mM dNTP mix (Fermentas), 10 U AMV-RT and 10 µl of the previously incubated reaction was diluted to a final volume of 20 µl using Milli-Q® water. The reaction was performed using the 2720 thermal cycler (Applied Biosystems) and included an initial incubation at 50 °C for 30 minutes, followed by an incubation at 85 °C for 5 minutes.

The cDNA was used in a PCR with the reaction mix consisting of 2.5 µl cDNA, 20 µM forward primer (IDT), 20 µM reverse primer (IDT), 10 mM dNTP mix (Fermentas), 1 U KAPA *Taq* (KAPA Biosystems), 1 x KAPA *Taq* Buffer A (KAPA Biosystems), 2.5 µl 5 x Cresol loading dye (30 % [w/v] sucrose; 125 mg cresol red dye) and diluted to a final volume of 25 µl using Milli-Q® water. The cycling conditions included an initial denaturing step at 95 °C for 5 minutes, followed by 35 cycles of 95 °C for 30 seconds, 50 °C for 30 seconds and 72 °C for 30 seconds, and a final elongation at 72 °C for 7 minutes.

The PCR products were resolved on a 1.5 % (w/v) TAE-agarose gel stained with EtBr, at 110 V for 40 minutes.

3.1.2. Dot-blot

The infected material was screened for the presence BMV by means of a dot-blot by using BMV-specific antiserum, obtained from the Biopharming Research Unit (BRU) at the University of Cape Town (UCT).

First, the nitrocellulose membrane was equilibrated by dipping it in methanol for 2 seconds, reverse osmosis (RO) water for 5 minutes and phosphate buffered saline (PBS) (0.8 % [w/v] NaCl, 0.02 % [w/v] KCl, 0.144 % [w/v] Na_2HPO_4, 0.024 % [w/v] KH_2PO_4, pH 7.5) with 0.05 % (v/v) Tween20 added (PBS-T), for 5 minutes. 2 µl of the sample was dried on the membrane and the membrane was subsequently incubated in blocking buffer (PBS-T, 5 % [w/v] milk powder) for 2 hours on a shaker at 37 °C. The membrane was washed with PBS-T for 5 minutes, repeated three times and then incubated with the BMV antiserum (1:100 dilution for a stock of 50 mg/ml, PBS-T, 5 % [w/v] milk powder) for 1 hour at room temperature. The wash step was repeated and the membrane incubated with the anti-rabbit IgG alkaline phosphatase conjugate (Sigma-Aldrich®) for 1 hour at room temperature (1:30,000 dilution, PBS-T, 5 % [w/v] milk powder). The wash step was repeated and the membrane was incubated with 10 ml alkaline phosphatase (AP) (100 mM Tris [pH 9.5], 100 mM NaCl, 5 M $MgCl_2$), 66 µl NBT (75 mg/ml stock) and 33 µl BCIP (50 mg/ml stock) in the dark until a color change was observed.

3.2. Virus Purification

3.2.1. Inoculation and propagation

Nicotiana benthamiana was seeded and grown under standard greenhouse conditions for 6 weeks. BMV-infected source material was homogenized in inoculation buffer (30 mM K_2HPO_4, 50 mM glycine, 1 % [w/v] celite, 1 % [v/v] bentonite, pH 9.2) and the inoculum was rubbed on 4 leaves per plant. The virus was allowed to propagate for three weeks after which the leaf material was harvested and stored at -80 °C.

3.2.2. Purification

3.2.2.1. Purification method 1

BMV was purified from infected leaf material using a protocol adapted from Bujarski (1998). Unless otherwise specified, all centrifugation steps were performed at 10,000 x *g* using the Beckman Coulter™ Allegra™ X-22R Centrifuge (F0850 rotor) at 4 °C. First, the frozen leaf material was ground in a chilled mortar and pestle in 1 ml extraction buffer (0.5 M sodium acetate, 0.01 M acetic acid, 0.01 M $MgCl_2$, pH 5.2) per gram of tissue. The homogenate was emulsified with 0.2 ml chloroform per gram of tissue and subjected to centrifugation at 5,000 x *g* for 5 minutes. The supernatant was filtered through course filter paper and incubated on ice for 30 minutes with one-third volume 30 % (w/v) polyethylene glycol (PEG) 8000. The precipitate was collected by centrifugation for 10 minutes and the pellet dissolved in 0.2 ml storage buffer (0.05 M sodium acetate, 0.01 M acetic acid, 1 mM Na_2EDTA, 1 mM $MgCl_2$, pH 5.2) per gram of tissue. The solution was emulsified with 0.4 ml chloroform per 1 ml of the solution and subjected to centrifugation for 5 minutes. The pellet was resuspended in 0.2 ml storage buffer per gram of tissue on ice overnight. The resuspended solution was centrifuged for 10 minutes and the supernatant subsequently subjected to two rounds of differential centrifugation using a Beckman Coulter Optima L-100 XP ultracentrifuge (Type 35 rotor). First, the sample was centrifuged at 100,000 x *g* for 2 hours, then the pellet was resuspended in the storage buffer. Finally, this was centrifuged at 30,000 x *g* for 10 minutes. The supernatant was subjected to another round of differential centrifugation, and the virus stored at -80 °C.

3.2.2.2. Purification method 2

A second protocol, from Michel *et al*. (2004), was used to purify BMV from infected leaf material. All steps were carried out at 4 °C and centrifugation steps were performed at 10,000 x *g* using the Beckman Coulter™ Allegra™ X-22R Centrifuge (F0850 rotor). Frozen leaf material was homogenized in grinding buffer (0.2 M sodium acetate, 0.01 M Na_2EDTA, pH 4.8) in a 1:2 ratio using a blender. The homogenate was squeezed through three layers of cheesecloth and subjected to centrifugation for 15 minutes. The supernatant was stirred with 10 % (w/v) PEG 8000 overnight after which it was centrifuged for 10 minutes. The pellet was resuspended in storage buffer (0.1 M sodium acetate, 0.001 M Na_2EDTA, pH 5.2), at one-tenth of the initial buffer used, and subjected to centrifugation for 10 minutes. The supernatant was stirred with 15 % (w/v) PEG 8000 for 2 hours and subsequently centrifuged for 10 minutes. The pellet was resuspended in 1 ml storage buffer, centrifuged for 10 minutes

and the supernatant collected. The purified virus were further purified by ultracentrifugation at 160,000 x *g* for 2.5 hours using the Beckman Coulter Optima L-100 XP ultracentrifuge (Type 70Ti rotor). The samples were layered on a 40 % (w/v) sucrose cushion prior to centrifugation.

3.3. Bioconjugation

3.3.1. Fluorescent labelling

The glutamic acid residues on the exterior surface of the BMV coat protein were modified using the 1-Ethyl-3-(3-dimethylaminopropyl)carbodiimide (EDC) and copper(I)-catalyzed alkyne-azide cycloaddition (CuAAC), also known as “click”, chemistries. The protocol for this reaction was adapted from Bruckman and Steinmetz (2014).

For all reactions the following formula was used to calculate the volume (in µl) of reagents to add for the number of molecular equivalents in the reaction:

$$\frac{\left(\frac{VNP}{MW\ VNP} \times \#\ CP\ per\ VNP\right) \times Equivalents}{Stock\ concentration} \times 1000$$

In the formula, VNP represents the concentration of the virus used in the reaction; for all reactions a concentration of 2 mg/ml was used. The molecular weight is given by $MW\ VNP$ while $\#\ CP\ per\ VNP$ is the number of coat protein subunits of the virus. For BMV this is 4.6 x 10^6 g/mol and 180 respectively. $Equivalents$ is the number of molecular equivalents (eq) of the reagents to ensure a great enough excess for the reaction to occur. This value differs for each reagent. $Stock\ concentration$ represents the concentration of the stock solution of the reagents to be added to the reaction.

3.3.1.1. EDC reaction

The EDC reaction was utilized in order to modify the glutamic acid residues on the surface of the BMV coat protein in order to produce alkyne-BMV particles. These will subsequently be used to conjugate the fluorescent molecules.

BMV particles (at a concentration of 2 mg/ml) was added to 0.1 M 4-(2-hydroxyethyl)-1-piperazineethanesulfonic acid (HEPES) buffer (pH 7.4) and mixed by vortexing for 2 seconds. The solution was then incubated for 24 hours at room temperature while agitating with 120 eq propargylamine (0.1 M stock) (Sigma-Aldrich®), 30 eq EDC (0.1 M stock) (Sigma-Aldrich®) and 3 mg Hydroxybenzotriazole (HOBt) (Sigma-Aldrich®) in a final volume

of 1 ml. The EDC was added at the start of the reaction, another 30 eq after 6 hours and a final 30 eq after incubating for 18 hours, equating to a final amount of 90 eq in the reaction. The modified particles were purified by ultracentrifugation at 160,000 x *g* for 2.5 hours using the Beckman Coulter Optima L-100 XP ultracentrifuge (Type 70Ti rotor). The samples were layered on a 40 % (w/v) sucrose cushion prior to centrifugation. The pellet was resuspended in a minimal volume of sodium acetate buffer (0.1 M sodium acetate, 0.001 M Na_2EDTA, pH 5.2), where an approximate of 50 µl buffer per 1 ml reaction was used. These were the ultracentrifugation conditions used for all subsequent reactions.

3.3.1.2. CuAAC reaction

The CuAAC reaction was used to conjugate an azide-fluorophore to the alkyne-BMV in order to produce a fluorescently labelled VNP. All subsequent reactions were performed in the dark as the fluorescent molecule is light sensitive.

Alkyne-BMV (at a concentration of 2 mg/ml) was added to cold sodium acetate buffer and mixed by vortexing for 2 seconds. The solution was incubated on ice for 30 minutes with 5 eq Cy5-azide (0.01 M stock) (Sigma-Aldrich®), 10 µl aminoguanidine (0.2 M stock) (Sigma-Aldrich®), 10 µl ascorbic acid (0.2 M stock) (Fluka Analytical), 10 µl copper (II) sulfate pentahydrate (0.1 M stock) (Sigma-Aldrich®) and 10 % (v/v) dimethyl sulfoxide (DMSO) in a final volume of 1 ml. The reaction was inactivated by the addition of 10 µl EDTA (0.5 M stock) and incubated on ice for 5 minutes. The samples were subjected to centrifugation at 14 000 x *g* for 5 minutes using the Eppendorf Centrifuge 5415R (F45-24-11 rotor) to separate unbound fluorescent molecules. The modified particles were purified by ultracentrifugation.

The following changes were made to the aforementioned protocols in order to optimize the outcome of the conjugation. Initially two different EDC reactions were performed, one using sodium acetate as the buffer and the other using a HEPES buffer as suggested by the protocol, due to BMV not being stable at a pH above 6. For the CuAAC reaction a final volume of 500 µl instead of 1 ml was used for the reaction that utilized the sodium acetate buffer. For this reaction Alexa Fluor® 647 (Molecular Probes®) was used as the fluorescent molecule.

Three different reactions were performed, one with a final reaction volume of 3 ml instead of 1 ml, ten 1 ml reactions and one with a final reaction volume of 10 ml. The pellet for the 3 ml reaction was resuspended in 50 µl and the other two reactions in 100 µl sodium acetate

buffer. As before, Alexa Fluor® 647 (Molecular Probes®) was used as the fluorescent molecule.

The EDC reaction was optimized by attempting different conditions for the reactions. Reaction 1 used the normal protocol as described previously. In reaction 2 the HOBt was omitted. In reaction 3 the HOBt was omitted and EDC was added only at 6 hours and at 18 hours. In reaction 4 a lower stock concentration of the virus was used and hence a higher volume of virus was added to the reaction. In reaction 5 the lower stock concentration of the virus was added and the HOBt was omitted. In reaction 6 the HOBt was omitted and only one addition of EDC was made at the beginning of the reaction.

Purified BMV obtained from the Biopharming Research Unit (BRU) at the University of Cape Town (UCT) was used with our purified BMV to test the viability of the different purified stocks. Two different BMV stocks from BRU was used with one of our own stocks.

The EDC reaction was again performed in a final volume of 10 ml.

3.3.2. Peptide conjugation

The lysine residues on the exterior surface of the BMV coat protein was modified for conjugation of the targeting peptides, PKRGFQD-C (which will further on be referred to as Peptide 1) and SNTRVAP-C (which will further on be referred to as Peptide 2). Crosslinker molecules, with an amine group (-NH_2) on the one end and a sulfhydryl group (-SH) on the other end, was used to conjugate the peptide to the VNP. During this reaction the amine group was conjugated to the lysine residues, while the sulfhydryl group on the peptide was conjugated to the sulfhydryl group on the crosslinker. The protocol for this reaction was adapted from Chariou *et al.* (2015). For calculating the volume of the peptides, to add to the reaction, the previous formula was adjusted to the following:

$$\frac{\left(\frac{VNP}{MW\ VNP} \times \#\ CP\ per\ VNP\right) \times Equivalents}{Stock\ concentration}$$

The Cy5-labelled BMV (at a concentration of 2 mg/ml) was added to sodium phosphate buffer (0.1 M, pH 7.4) and mixed by vortexing. The reaction was incubated with 6 eq (0.250 M stock) (succinimidyl-[(*N*-maleimidopropionamido)-diethyleneglycol] ester) $SM(PEG)_n$ crosslinkers (Thermo Scientific) and 10 % (v/v) DMSO in a final volume of 1 ml for 2 hours on ice. Three different lengths of crosslinkers were used, namely $SM(PEG)_8$, $SM(PEG)_{12}$ and $SM(PEG)_{24}$. After the incubation, 6 eq of the peptide (10 x 10^{-6} M stock, 0.1 % [v/v] trifluoroacetic anhydride [TFAA] in MilliQ® water) (GL Biochem Shanghai Ltd)

was added and incubated overnight at 4 °C (this was later amended to room temperature on a shaker). The modified particles were subjected to ultracentrifugation.

The following changes were made to the aforementioned protocol in order to optimize the outcome of the conjugation. The reaction was performed on native, unconjugated BMV to test whether the peptides bind to BMV. Both Peptide 1 and Peptide 2 were used with crosslinker $SM(PEG)_{24}$. The reaction with the native, unconjugated BMV was repeated with crosslinkers $SM(PEG)_8$ and $SM(PEG)_{12}$ and both peptides to test whether the peptides bind to BMV.

As an alternative, the conjugation process was reversed, i.e. the peptide conjugation was performed first and the peptide-conjugated virus was subsequently conjugated with the fluorescent molecule.

During the peptide conjugation, the crosslinker was first incubated with the peptide for 2 hours on ice and the Cy5-BMV subsequently added and incubated overnight at room temperature while agitating.

3.3.3. Alternative conjugation method

An alternative conjugation method was used to conjugate both the peptide and the fluorescent molecule to the lysine residues (Chariou *et al*., 2015) on the coat protein of BMV.

BMV (at a concentration of 2 mg/ml) was incubated with 2 eq Cy™5 NHS Ester (GE Healthcare UK Limited), 2 eq $SM(PEG)_{24}$ and 10 % (v/v) DMSO in 100 mM potassium phosphate buffer (pH 7) in a final volume of 1 ml for 2 hours at room temperature while agitating. The modified BMV was subjected to ultracentrifugation. The pellet was resuspended in 100 mM potassium phosphate buffer and incubated with 20 eq Peptide 1 and Peptide 2 in a final volume of 1 ml overnight at room temperature while agitating. The modified BMV was purified by ultracentrifugation and the pellet resuspended in sodium acetate buffer.

3.4. Quality control

The modified VNPs were subjected to a variety of quality control steps to verify whether the conjugation methods were successful and have produced particles of high quality, as assessed by the purity and integrity of the particles.

3.4.1. Electron microscopy

Samples were visualized using electron microscopy to ensure that the particles were intact before proceeding with subsequent steps. 20 µl of the sample (between 0.5 and 1 mg/ml) was incubated on a carbon film 200 mesh copper grid (Electron Microscopy Sciences) for 10 minutes. The grids were washed with two drops of Milli-Q® water and dried on filter paper. The samples were subsequently stained with 2 % (w/v) uranyl acetate for 10 minutes and blotted dry on filter paper. The grids were allowed to dry in a desiccator (Nalgene™) before visualization.

3.4.1.1. Scanning transmission electron microscope (STEM)

The samples were visualized using the Zeiss MERLIN Field Emission Scanning Electron Microscope (FE-SEM) at the Electron Microbeam Unit of the Central Analytical Facility (CAF) at Stellenbosch University for initial analysis before proceeding with subsequent steps.

A Zeiss five-diode Scanning Transmission Electron Detector (Zeiss aSTEMA Detector) and Zeiss Smart SEM software were used to generate the STEM images. The beam conditions during analysis on the Zeiss MERLIN FE-SEM were set to 20 kV accelerating voltage, 250 pA probe current and a working distance of 4 mm. The images were acquired by using the orientated dark field (ODF) bright fields (BF) mode with the S1 and S2 diodes activated and the S3 diode inverted.

3.4.1.2. Transmission electron microscope (TEM)

Some of the samples were submitted to the Electron Microscope Unit (EMU) at The Centre for Imaging and Analysis at the University of Cape Town (UCT). The negatively stained samples were visualized using a Tecnai F20 FEGTEM operating at 200 kV and the images were obtained using a Gatan US4000 digital camera controlled by the Digital Micrograph software suite.

3.4.2. Spectrophotometry

The samples were analyzed using the Nanodrop 2000 spectrophotometer (Thermo Scientific) to assess the concentration and purity of the particles after conjugation. The absorbance at 260 nm was used to calculate the concentration of the samples and the 260/280 ratio indicated the level of purity. The number of fluorescent molecules conjugated to the particles could also be calculated by using the absorbance of the fluorescent molecules at 647 nm as well as the absorbance of the virus particles at 260 nm. The following formula was used to calculate the number of bound fluorescent molecules:

$$\frac{A\,647}{\varepsilon\,fluorophore} \times \frac{MW\,VNP}{\frac{A\,260}{\varepsilon\,VNP}}$$

Here, $A\,647$ represents the absorbance of the fluorescent molecule and $A\,260$ the absorbance of the virus particle. The $\varepsilon\,fluorophore$ represents the extinction coefficient of the fluorescent molecules. For the Alexa Fluor® 647 fluorophore this value is 239,000 and for the Cy5-azide this value is 250,000. The $\varepsilon\,VNP$ represents the extinction coefficient of the virus particle, which for BMV is 5.15, and the $MW\,VNP$ represents the molecular weight of the virus particle. For BMV this value is 4.6 x 10^6 g/mol.

3.4.3. SDS-PAGE

The modified BMV particles were subjected to polyacrylamide gel electrophoresis to assess whether the peptides were successfully conjugated to the particles. An amount of between 20 and 50 µg sample was loaded into each well, in the case where enough sample was obtained during the conjugation process. In the case where less than 20 µg was available after conjugation, a maximum of 37.5 µl was used. The samples were first denatured in a 4x Laemmli sample buffer (Bio-Rad) in a ratio of 1:4 by incubating for 5 minutes at 95 °C. The samples were loaded onto a 4-15 % Mini-PROTEAN® TGX™ Precast Gel (Bio-Rad) along with a Precision Plus Protein™ Standard (Bio-Rad). The samples were allowed to separate on the gel for 1 hour at 120 V. The gel was visualized using the Bio-Rad Gel Doc™ XR+ Molecular Imager® and the images were analyzed using the Image Lab™ Software (*Image Lab*, 2014).

3.4.4. MALDI-TOF MS

The modified particles were assessed by means of Matrix-Assisted Laser Desorption/Ionization Time-of-Flight Mass Spectrometry (MALDI-TOF MS) to verify whether the peptides were conjugated to the particles. The samples were analyzed at the Proteomics Research & Services Unit in the Department of Biotechnology at the University of the Western Cape (UWC). All the samples were prepared according to the protocol described by Bruckman and Steinmetz (2014) prior to analysis.

The measurements were performed using an UltrafleXtreme MALDI ToF/ToF system (Bruker Daltonics) with instrument control through Flex control 3.4. Approximately 2 µl of the prepared sample was spot onto a MTP 384 MALDI target plate and allowed to dry. The samples were ionized with a 337 nm laser and the spectra were acquired in a linear positive

mode at 17 kV using 500 laser shots per spectrum. A scan range of m/z = 0 – 35,000 Da was used. The spectra was internally calibrated using a protein mixture (Insulin $[M+H]^+$ 5,734.51 Da, Cytochrome C $[M+H]^+$ 12,360.97 Da, Cytochrome C $[M+2H]^{2+}$ 6,180.99 Da, Myoglobin $[M+H]^+$ 16,952.30 Da, Trypsinogen $[M+H]^+$ 23,982 Da) and the spectra were automatically processed using the FlexAnalysis Software (Bruker Daltonics) for data interpretation.

3.5. Cell uptake experiments

3.5.1. Cell culture

3.5.1.1. Prostate cancer cell lines

Three different prostate cell lines was used to assess the VNPs *in vitro*. The first cell line was a normal prostate cell line, PNT2. This cell line was derived from prostate epithelial cells and was immortalized by transfection with *Simian virus* 40 (Berthon *et al*., 1995). The second cell line, VCaP, is representative of an androgen dependent (early stage cancer) cell line. This cell line was derived from a metastatic site at the lumbar vertebrae in a prostate cancer patient (Korenchuk *et al.*, 2001). The third cell line, PC3, represents late stage cancer in which the tumours have become androgen independent. This cell line was derived from a adenocarcinoma metastatic to bone tissue (Kaighn *et al*., 1979).

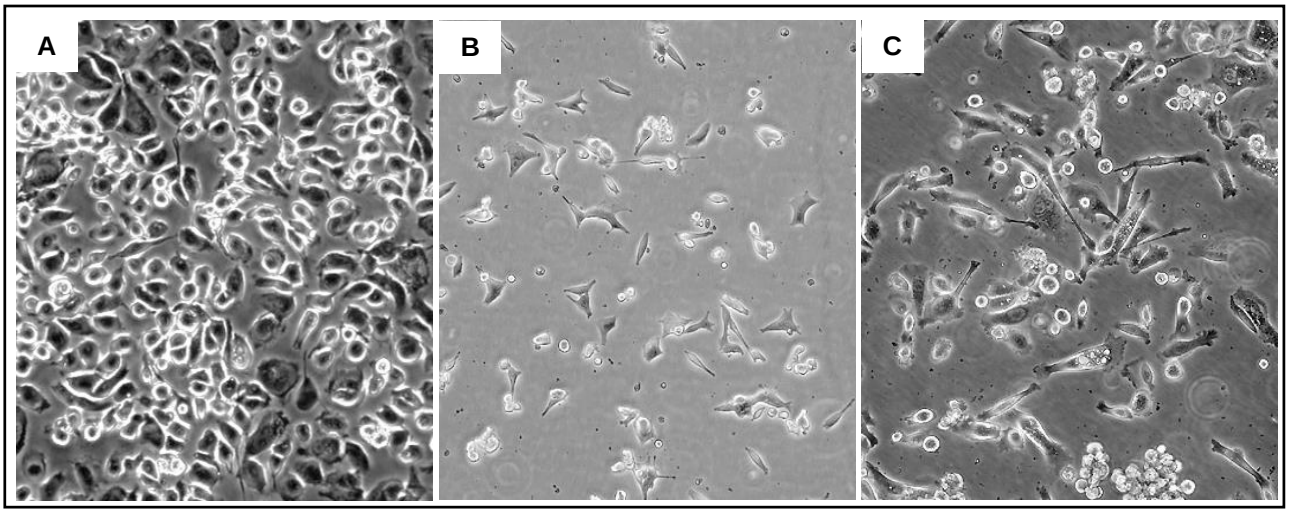

Figure 3.1: Micrographs of the three different prostate cell lines, **(A)** PNT2, **(B)** VCaP, **(C)** PC3. Obtained from http://www.phe-culturecollections.org.uk/ and https://www.atcc.org.

3.5.1.2. Culturing of cells

PNT2, PC3 and VCaP cell lines were obtained from the Biochemistry Department at Stellenbosch University. PNT2 and PC3 cells were maintained in Advanced Roswell Park

Memorial Institute (RPMI) 1640 reduced serum medium (Gibco®, Life Technologies), supplemented with 1 x GlutaMAX™ (Gibco®, Life Technologies), 1 % (v/v) Gentamicin (Gibco®, Life Technologies) and 6 % (v/v) fetal bovine serum (FBS) Superior (Biochrom GmbH). VCaP cells were maintained in Dulbecco's Modified Eagle Medium (DMEM) + GlutaMAX™ (Life Technologies), supplemented with 1 % (v/v) Gentamicin and 10 % (v/v) FBS Superior.

Cells were stored in a liquid nitrogen tank, in the appropriate medium supplemented with 10 % (v/v) DMSO. Cells were thawed and added to a 25 cm^2 flask with pre-warmed media and cultured at 37 °C in an ESCO CelCulture CO_2 incubator within a humidified atmosphere and 5 % CO_2. The medium was initially refreshed 24 hours after it was first seeded into a new flask. Thereafter the medium was refreshed after every 48 hours.

Cells were subcultured by first removing old medium and washing the bottom of the flask with Dulbecco's Phosphate Buffered Saline (DPBS), without $CaCl_2$ and $MgCl_2$, (Gibco®, Life Technologies). The cells were incubated with pre-warmed (0.25 %) Trypsin-EDTA (Life Technologies) for a maximum of 10 minutes at 37 °C. The flasks were visualized under the Olympus IX51 inverted light microscope to verify whether they have dissociated from the bottom of the flask. The trypsin was inactivated by adding twice the volume of medium and subjected to centrifugation at 1,500 rpm using a IEC Centra® CL2 centrifuge (IEC 236 rotor). The pellets were resuspended in 1 ml media and seeded at a 1:3 ratio into 75 cm^2 flasks containing pre-warmed media. Cells were maintained at 80 % confluency.

3.5.2. Flow cytometry

The cells were removed from the flasks similarly to what was described previously, with the exception of cell dissociation buffer (Gibco®, Life Technologies) used as opposed to trypsin. The cells were incubated at 37 °C for a maximum of 30 minutes. The cell dissociation buffer is enzyme-free which keeps the receptors on the surface of the cells intact for uptake experiments. After centrifugation the pellets were again resuspended in 1 ml of the appropriate medium and cells were counted using in an Invitrogen™ Countess™ Automated Cell Counter. For the counting, 10 µl of the cells were added to 10 µl Trypan blue stain (0.4 %) (Life Technologies) and 10 µl of the mixture was loaded onto a Countess™ cell counting chamber slide (Invitrogen) which was used in the cell counter. A total of 500,000 cells were seeded into a 96 well v-bottom plate and medium was added to a final volume of 200 µl where needed.

Cells were treated with particles in triplicate (three biological repeats, each with three technical repeats) and a negative control was left untreated, also with three biological repeats. The number of particles added per well was calculated using the following formula:

$$g\ VNP\ per\ cell = \frac{100{,}000}{6.022x10^{23}} \times 4.6 \times 10^{6} = 7.638 \times 10^{-13} g\ BMV\ per\ cell$$

Here, $100{,}000$ refers to the number of VNPs added per cell. $6.022x10^{23}$ is Avogadro's constant which is equivalent to the number of molecules in one mole. The molecular weight of the VNP is given by 4.6×10^{6}.

Each well has 500,000 cells, therefore 7.638 x 10^{-13} g of BMV per cell multiplied by 500,000 equals 3.82 x 10^{-7} g BMV per well. This translates to 0.382 µg of BMV per well. A stock solution of 38 µg/ml was made up in order for 10 µl BMV to be added to each well for a total 0.382 µg BMV per well. The plates were incubated with the particles for 2 hours at 37 °C, covered with foil.

After incubation, the cells were subjected to centrifugation at 1500 x *g* for 5 minutes using the Eppendorf Centrifuge 5430 R (5430/R rotor). The pellets were resuspended in 200 µl FACS buffer (0.1 ml 0.5 M EDTA, 0.5 ml FBS, 1.25 ml 1 M HEPES pH 7, in a final volume of 50 ml in 1 x PBS). This step was repeated twice and the cells were then fixed in 200 µl of 2 % (v/v) paraformaldehyde (in FACS buffer) for 10 minutes. The cells were again subjected to centrifugation and the wash steps in FACS buffer was repeated. The cells were stored in FACS buffer at 4 °C, for a maximum of 24 hours, until flow cytometry.

The samples were analyzed using the BD FACSAria™ Cell Sorter (Becton Dickinson) at the Fluorescence Microscopy Unit of the CAF at Stellenbosch University. The analysis was performed by collecting a minimum of 20,000 cells at a flow rate of 2 using the 633 nm laser. Fluorescence intensity signal was measured using the geometric mean on the intensity histogram and data was obtained using the BD FACSDiVa v6.1.3 Software. The data was subsequently analyzed by using the FlowJo™ (*FlowJo*, 2016) and GraphPad Prism Software (*GraphPad Prism*, 2012). The percentage uptake of the VNPs was calculated by the BD FACSDiVa v6.1.3 Software from the number of positive events recorded.

3.5.3. Fluorescence microscopy

The cells were prepared and counted using the same protocol for flow cytometry (Section 3.5.2, pages 32-33). A total of 500,000 cells were seeded onto coverslips in a 6 well flat bottom plate. Prior to adding the cells, the coverslips were sterilized by washing with 70 %

(v/v) ethanol three times and subsequently with PBS three times. The coverslips were covered by adding 1 ml of the appropriate medium into each well. The cells were allowed to adhere and grow on the coverslips overnight.

Particles were added in triplicate (with three biological repeats), but in some cases only one biological sample was treated with the particles. One negative control was left untreated. The same formula was used to calculate the number of particles to add to each well, with a total of 0.382 µg BMV added per well. The cells were incubated with the particles for 4 hours at 37 °C, covered with foil.

After the incubation, the cells were washed three times with PBS and then fixed at room temperature for 5 minutes with 1 ml of the fixative (2.94 ml PBS [1 x stock], 60 µl 2.5 % [v/v] glutaraldehyde, 2 ml paraformaldehyde [4 % (w/v) stock]). The cells were again washed three times with PBS and stained with DAPI (Sigma-Aldrich®) in a ratio of 1:500 (300 mM stock) in PBS for 15 minutes. The cells were washed with PBS three times for 5 minutes per wash step and subsequently stained with wheat germ agglutinin (WGA) Alexa Fluor® 488 conjugate (Life Technologies) in a ratio of 1:500 (1 mg/ml stock) in PBS for 45 minutes. The cells were washed with PBS three times for 5 minutes per wash step. The cover slips were then mounted onto microscope slides with the aiding of Fluoroshield™ histology mounting medium (Sigma-Aldrich®) and the edges of the coverslips were sealed using clear nail polish. The slides were kept in the dark at 4 °C until visualization.

The microscope images were obtained using the Carl Zeiss Laser Scanning Microscope (LSM780) ELYRA S.1 (Carl Zeiss) at the Fluorescence Microscopy Unit of the CAF at Stellenbosch University. Cells were imaged using the LCI Plan-Apochromat 63x/1.4 Oil DIC M27 objective and detected by means of a 633 nm, 488 nm and a diode 405 nm CW/PS laser. Images were processed using the Zen 2.1 (black) Software (Zeiss) (*Zen 2.1 (black)*, 2015).

Chapter 4

Results and discussion

4.1. Diagnostics

4.1.1. RT-PCR

In order to amplify the coat proteins, RT-PCR was performed. The infected *N. benthamiana* (Figure 4.1, panel A, lane 2) received from DAFF and the *N. benthamiana* inoculated with the virus (Figure 4.1, panel A, lane 3) were screened. The one-step RT-PCR did not amplify the expected amplicon (Figure 4.1, panel A). We therefore extracted RNA and rather did a two-step reaction; an initial cDNA synthesis followed by the PCR. Good quality RNA was extracted and BMV was positively diagnosed with the RT-PCR (Figure 4.1, panel B). The band corresponds to the expected amplicon size of 521 bp. This result indicates that the primers successfully amplified the coat protein of BMV. The inoculated *N. benthamiana* was also positively diagnosed after sufficient propagation.

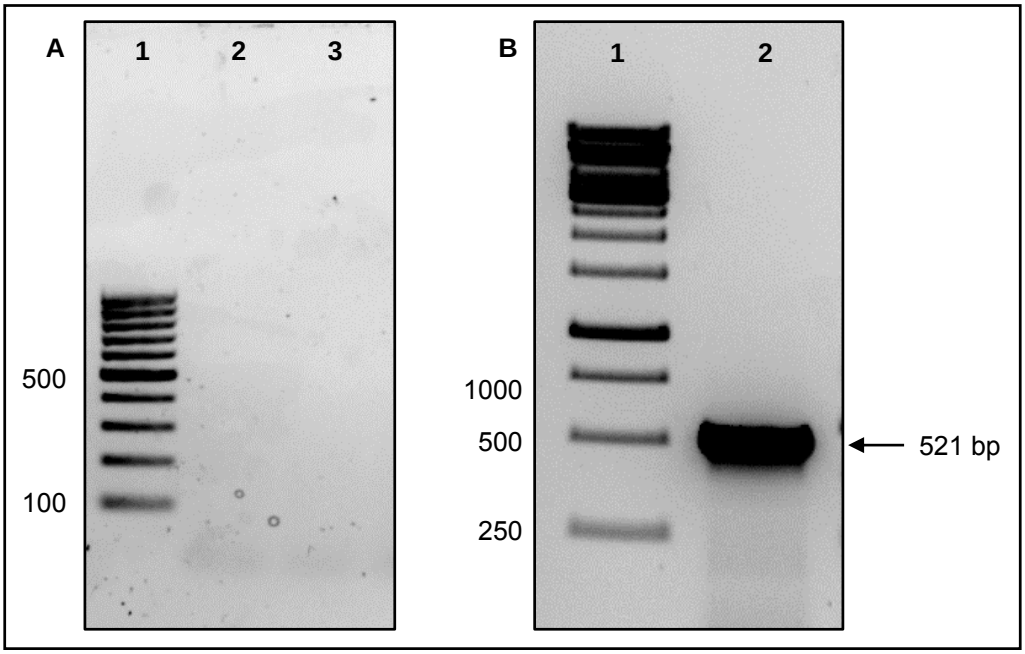

Figure 4.1: RT-PCR of BMV infected source material. **(A)** 1.5 % TAE-agarose gel with ethidium bromide staining, of one-step RT-PCR amplicons generated using BMV primers. Lane 1: O'GeneRuler™ 100 bp Plus DNA Ladder (Thermo-Scientific), Lane 2: Infected *N. benthamiana*, Lane 3: Inoculated *N. benthamiana*. **(B)** 1.5 % TAE-agarose gel with ethidium bromide staining, of two-step RT-PCR amplicons generated using BMV primers. Lane 1: GeneRuler™ 1 kb ladder (Thermo-Scientific), Lane 2: Amplicon.

4.1.2. Dot-blot

An immuno dot-blot was performed in order to diagnose BMV in the infected leaf material. BMV was positively diagnosed by means of the immuno dot-blot. This is presented as dark spots in Figure 4.2. Purified BMV samples were obtained from the Biopharming Research Unit (BRU) at the University of Cape Town (UCT) and were used as a positive control (Figure 4.2, 2). The negative control (Figure 4.2, 1) represents uninfected *N. benthamiana* leaves that were ground in sodium acetate buffer and blotted on the membrane to test for any nonspecific binding of the antibody. From Figure 4.2 we observe that a faint spot is present at the negative control, however, the BMV samples are much darker which indicates true binding of the antibody. From this analyses we conclude that we successfully infected *N. benthamiana* with BMV.

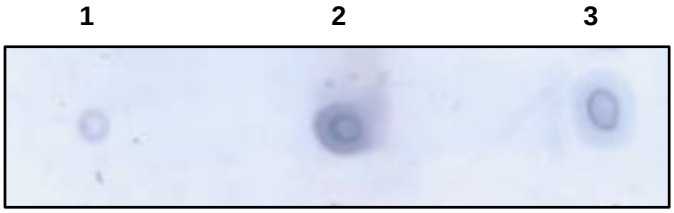

Figure 4.2: Dot-blot of purified BMV. 1) Negative control, 2) BMV positive control, 3) Purified BMV

4.2. Virus Purification

4.2.1. Inoculation and propagation

BMV was propagated in *N. benthamiana* in order to increase the virus concentration. Characteristic mosaic and chlorotic symptoms appeared in *N. benthamiana* after propagating for two weeks (Figure 4.3), which is consistent with literature (Lane, 1974) . The leaves were harvested after three weeks to ensure high virus titer in the infected plants.

Figure 4.3: *N. benthamiana* infected with BMV. Characteristic symptoms are visible.

4.2.2. Purification

BMV was purified from the leaf material in order to produce pure particles for bioconjugation experiments. The purification of BMV using method 1 was unsuccessful (Figure 4.4, panel A). The virus particles were present in the aqueous phase during the chloroform step and not in the pellet as indicated by the protocol. The second purification method, which utilized a longer PEG precipitation incubation time and omitted a chloroform step, could successfully purify BMV from the infected leaf material. The purified particles could be visualized on the TEM as is shown on Figure 4.4, panel B. Their average diameter was found to be 28 nm, as expected.

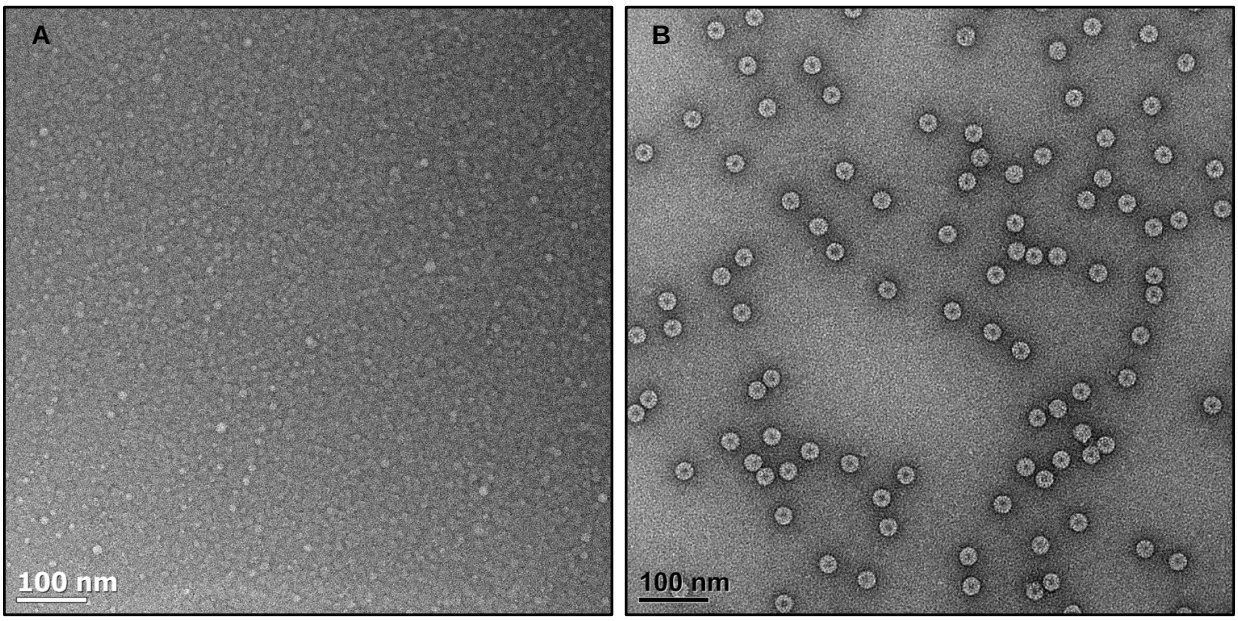

Figure 4.4: Electron micrograph of purified BMV. **(A)** BMV purified using method 1, no particles are present. **(B)** BMV purified using method 2. The average diameter of the particles is 28 nm.

Table 4.1 indicates the protein concentrations and absorbance ratios of 260/280 for both methods. The protein concentration indicates that method 2 is more efficient for purifying BMV, since the yield is twice as high. The absorbance ratio of 260/280 is used to assess the purity and integrity of the virus (Yildiz *et al*., 2012) and this also indicates a successful purification. For BMV a 260/280 absorbance ratio of 1.7 indicates pure and intact virus particles (Bockstahler and Kaesberg, 1962; Yildiz *et al*., 2012). The electron micrograph also confirmed that the particles were intact (Figure 4.4, B). This was therefore the preferred method for purification of BMV from *N. benthamiana* for the remainder of the study. The purifications yielded an average of 800 mg purified particles per kilogram of leaf material and had a 260/280 ratio of 1.73 (Table 4.1, Sample: Purified BMV).

Table 4.1: Spectrophotometer results for purified BMV produced using two different purification methods

Sample	Protein concentration (mg/ml)	260/280
BMV from method 1 (aqueous layer)	3.597	1.55
BMV from method 2	10.274	1.74
Purified BMV	80.155	1.73

4.3. Bioconjugation

BMV was labeled with a fluorescent molecule in order to facilitate the movement of the VNPs *in vitro*. It was also conjugated with a targeting peptide with the aim of increasing the internalization into the cells. Initially two different buffers were used in the EDC reaction, namely a sodium acetate buffer and a HEPES buffer. Since BMV is usually not stable at a pH higher than 6 (Pfeiffer and Hirth, 1975), we decided that the low pH sodium acetate buffer may be more suitable for the virus. The preparation from the fluorescent labeling did not indicate a significant difference in yield or integrity for the two different buffers (Table 4.2). However, a total of 8 fluorescent molecules were found to be bound for the HEPES buffer, whereas for the sodium acetate buffer no molecules were bound. The STEM analysis[3] indicated that the sodium acetate buffer produced particles that were not intact, while the particles from the HEPES buffer were all intact. These results suggest that the HEPES

[3] These images will not be presented here due to low resolution of the images produced. The STEM analysis was performed to validate the integrity of the particles before proceeding with subsequent steps.

buffer, with a pH of 7.4, is necessary to facilitate the reaction as suggested by the protocol from Bruckman and Steinmetz (2014).

Table 4.2: Virus concentration, based on the absorbance at 260 nm, for EDC and CuAAC reaction utilizing both sodium acetate and HEPES buffer

Sample	Concentration (mg/ml)	260/280	Fluorescent molecules bound
BMV-Alkyne (sodium acetate buffer)	0.83	1.42	N/A*
BMV-Alkyne (HEPES buffer)	1.18	1.38	N/A*
BMV-AlexaFluor 647 (sodium acetate buffer)	0.62	1.73	<1
BMV-AlexaFluor 647 (HEPES buffer)	0.71	1.68	8

*N/A – not applicable to this sample

We proceeded with an upscale reaction as a larger volume of the preparation was needed for subsequent conjugations. However, a larger reaction volume (10 ml) resulted in precipitation and the absorbance ratio was lower when compared to the 1 ml reaction volume (Table 4.3). The 1 ml reaction volume produced a higher yield, and more intact particles were obtained. For this reason, we proceeded with 1 ml reaction volumes, which were combined during the ultracentrifugation step.

Table 4.3: Spectrophotometer results for the concentration, purity and fluorescent labeling efficiency of BMV-Alkyne and BMV-AlexaFluor 647 using either a 10 ml, or multiple 1 ml reactions.

Sample	Concentration (mg/ml)	260/280	Fluorescent molecules bound
BMV-Alkyne (10 ml)	53.979	1.03	N/A*
BMV-Alkyne (1 ml)	61.413	1.2	N/A*
BMV-AlexaFluor 647 (1 ml)	0.16	1.39	120

*N/A – not applicable to this sample

The results for the CuAAC reaction using the BMV-Alkyne from the separate 1 ml reactions were favorable (Table 4.3). This sample was used for an initial passive uptake experiment in the different cell lines (Figures 4.17 and 4.18). We proceeded with another EDC and

CuAAC reaction, and the resulting preparation was used in a peptide conjugation experiment. The spectrophotometer results for these preparations were favorable (Table 4.4). The first peptide conjugation produced intact particles as indicated by the STEM visualization.

Table 4.4: Virus concentrations, purity and fluorescent labeling efficiency, based on the absorbance at 260 nm, of BMV-Alkyne, BMV-AlexaFluor 647 and peptide conjugated BMV

Sample	Concentration (mg/ml)	260/280	Fluorescent molecules bound
BMV-Alkyne	68	1.46	N/A*
BMV-AlexaFluor 647	34.66	1.68	35
BMV-SM$(PEG)_8$-P1	0.22	1.63	35
BMV-SM$(PEG)_{12}$-P1	0.34	1.71	35
BMV-SM$(PEG)_{24}$-P1	0.25	1.61	35

*N/A – not applicable to this sample

The SDS-PAGE gel (Figure 4.5) shows the separation of the different samples. An amount of 10 µg per sample was loaded onto the gel. We expected to see two bands, which indicate that the reaction was successful. The bottom band corresponds to the coat protein of BMV (Figure 4.5, panel A, lane 2 and panel B, lane 5), which is 20 kDa in size. The top band represents the BMV-peptide conjugate, which shows a size increase and therefore migrates slower on the gel. The bands are very light as only 10 µg could be loaded onto the gel.

The coat protein band for BMV is lower than the expected 20 kDa size. It has previously been demonstrated that the native T=3 conformation of BMV is able to transform into a T=1 conformation at pH higher than 7, and a high salt concentration. This T=1 BMV has a molecular weight of approximately 16,450 Da, as confirmed by SDS-PAGE and mass spectrometry (Larson *et al*., 2005; Lucas *et al*., 2001). This could indicate that the native BMV particles transform into T=1 particles in the presence of the sample buffer.

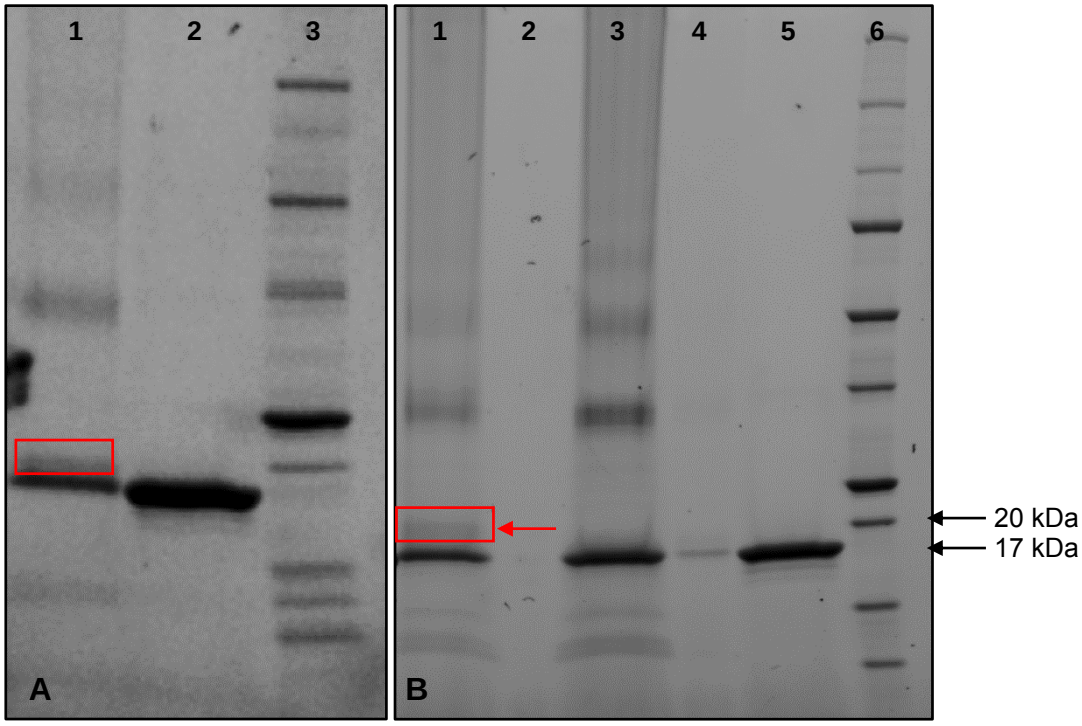

Figure 4.5: SDS-PAGE gel of BMV-AlexaFluor® 647 conjugated with Peptide 1 and three different crosslinkers, run at 120 V. **(A)** Lane 1: BMV-SM(PEG)$_8$-P1, conjugate indicated by the red block, Lane 2: Unmodified BMV, Lane 3: Precision Plus Protein™ Standard Ladder. **(B)** Lane 1: BMV-SM(PEG)$_{24}$-P1, conjugate indicated by the arrow and red block, Lane 2: BMV-SM(PEG)$_{24}$, Lane 3: BMV-SM(PEG)$_{12}$-P1, Lane 4: BMV-SM(PEG)$_{12}$, Lane 5: Unmodified BMV, Lane 6: Precision Plus Protein™ Standard Ladder

In panel B, lanes 2 and 4 correspond to only the BMV-crosslinker conjugate, before the peptide was added to the reaction.[4] Only the BMV-SM(PEG)$_{24}$-P1 reaction (panel B, lane 1) indicated a second band, as indicated by the red block and arrow. This shows that the peptide is bound to the coat protein. These samples were used for an initial active uptake experiment in all three cell lines (Figures 4.19 and 4.20).

Due to a limited volume of the preparation that was available, repeated upscale reactions were required. However, in the 1 ml EDC reaction, a precipitation was observed. This was unexpected as it previously only occurred when a reaction volume greater than 1 ml was used. We first performed a 1 ml CuAAC reaction to validate whether the precipitation affected the fluorescent labeling, and then proceeded with the upscale reaction. The results were favorable, except for the low absorbance ratio and lower yield of the upscale reaction (Table 4.5).

[4] During the reaction 10 µl of the reaction was stored before the peptide was added to the reaction, but this was too little to visualize on the gel.

We investigated whether the purified stock of BMV led to the precipitation and therefore included two purified BMV stocks obtained from UCT (BMV 1 and BMV 2). The results (Table 4.5) indicated that our own purified BMV had comparable fluorescent binding and therefore we conclude that this is not the cause of the precipitation.

Table 4.5: Virus concentrations, based on the absorbance at 260 nm, of BMV-Alkyne and BMV-Cy5 for various optimization steps

Sample	Concentration (mg/ml)	260/280	Fluorescent molecules bound
BMV-Alkyne	94.3	1.28	N/A*
BMV-Cy5 (1 ml)	3.322	1.68	60
BMV-Cy5 (upscale)	3.761	0.89	28
BMV-Alkyne (our sample)	18.252	1.23	N/A*
BMV-Alkyne (BMV 1)	14.425	1.07	N/A*
BMV-Alkyne (BMV 2)	19.423	1.22	N/A*
BMV-Cy5 (our sample)	0.594	1.62	41
BMV-Cy5 (BMV 1)	0.478	1.56	47
BMV-Cy5 (BMV 2)	0.433	1.59	49

*N/A – not applicable to this sample

We performed another scaled-up reaction with good yield and a total of 32 fluorescent molecules bound. The particles were visualized on a TEM to ensure that they were intact before proceeding with subsequent reactions.[5] The particles produced from the EDC (Figure 4.6, panel A) and CuAAC reactions (Figure 4.6, panel B) were intact.

The peptide conjugations from this preparation were successful with regards to yield and absorbance ratio (Table 4.6). The particles were all intact (Figure 4.6, panels C-F and panel H), with the exception of BMV-SM(PEG)$_{12}$-P2 (Figure 4.6, panel G). The SDS-PAGE gel indicated a second band for BMV-SM(PEG)$_{24}$-P1 (Figure 4.7, lane 5) and BMV-SM(PEG)$_{24}$-P2 (Figure 4.7, lane 8), as shown by the red blocks and red arrows. This indicates that the

[5] The TEM does not have a high enough resolution power to indicate the modifications on the surface of the virus coat protein and therefore the images are only an indication of the integrity of the particles.

peptide is bound to BMV. These samples were used in uptake experiments in the all the cell lines (Figures 4.21, 4.22 and 4.27).

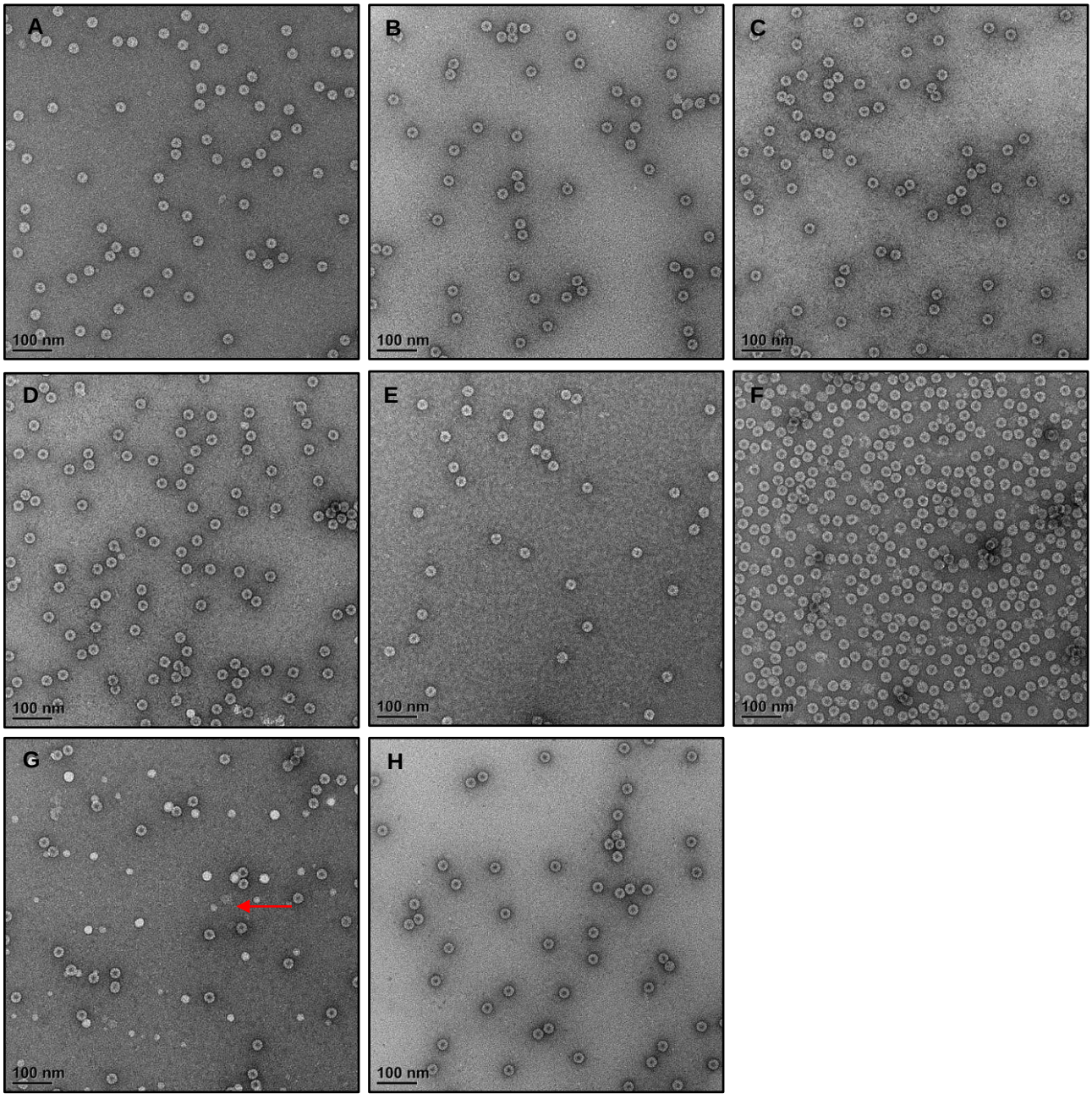

Figure 4.6: Electron micrograph of **(A)** BMV modified using the EDC reaction, **(B)** BMV conjugated with the Cy5 fluorescent molecule, **(C)** BMV-Cy5 conjugated with $SM(PEG)_8$ and Peptide 1, **(D)** BMV-Cy5 conjugated with $SM(PEG)_{12}$ and Peptide 1, **(E)** BMV-Cy5 conjugated with $SM(PEG)_{24}$ and Peptide 1, **(F)** BMV-Cy5 conjugated with $SM(PEG)_8$ and Peptide 2, **(G)** BMV-Cy5 conjugated with $SM(PEG)_{12}$ and Peptide 2, the red arrow indicates particles that are not intact, **(H)** BMV-Cy5 conjugated with $SM(PEG)_{24}$ and Peptide 2

Table 4.6: Virus concentrations, based on the absorbance at 260 nm, for BMV modified with the Peptide 1 and 2 using two different BMV-Cy5 samples

Sample	Concentration (mg/ml)	260/280
BMV-SM(PEG)$_8$-P1	0.831	1.66
BMV-SM(PEG)$_{12}$-P1	0.810	1.7
BMV-SM(PEG)$_{24}$-P1	0.326	1.65
BMV-SM(PEG)$_8$-P2	0.965	1.56
BMV-SM(PEG)$_{12}$-P2	1.254	1.66
BMV-SM(PEG)$_{24}$-P2	1.468	1.63

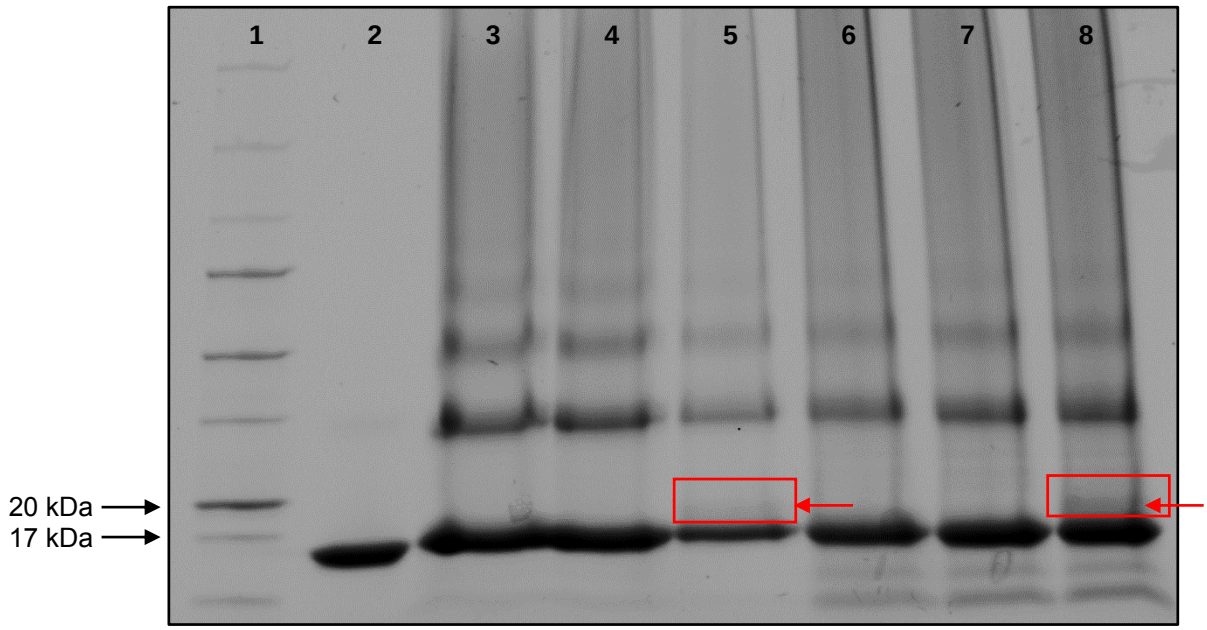

Figure 4.7: SDS-PAGE gel of BMV-Cy5 conjugated with Peptide 1 and 2 and three different crosslinkers, run at 120 V. Lane 1: Precision Plus Protein™ Standard Ladder, Lane 2: Unmodified BMV, Lane 3: BMV-SM(PEG)$_8$-P1, Lane 4: BMV-SM(PEG)$_{12}$-P1, Lane 5: BMV-SM(PEG)$_{24}$-P1, conjugate indicated by the arrow, Lane 6: BMV-SM(PEG)$_8$-P2, Lane 7: BMV-SM(PEG)$_{12}$-P2, Lane 8: BMV-SM(PEG)$_{24}$-P2, conjugate indicated by the arrow

The samples were also analyzed using MALDI-TOF MS. The two peptides were found to be intact with their expected sizes of 950.08 Da and 846.96 Da, while the size of BMV was determined to be 20,284 Da, as expected. In Figure 4.8, an approximate size of 20,380 Da can be observed for BMV-Cy5, as indicated by the largest peak. A second peak is observed

for BMV-SM(PEG)$_{12}$-P1 (Figure 4.8, panel B), BMV-SM(PEG)$_{24}$-P1 (Figure 4.8, panel C), BMV-SM(PEG)$_{8}$-P2 (Figure 4.8, panel D) and BMV-SM(PEG)$_{12}$-P2 (Figure 4.8, panel E).

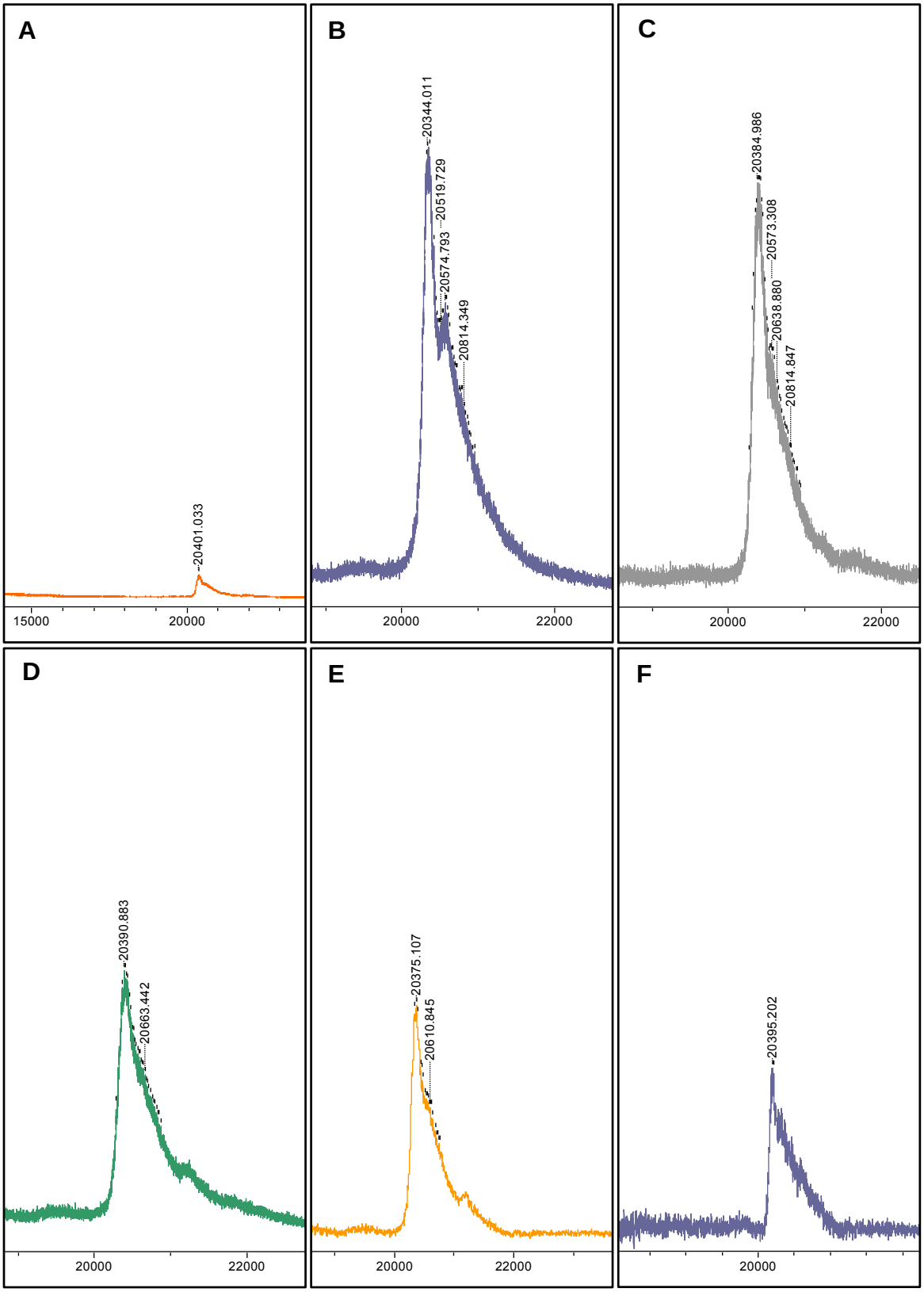

Figure 4.8: MALDI-TOF MS analysis of BMV-Cy5 conjugated with **(A)** SM(PEG)$_{8}$-P1, **(B)** SM(PEG)$_{12}$-P1, **(C)** SM(PEG)$_{24}$-P1, **(D)** SM(PEG)$_{8}$-P2, **(E)** SM(PEG)$_{12}$-P2, **(F)** SM(PEG)$_{24}$-P2

This is contradictory to the result from SDS-PAGE (Figure 4.7), which showed that only conjugates BMV-SM(PEG)$_{24}$-P1 and BMV-SM(PEG)$_{24}$-P2 was successfully conjugated with the peptides.

We confirmed the successful conjugation of BMV with Peptide 1 and Peptide 2 by using the crosslinker SM(PEG)$_{24}$ (Figure 4.9). Unmodified BMV was used and the presence of the peptide conjugate is indicated by the second band.

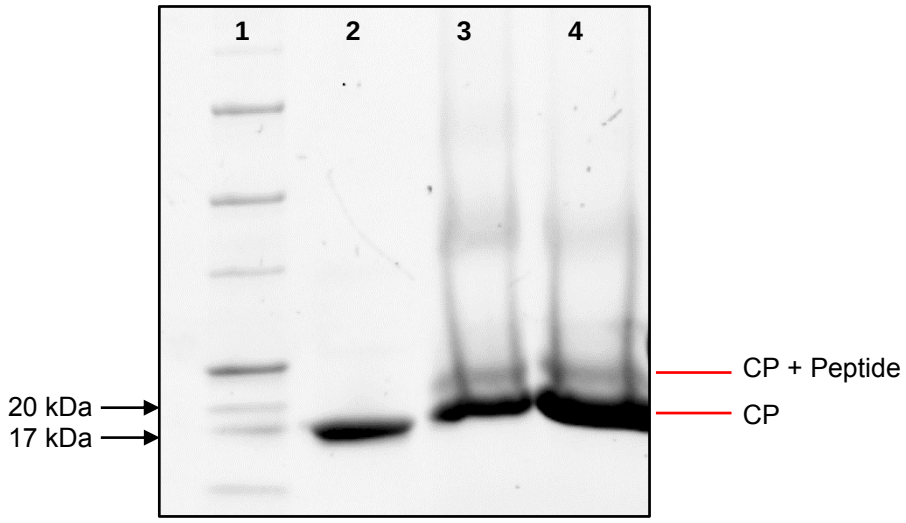

Figure 4.9: SDS-PAGE gel of native BMV conjugated with Peptide 1 and 2 and crosslinker SM(PEG)$_{24}$, run at 120 V. Lane 1: Precision Plus Protein™ Standard Ladder, Lane 2: Unmodified BMV, Lane 3: BMV-SM(PEG)$_{24}$-P1, Lane 4: BMV-SM(PEG)$_{24}$-P2

In a following EDC reaction, no precipitation was observed for the 1 ml reaction volume.[6] The particles for the EDC modification (Figure 4.10, panel A) and fluorescent labeling (Figure 4.10, panel B) were intact. An excellent yield was obtained and 50 fluorescent molecules were bound. The spectrophotometry results (Table 4.7) for the peptide conjugation indicate excellent yield and that intact particles were produced. TEM images were obtained for BMV-SM(PEG)$_{24}$-P1 (Figure 4.10, panel C) and BMV-SM(PEG)$_{24}$-P2 (Figure 4.10, panel D).

[6] The previously observed precipitation was found to be due to crystals forming in the propargylamine. For the subsequent reactions a new tube was used.

Table 4.7: Virus concentrations, based on the absorbance at 260 nm, for BMV-Cy5 modified with Peptide 1 and 2 and crosslinkers SM(PEG)$_8$, SM(PEG)$_{12}$ and SM(PEG)$_{24}$

Sample	Concentration (mg/ml)	260/280
BMV-SM(PEG)$_8$-P1	2.998	1.64
BMV-SM(PEG)$_{12}$-P1	1.581	1.64
BMV-SM(PEG)$_{24}$-P1	3.522	1.60
BMV-SM(PEG)$_8$-P2	1.342	1.62
BMV-SM(PEG)$_{12}$-P2	2.732	1.64
BMV-SM(PEG)$_{24}$-P2	1.592	1.63

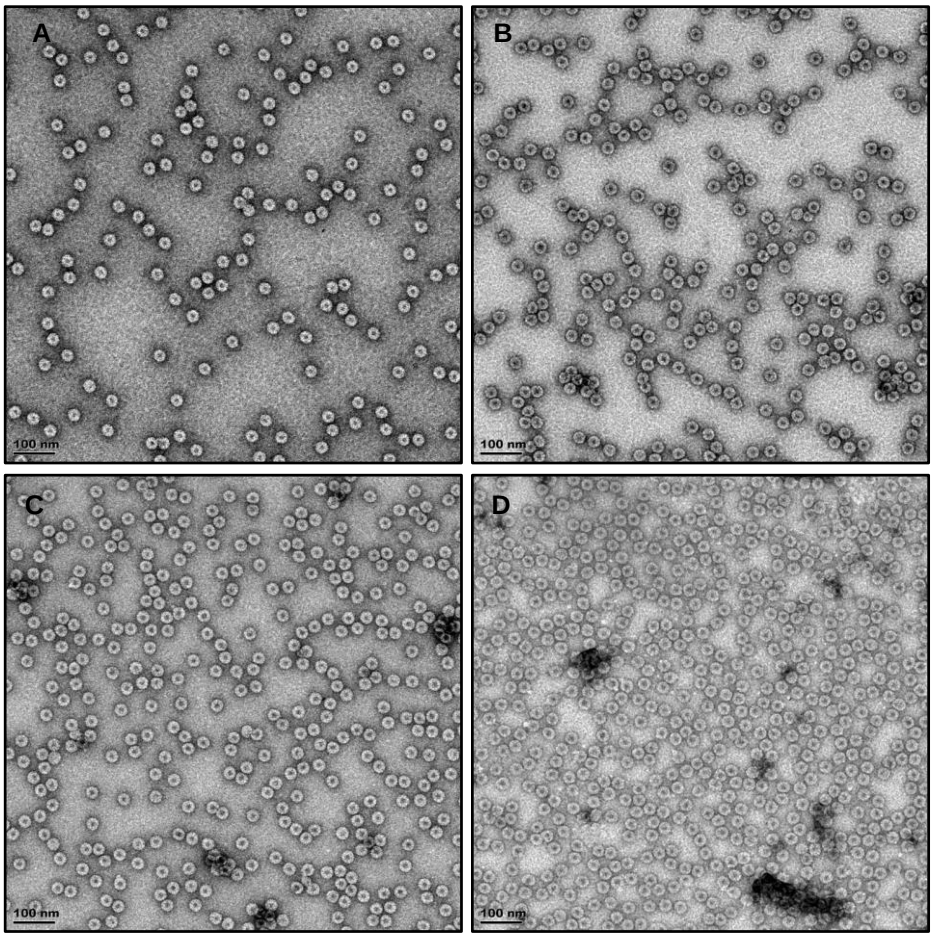

Figure 4.10: Electron micrograph of **(A)** BMV modified using the EDC reaction, **(B)** BMV conjugated with the Cy5 fluorescent molecule, **(C)** BMV-Cy5 conjugated with SM(PEG)$_{24}$ and Peptide 1, **(D)** BMV-Cy5 conjugated with SM(PEG)$_{24}$ and Peptide 2

There was no second conjugate band present on the SDS-PAGE gel (Figure 4.11). The previous peptide conjugation to the native BMV was used as a control (Figure 4.11, lane 9 and 10) as this was previously confirmed on the gel. This indicates that the peptide is not bound. These samples were still used in the cell uptake experiments (Figures 4.23, 4.24 and 4.28).

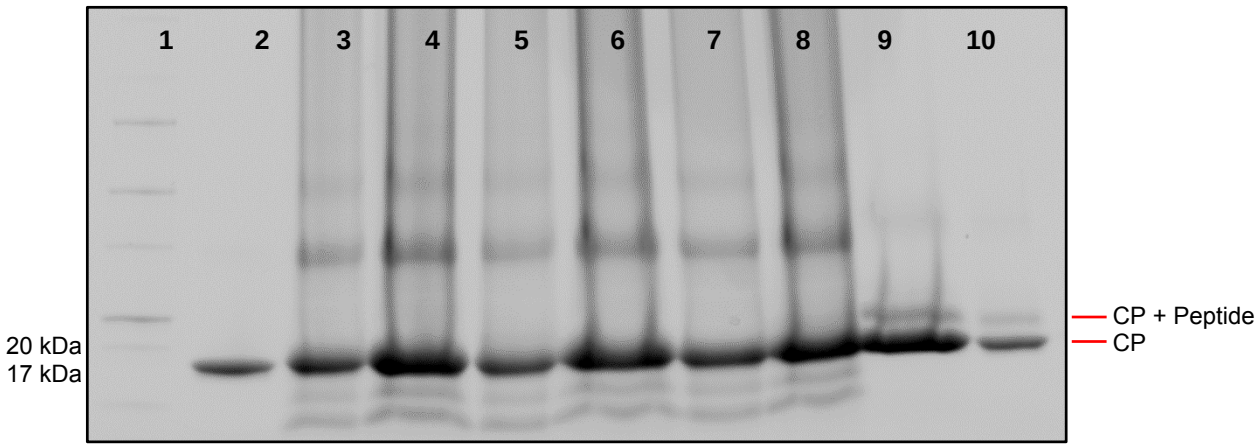

Figure 4.11: SDS-PAGE gel of BMV-Cy5 conjugated with Peptide 1 and 2 and crosslinkers $SM(PEG)_8$, $SM(PEG)_{12}$ and $SM(PEG)_{24}$, run at 120 V. Lane 1: Precision Plus Protein™ Standard Ladder, Lane 2: Unmodified BMV, Lane 3: BMV-$SM(PEG)_8$-P1-Cy5, Lane 4: BMV-$SM(PEG)_{12}$-P1-Cy5, Lane 5: BMV-$SM(PEG)_{24}$-P1-Cy5, Lane 6: BMV-$SM(PEG)_8$-P2-Cy5, Lane 7: BMV-$SM(PEG)_{12}$-P2-Cy5, Lane 8: BMV-$SM(PEG)_{24}$-P2-Cy5, Land 9: BMV positive control BMV-$SM(PEG)_{24}$-P1, Lane 10: BMV positive control BMV-$SM(PEG)_{24}$-P1 (lower concentration)

We validated the conjugation of the different crosslinkers with both peptides, by conjugating them to unmodified BMV. The SDS-PAGE gel confirmed that only crosslinker $SM(PEG)_{24}$ successfully conjugated both Peptide 1 and 2 to the BMV coat protein (Figure 4.12, lanes 4 and 7). These results are contradictory to those received from the MALDI-TOF MS analysis, nevertheless we decided to proceed with only crosslinker $SM(PEG)_{24}$ for the remainder of the study. This successful conjugation is contradictory to the previous results (Figure 4.11) where none of the crosslinkers bound the peptide to BMV.

We suspected that the fluorescent labeling may inhibit the subsequent peptide conjugation. This was investigated by first conjugating the peptide to the virus and then proceeding with the fluorescent labelling. We confirmed that the peptide was bound to the virus after the initial peptide conjugation (Figure 4.13, panel A) and after the fluorescent labeling (Figure 4.13, panel B, lane 3). Good yield and mostly intact particles were obtained. We calculated a total of 51 fluorescent molecules bound, which indicated that conjugation of the peptide before the fluorescent molecule does not impact the efficiency of fluorescent labeling.

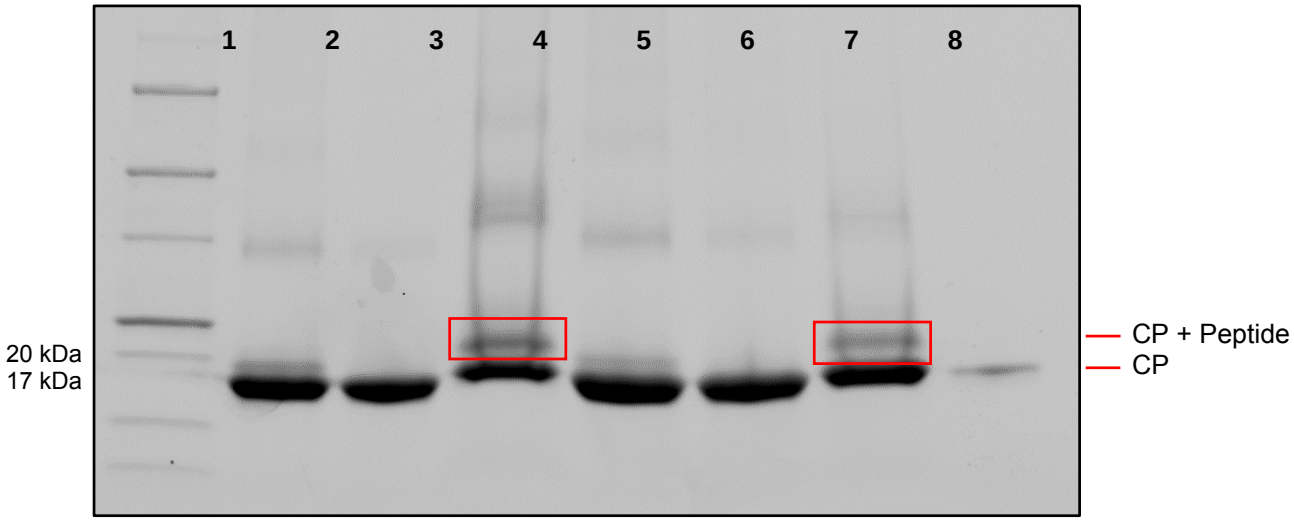

Figure 4.12: SDS-PAGE gel of native BMV conjugated with Peptide 1 and 2 and crosslinkers SM(PEG)$_8$, SM(PEG)$_{12}$ and SM(PEG)$_{24}$, run at 120 V. Lane 1: Precision Plus Protein™ Standard Ladder, Lane 2: BMV-SM(PEG)$_8$-P1, Lane 3: BMV-SM(PEG)$_{12}$-P1, Lane 4: BMV-SM(PEG)$_{24}$-P1, conjugate indicated in red block, Lane 5: BMV-SM(PEG)$_8$-P2, Lane 6: BMV-SM(PEG)$_{12}$-P2, Lane 7: BMV-SM(PEG)$_{24}$-P2, conjugate indicated in red block, Lane 8: Unmodified BMV

We also attempted to first incubate the peptide and the linker together and then conjugate it to the fluorescently labeled virus. This was to investigate whether the problem lies with the linker binding to the virus or the peptide binding to the linker after the fluorescent labeling.

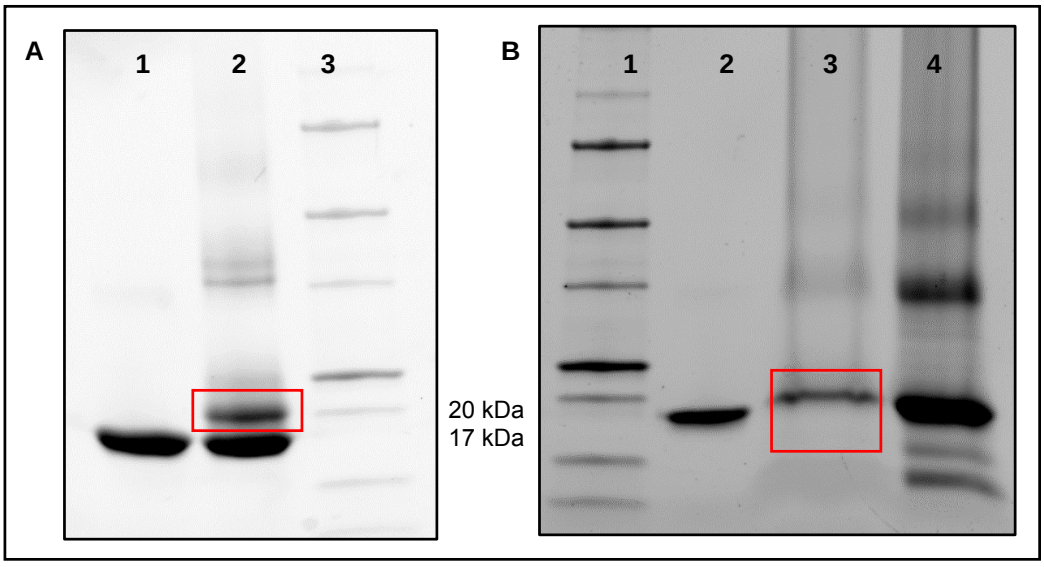

Figure 4.13: SDS-PAGE gel of BMV conjugated with Peptide 1 and SM(PEG)$_{24}$, run at 120 V. **(A)** Lane 1: Unmodified BMV, Lane 2: BMV-SM(PEG)$_{24}$-P1 of native BMV, Lane 3: Precision Plus Protein™ Standard Ladder. **(B)** Lane 1: Precision Plus Protein™ Standard Ladder, Lane 2: Unmodified BMV, Lane 3: BMV-SM(PEG)$_{24}$-P1-Cy5 (reverse), Lane 4: BMV-SM(PEG)$_{24}$-P1-Cy5 (peptide-linker incubated)

The fluorescent labeling achieved 52 molecules bound and all the particles were intact. The peptide was however not bound (Figure 13, panel B, lane 4), as only a single band of

17 kDa was present. This provided further evidence that the fluorescent labeling might impede peptide conjugations.

4.3.1. Alternative conjugation method

We investigated the structure of the coat protein to verify whether the glutamic acids and lysines could cause steric hindrance during conjugation. We generated an image of the coat protein structure (Figure 4.14) using Chimera (v.1.11.2) (Pettersen *et al*., 2004). The red arrow indicates a representative section of the interaction between the glutamic acid and the lysine residues. Here we observe that a large proportion of the two amino acids appear in the same location. This might explain why the peptide conjugation is less efficient when the fluorescent labeling is performed first. The fluorescent molecule, bound to the glutamic acid, could cause steric hindrance which prevents the peptides from conjugating. This may not be the case for every lysine residue, but could affect enough of them for too few of the conjugates to be separated on the SDS-PAGE gel, thereby explaining the lack of a double band. This might also explain why the gel was negative for the peptide conjugation, but was positively confirmed with the MALDI-TOF MS. Due to this interference and the reverse reaction not being efficient, we proceeded with a different approach.

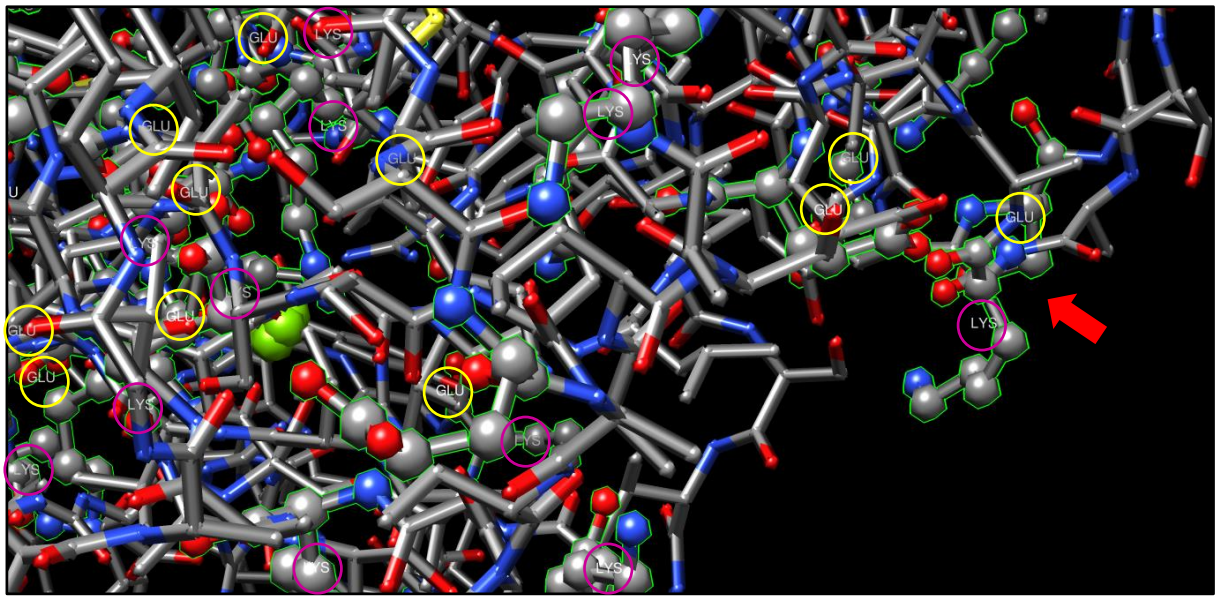

Figure 4.14: Section of the exterior coat protein of BMV indicating the glutamic acid and lysine residues. The arrow indicates where the glutamic acid and lysine co-occur. The glutamic acids are highlighted in the yellow circles and the lysines in the pink circles.

We conjugated both the fluorescent molecule and the peptide to the lysine residues. Fluorescent binding for Peptide 1 and 2 was 40 and 60 molecules respectively. TEM analysis showed that the particles produced in the Peptide 2 reaction (Figure 4.15, panel B)

were completely intact, but the particles from the Peptide 1 reaction (Figure 4.15, panel A) were not all intact with only a few aggregated particles present.

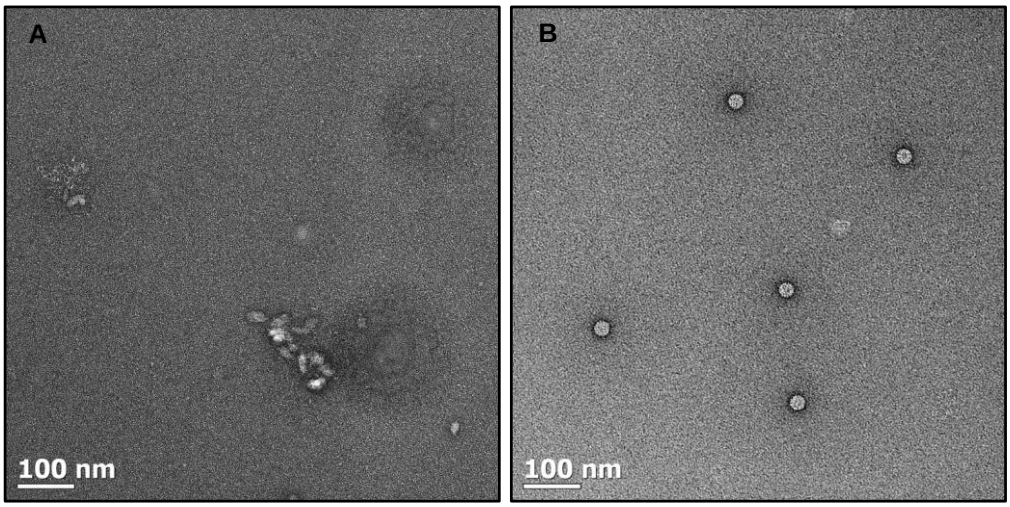

Figure 4.15: Electron micrograph of BMV-Cy5 conjugated with a crosslinker and two peptides. **(A)** SM(PEG)$_{24}$ and Peptide 1, particles are not intact. **(B)** SM(PEG)$_{24}$ and Peptide 2, particles are intact.

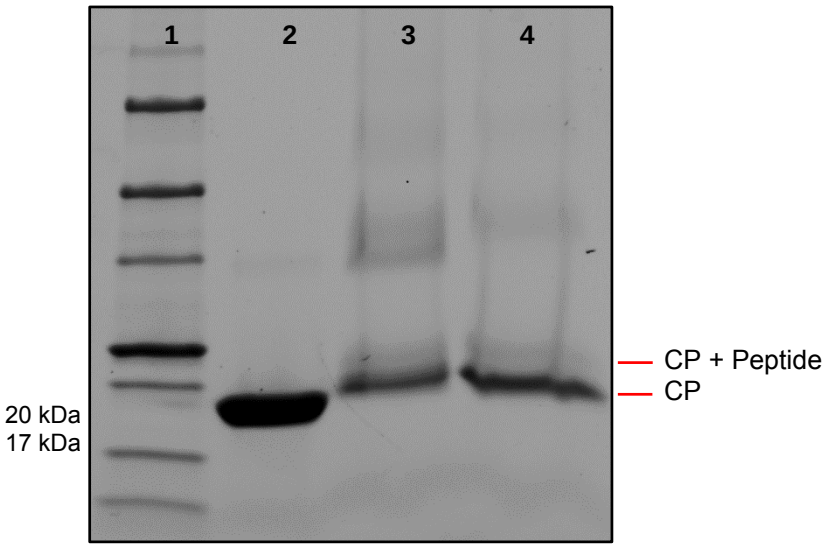

Figure 4.16: SDS-PAGE gel of BMV conjugated with Peptide 1 and 2 and SM(PEG)$_{24}$ using an alternative method, run at 120 V. Lane 1: Precision Plus Protein™ Standard Ladder, Lane 2: Unmodified BMV, Lane 3: BMV-SM(PEG)$_{24}$-P1, Lane 4: BMV-SM(PEG)$_{24}$-P2

The peptide binding was successful as indicated by double bands for both reactions (Figure 4.16). This indicates that this conjugation method not only produced intact particles, at least for Peptide 2, but also excellent fluorescent labeling and peptide conjugation. This is therefore the conjugation method of choice for BMV. These samples were used in uptake experiments in all cell lines (Figures 4.25, 4.26 and 4.29).

4.4. Cell uptake experiments

4.4.1. Flow cytometry

The internalization of the VNPs were assessed in three different prostate cell lines by means of flow cytometry. Previous studies on BMV (Daniel *et al*., 2010; Dixit *et al*., 2006; Huang *et al*., 2011, 2007; Sun *et al*., 2007; Yildiz *et al*., 2012) have not accessed the uptake of the VNPs into cell lines even though the encapsulation and bioconjugation was successful. Jung *et al*., (2011) demonstrated that BMV encapsulated with a fluorescent molecule is internalized into human bronchial epithelial cells. It is therefore unclear with what percentage BMV will be taken up into the prostate cells.

The initial flow cytometry experiments for the passive uptake of BMV into the three cell lines (Figure 4.17) indicated significant uptake in only the PNT2 cell line. This is also demonstrated by the mean fluorescence intensity in the cells (Figure 4.18). The uptake is quite high for PNT2, which is expected since this is only passive uptake and we would expect the normal cell line to allow more molecules to enter, whereas the physiological characteristics of the cancer cells may prevent this.

The first active uptake results (Figure 4.19) indicate that the presence of a targeting ligand improves the efficiency of the internalization of the VNPs. The ligand facilitates the internalization of the VNPs by means of receptor-mediated endocytosis. This form of endocytosis makes use of a selective internalization in which only molecules with the complementary ligand to the receptor on the cell will be internalized. When the ligand binds to the receptor on the cell surface, the membrane will form a vesicle around the molecule and release it in the interior of the cell (Cooper, 2000). Previous studies on CPMV as a VNP indicated that when conjugated with a bombesin ligand, targeting the GRP receptor, the internalization was increased (Steinmetz *et al*., 2011). We would therefore expect that the VNPs with the targeting ligand will be internalized with a higher percentage.

We also observed that the passive uptake was not significant. The VCaP cell line had the highest uptake, while PNT2 and PC3 had similar uptake. We observe a significant increase in uptake for $SM(PEG)_{12}$ and $SM(PEG)_{24}$ compared to $SM(PEG)_8$ ($p<0.0001$) for VCaP. For PC3 and PNT2 there is no significant difference in uptake among the different linkers. The mean fluorescent intensity (Figure 4.20) differs slightly from the percentage uptake in the

cell lines.[7] The higher uptake of VCaP compared to PC3 is unexpected, since the peptides are designed specifically for the receptors on androgen-independent cell lines.

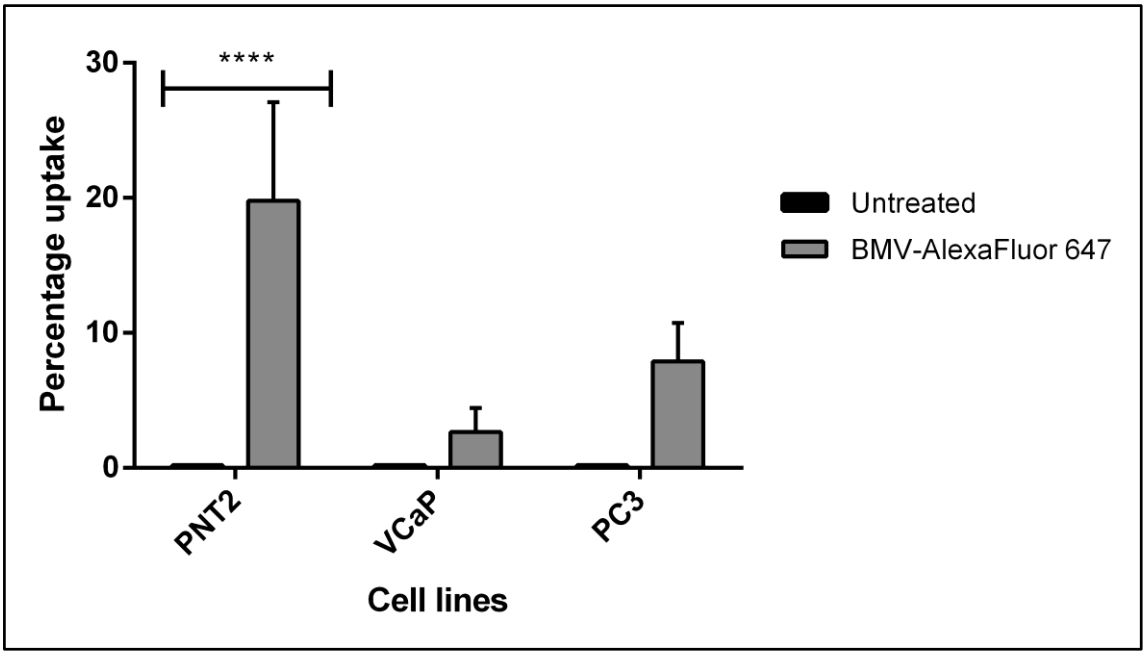

Figure 4.17: Percentage passive uptake of BMV-AlexaFluor® 647 in three different prostate cells, PNT2, VCaP and PC3. Significance was calculated using a two-way ANOVA with Bonferroni correction. Significance is indicated between treated and untreated cells: **** = p<0.0001.

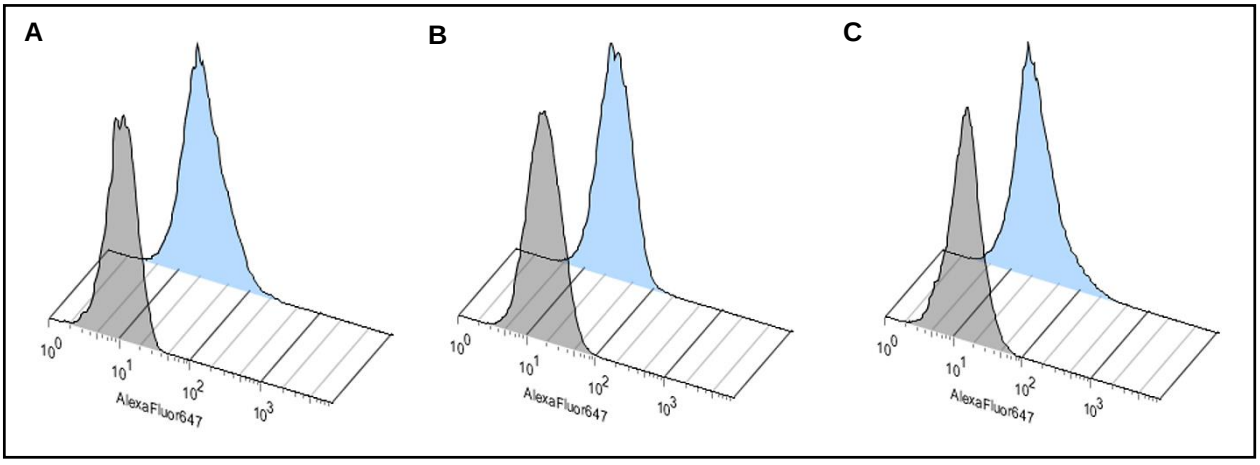

Figure 4.18: Mean fluorescence intensity indicating passive uptake into **(A)** PNT2, **(B)** VCaP and **(C)** PC3. Grey = Untreated cells, Blue = BMV-AlexaFluor 647

[7] This could be caused by fewer cells containing VNPs, but each cell which does contain VNPs, has a large number of them.

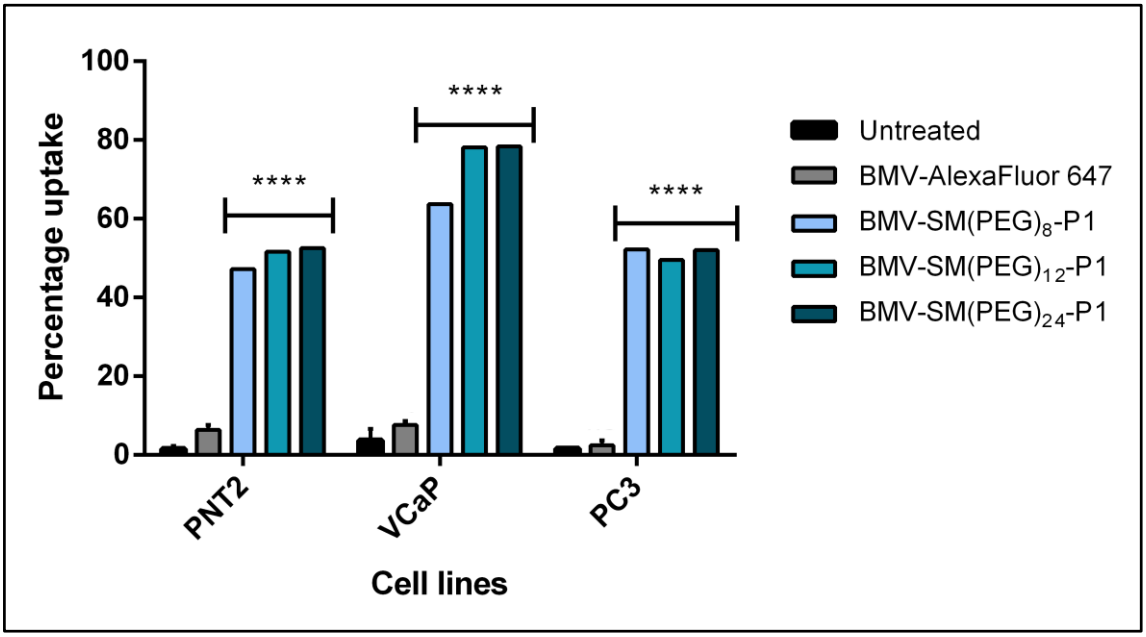

Figure 4.19: Percentage passive and active uptake of BMV-AlexaFluor® 647, conjugated to Peptide 1 and three different crosslinkers, in three different prostate cells, PNT2, VCaP and PC3. Significance was calculated using a two-way ANOVA with Bonferroni correction. Significance is indicated between treated and untreated cells: **** = $p<0.0001$

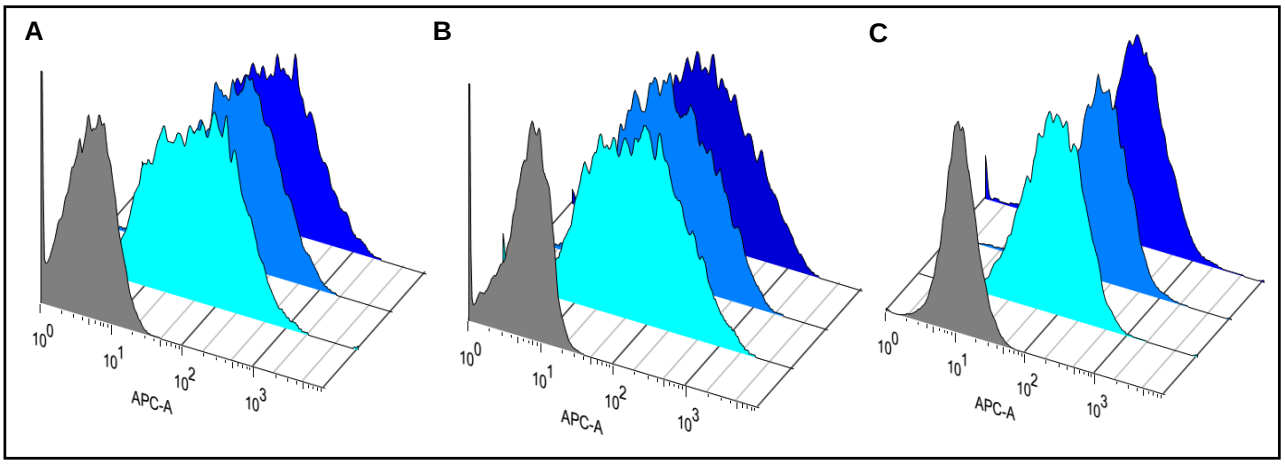

Figure 4.20: Mean fluorescence intensity indicating passive and active uptake into **(A)** PNT2, **(B)** VCaP and **(C)** PC3. Grey = Untreated cells, Light blue = BMV- SM(PEG)$_8$-P1, Medium blue = BMV- SM(PEG)$_{12}$-P1, Dark blue = BMV- SM(PEG)$_{12}$-P1

In Figure 4.21 we present the first uptake data with three and more biological and technical repeats. In this case we observed that VCaP did not have any significant uptake, for both the passive and active uptake. Both PNT2 and PC3 had significant uptake, with the exception of BMV-SM(PEG)$_8$-P1 in PNT2. Even though the uptake for PNT2 was still high, PC3 had significantly more uptake of the VNPs ($p<0.0001$). This suggests that the VNPs will tend to target the PC3 cells, which is the expected outcome. BMV-SM(PEG)$_{24}$-P1 had the highest uptake and was significant compared to the passive ($p<0.005$) in PC3. This

sample also had a high fluorescent intensity (Figure 4.22, C), suggesting that a large number of VNPs enter the cells. The high passive uptake may be attributed to the normal endocytosis of molecules into the cells, but the targeting ligand present on the VNPs utilizes a receptor-mediated endocytosis which is more efficient and therefore a higher uptake is observed.

The results correspond to the double band that was observed on the SDS-PAGE gel and was confirmed with MALDI-TOF MS analysis, and suggests that the peptide is bound to BMV and contributes to an increased internalization into the cancer cells. The results for BMV-SM(PEG)$_{12}$-P1 are contradictory, since the MALDI-TOF MS analysis suggested that the peptide is bound, whereas the gel indicated that it is not bound. Further investigation confirmed that crosslinker SM(PEG)$_{12}$ does not bind the peptide to BMV. This is also the case for crosslinker SM(PEG)$_8$.

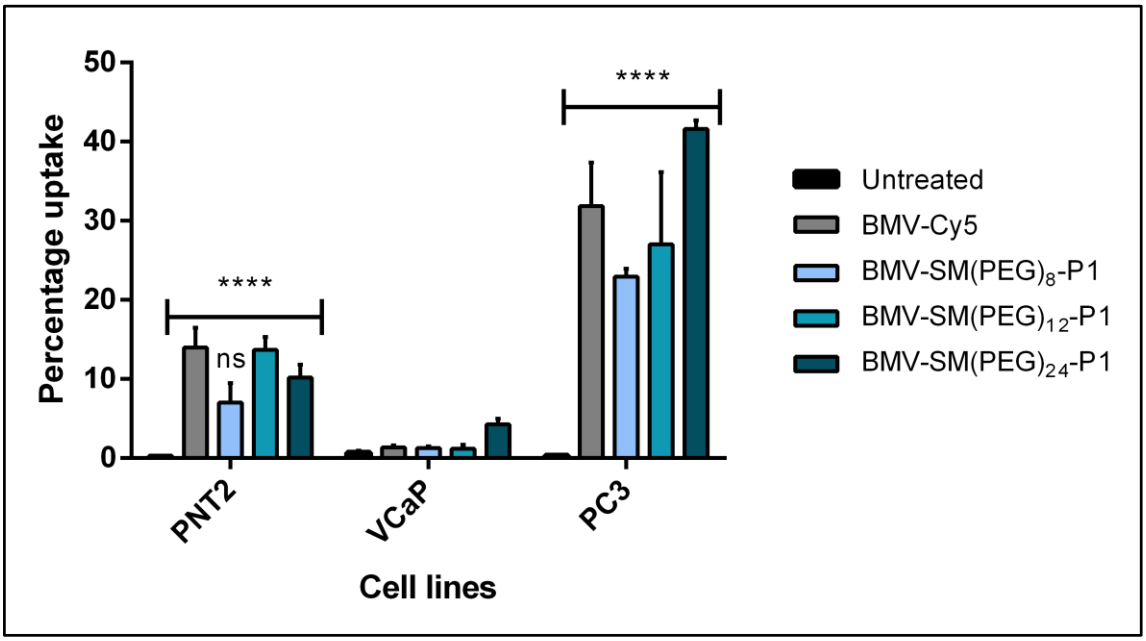

Figure 4.21: Percentage passive and active uptake of BMV-Cy5, conjugated to Peptide 1 and three different crosslinkers, in three different prostate cells, PNT2, VCaP and PC3. Significance was calculated using a two-way ANOVA with Bonferroni correction. Significance is indicated between treated and untreated cells: ns = $p>0.05$, **** = $p<0.0001$

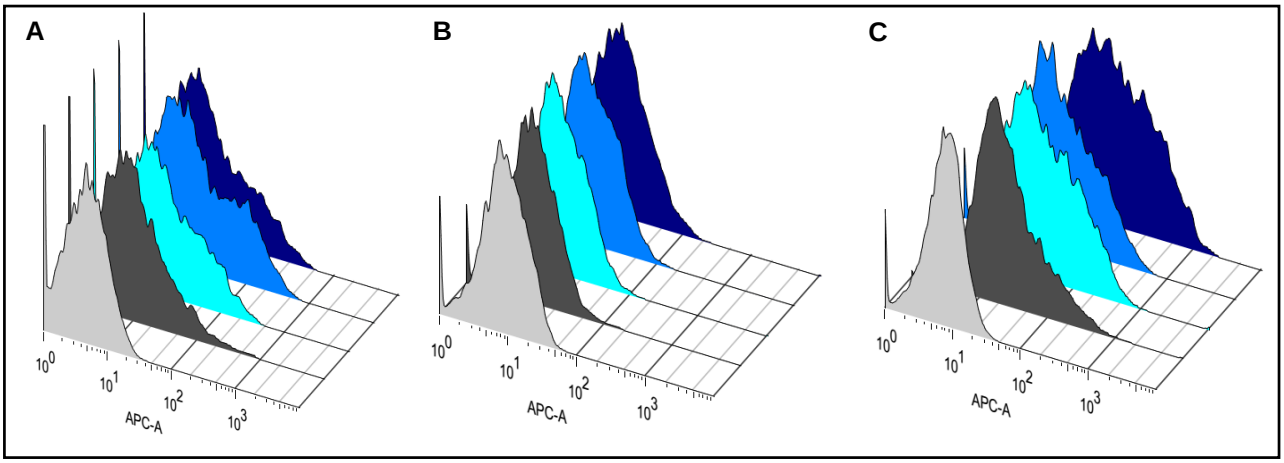

Figure 4.22: Mean fluorescence intensity indicating passive and active uptake into **(A)** PNT2, **(B)** VCaP and **(C)** PC3. Light grey = Untreated cells, Dark grey = BMV-Cy5, Light blue = BMV- SM(PEG)$_8$-P1, Medium blue = BMV- SM(PEG)$_{12}$-P1, Dark blue = BMV- SM(PEG)$_{12}$-P1

For the final samples that utilized the conjugation of the fluorescent molecule to the glutamic acids and the peptide to the lysines, we did not observe significant uptake (Figure 4.23). This result was expected since we did not confirm any peptide bound on the gel. The passive uptake is significantly lower than expected. From the mean fluorescent intensity (Figure 4.24) we also did not see high fluorescence, which suggests that the VNPs were not internalized.

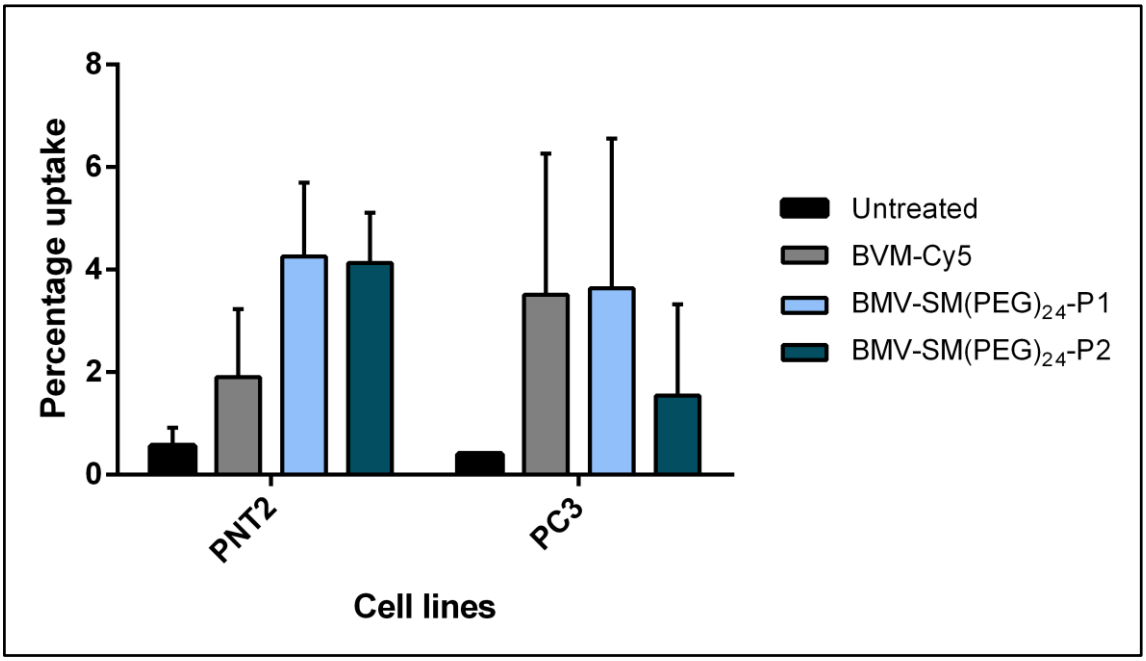

Figure 4.23: Percentage passive and active uptake of BMV-Cy5, conjugated to Peptide 1 and 2 and crosslinker SM(PEG)$_{24}$, in two different prostate cells, PNT2 and PC3. Significance was calculated using a two-way ANOVA with Bonferroni correction. Non-significant uptake was observed.

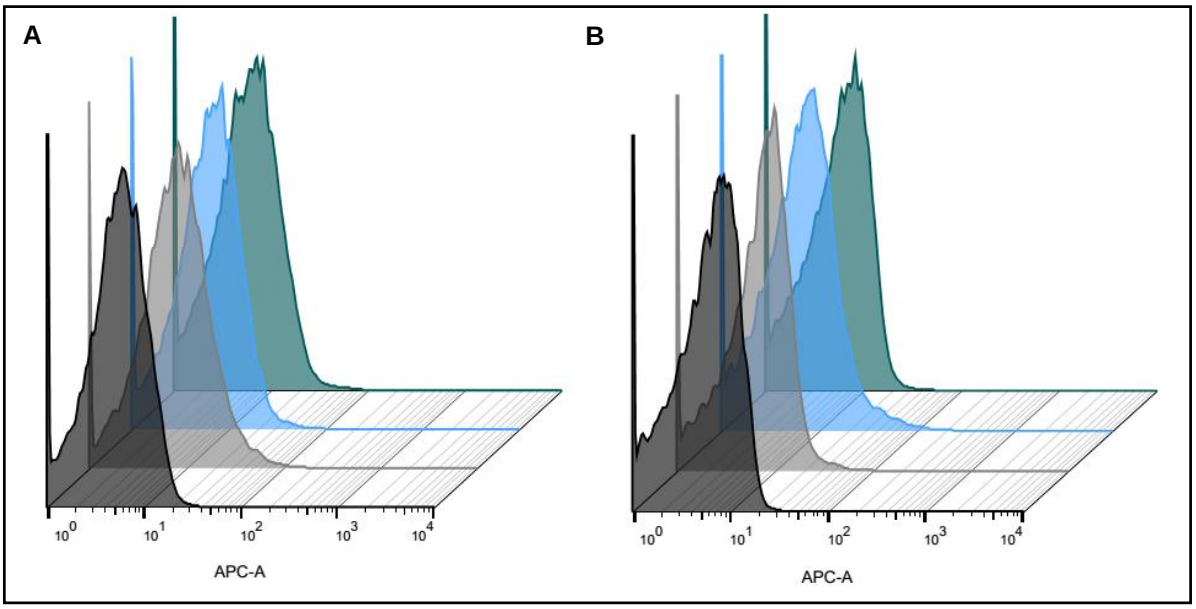

Figure 4.24: Mean fluorescence intensity indicating passive and active uptake into **(A)** PNT2, **(B)** PC3. Dark grey = Untreated cells, Light grey = BMV-Cy5, Light blue = BMV- SM(PEG)$_{24}$-P1, Dark blue = BMV-SM(PEG)$_{24}$-P2

The percentage uptake and mean fluorescent intensity for the VNPs produced by conjugating to only the lysines are presented in Figures 4.25 and 4.26. BMV-SM(PEG)$_{24}$-P2 had the highest uptake for all the cell lines. For the passive uptake we used the same sample that was reported in Figure 4.23, but in this case we have significant uptake. The result for PC3 was expected as the peptides are specific to the receptors on androgen-independent cancer cells. This could also explain why the uptake for Peptide 1 was much higher in PC3 than for the other two cell lines. Even though PNT2 still had very high uptake, the uptake for PC3 was significantly higher ($p<0.0001$) for both Peptide 1 and 2 as calculated by the two-way ANOVA. The high uptake for the PC3 cell line is consistent with findings in literature (Mandelin *et al*., 2015) where both peptides were targeted to the PC3 cells and not the control sarcoma cells that were used. They have identified that the receptors for the peptides are present on prostatic cell lines, but they have not investigated the presence on normal prostate cells. Therefore the PNT2 cell lines may also present with the respective receptors which would explain the high uptake. The significantly higher uptake in the PC3 cell lines would however suggest that the VNPs would rather internalize into the cancer cells than into the normal prostate cells.

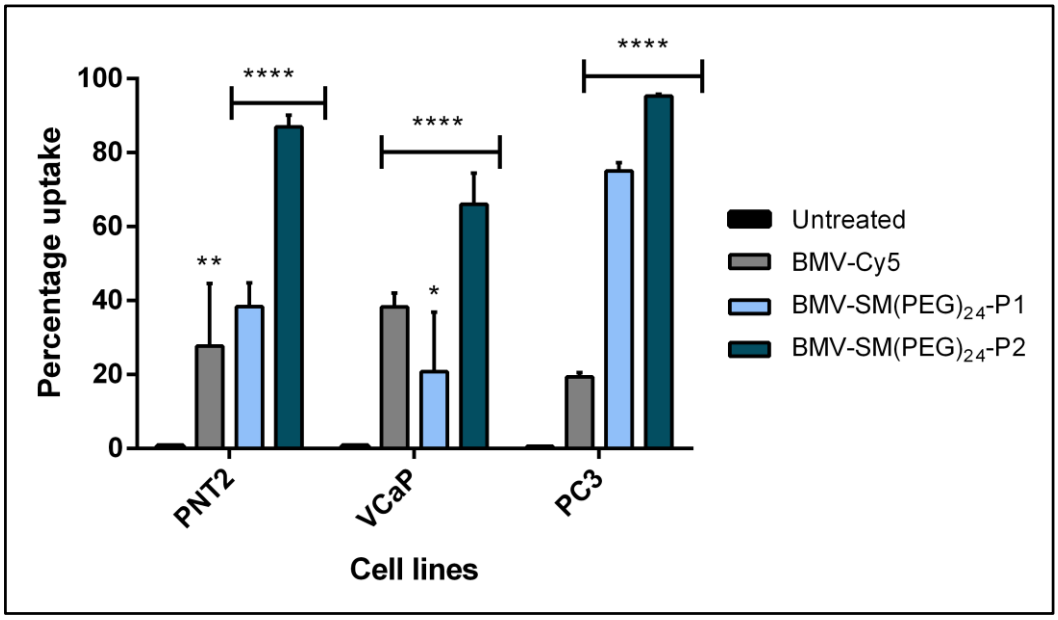

Figure 4.25: Percentage passive and active uptake of VNPs produced by the conjugation to the lysines. BMV-Cy5 conjugated to Peptide 1 and 2 and crosslinker SM(PEG)$_{24}$ uptake in three different prostate cells, PNT2, VCaP and PC3. Significance was calculated using a two-way ANOVA with Bonferroni correction. Significance is indicated between treated and untreated cells: * = p<0.05, ** = p<0.005, **** = p<0.0001.

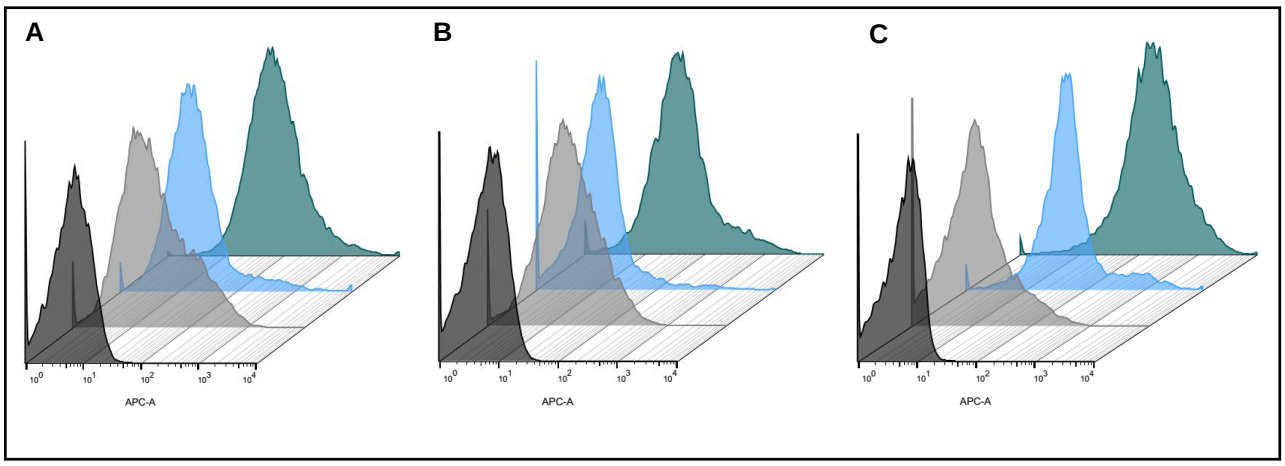

Figure 4.26: Mean fluorescence intensity indicating passive and active uptake into **(A)** PNT2, **(B)** VCaP and **(C)** PC3. Dark grey = Untreated cells, Light grey = BMV-Cy5, Light blue = BMV- SM(PEG)$_{24}$-P1, Dark blue = BMV- SM(PEG)$_{24}$-P2

4.4.2. Fluorescence microscopy

The internalization of the VNPs were also assessed in the three prostate cell lines by means of florescence microscopy. The image acquisitions included a z-stack in order to assess the localization of the VNPs in the cells. The uptake for the different VNPs in PC3 is shown in Figure 4.27. We observed that the passive and active uptake for BMV-SM(PEG)$_8$-P1 and BMV-SM(PEG)$_{12}$-P1 corresponded with the findings from the flow cytometry. However, for

BMV-SM$(PEG)_{24}$-P1 the uptake was significantly lower. This could be explained by the fact that only a single focal plane was acquired.

The results for the uptake of BMV-P1 and BMV-P2 (Figure 4.28) contradicted the non-significant results we obtained from flow cytometry. In this case, the uptake of the virus in the cells was comparable to the uptake in Figure 4.27, which had significant flow cytometry results. This could be due to the difference in incubation time for flow cytometry and fluorescence microscopy. We can also see that the passive uptake (Figure 4.28, A and B) corresponds to the percentage uptake observed in Figure 4.25.

In Figure 4.29 the uptake corresponds perfectly with the flow cytometry results and we observed high uptake of BMV-SM$(PEG)_{24}$-P2 in all three cell lines and BMV-SM$(PEG)_{24}$-P1 in PC3. We performed a z-stack of the cells and confirmed that the particles were internalized. This confirms the positive result that we obtained earlier.

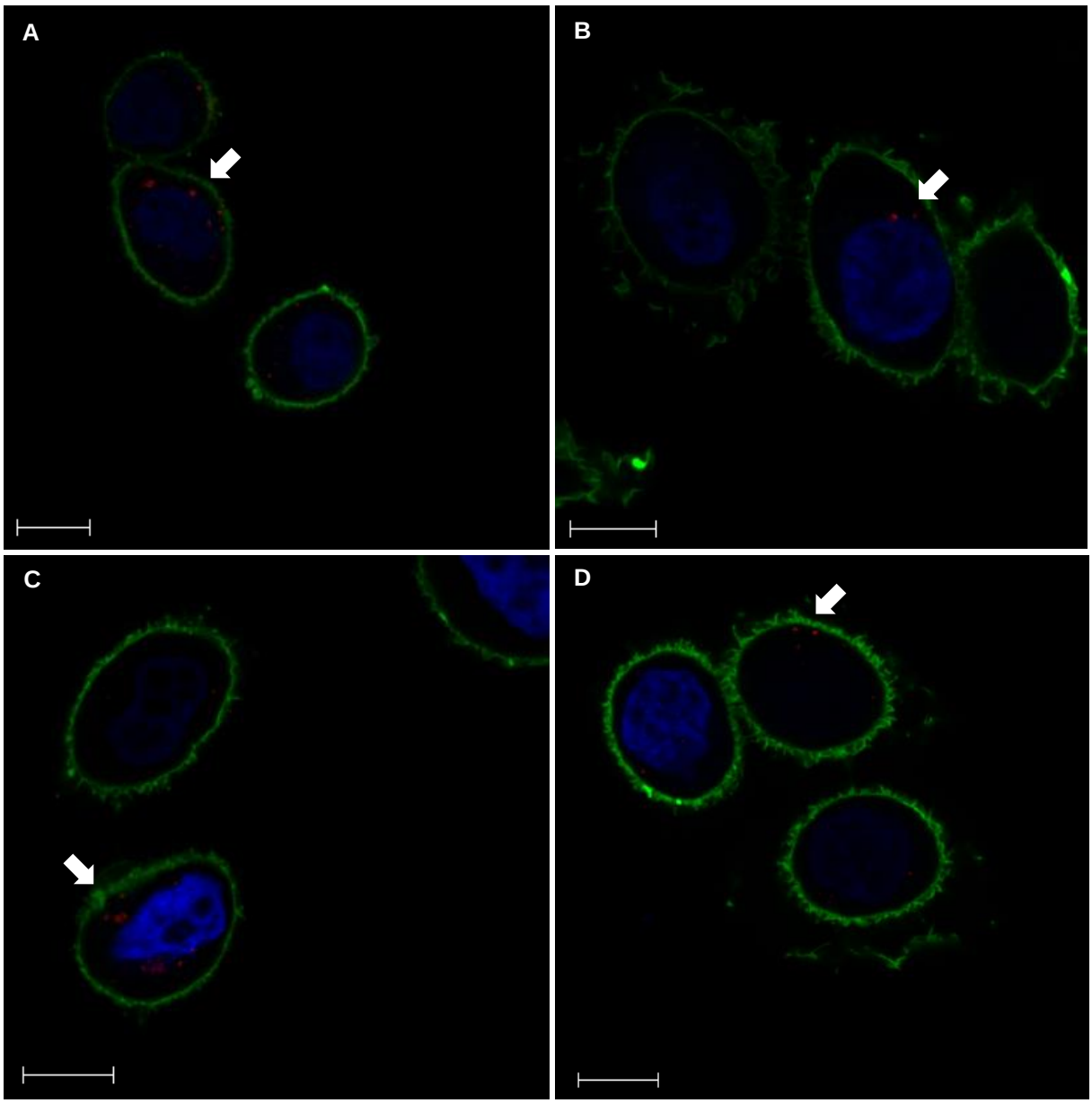

Figure 4.27: Micrograph of passive and active uptake of BMV-Cy5 conjugated with Peptide 1 and three different crosslinkers, uptake into PC3 cells. **(A)** BMV-Cy5, **(B)** BMV-SM(PEG)$_8$-P1, **(C)** BMV-SM(PEG)$_{12}$-P1, **(D)** BMV-SM(PEG)$_{24}$-P1. The nucleus is stained in blue (DAPI) and the cell membrane in green (WGA). The VNPs are in red and can be located with the white arrows. The scale bar represents 10 µm.

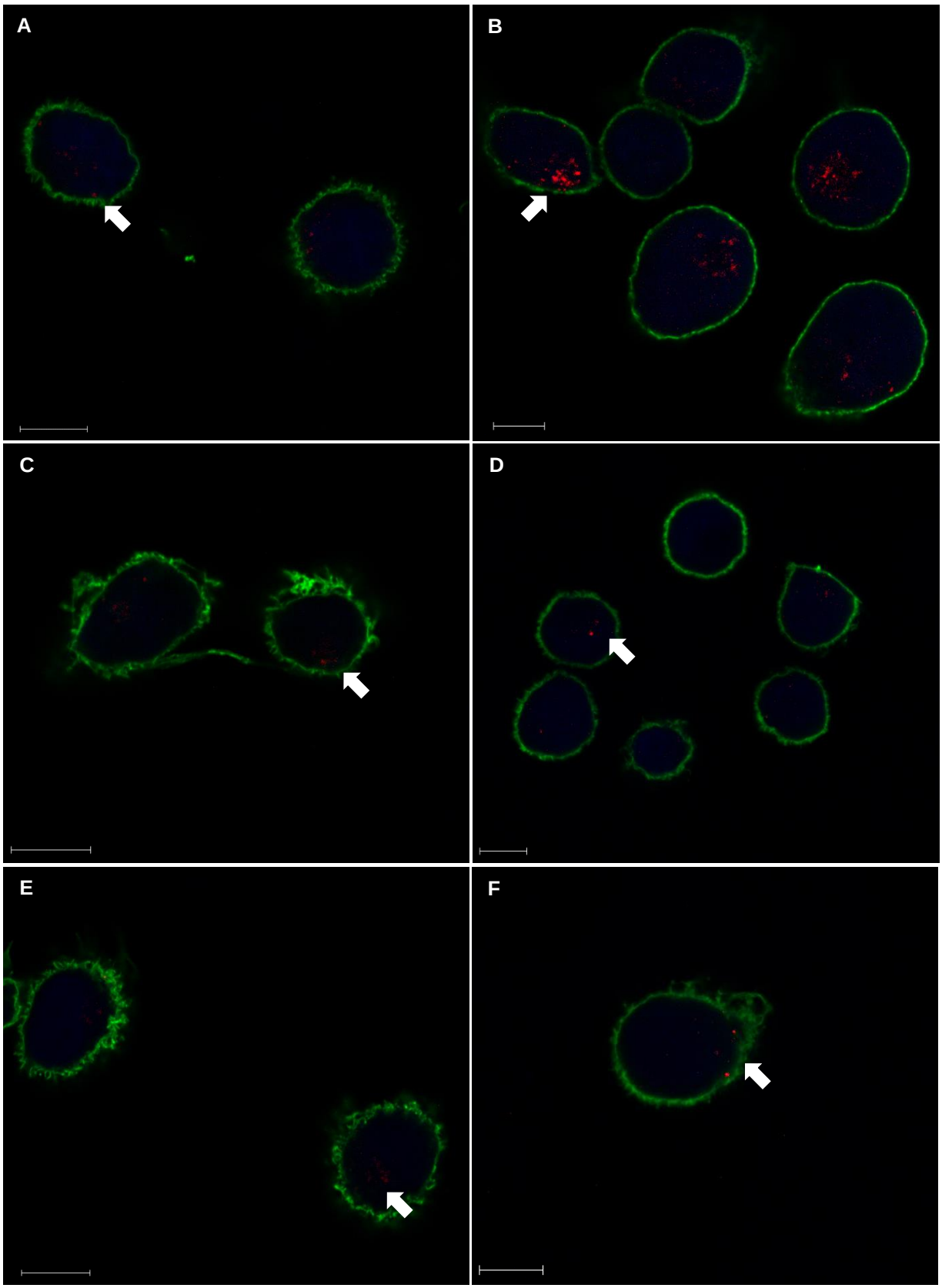

Figure 4.28: Micrograph of passive and active uptake of BMV-Cy5 conjugated with Peptide 1 and 2 and crosslinker SM(PEG)$_{24}$, uptake into PNT2 and PC3. **(A)** BMV-Cy5 in PNT2, **(B)** BMV-Cy5 in PC3 **(C)** BMV-SM(PEG)$_{24}$-P1 in PNT2, **(D)** BMV-SM(PEG)$_{24}$-P1 in PC3, **(E)** BMV-SM(PEG)$_{24}$-P2 in PNT2, **(F)** BMV-SM(PEG)$_{24}$-P2 in PC3. The nucleus is stained in blue (DAPI) and the cell membrane in green (WGA). The VNPs are in red and can be located with the white arrows. The scale bar represents 10 µm.

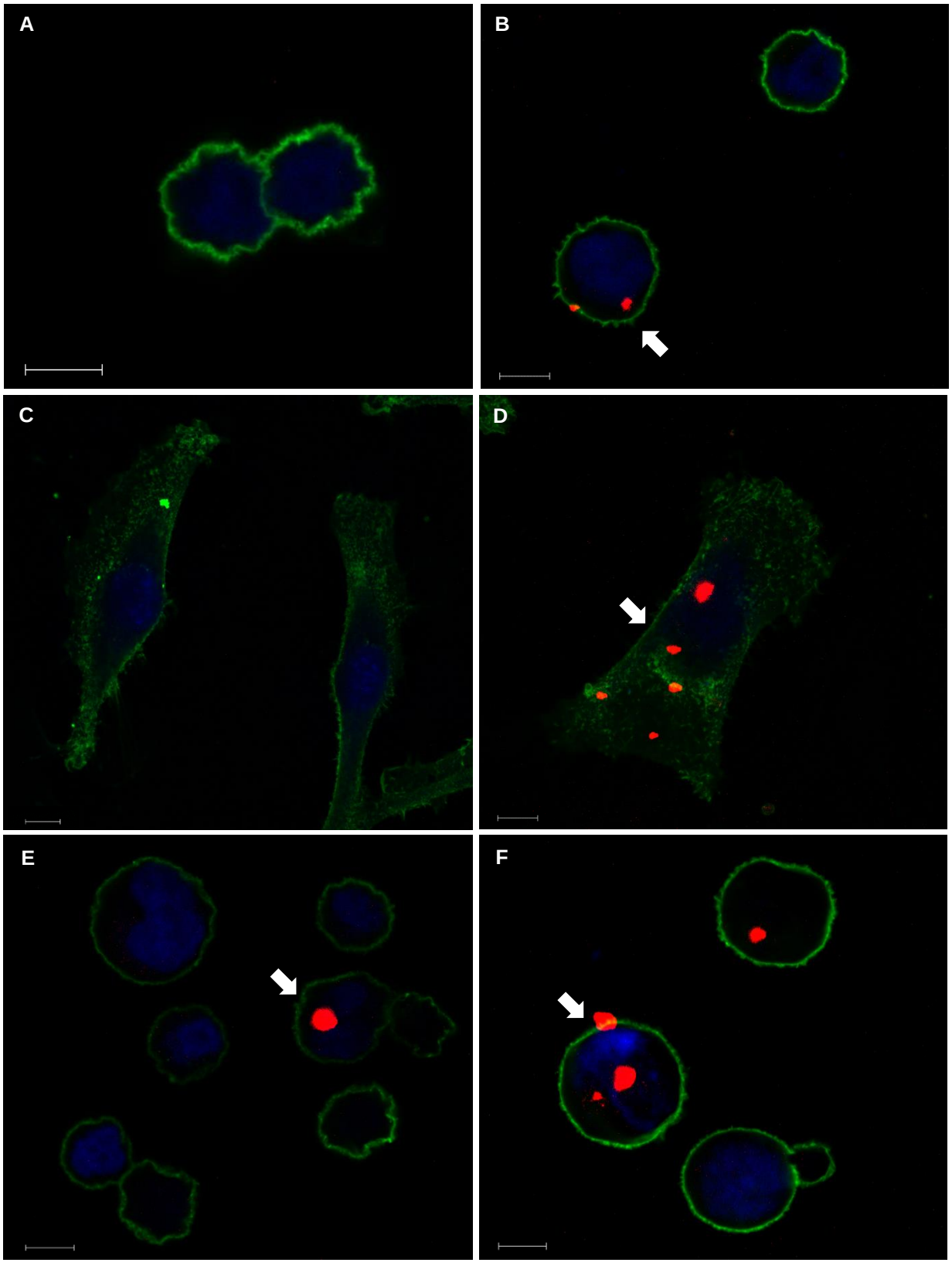

Figure 4.29: Micrograph of passive and active uptake of BMV-Cy5 conjugated with Peptide 1 and 2 and crosslinker SM(PEG)$_{24}$, uptake into three different prostate cells. **(A)** BMV-SM(PEG)$_{24}$-P1 in PNT2, **(B)** BMV-SM(PEG)$_{24}$-P2 in PNT2, **(C)** BMV-SM(PEG)$_{24}$-P1 in VCaP, **(D)** BMV-SM(PEG)$_{24}$-P2 in VCaP, **(E)** BMV-SM(PEG)$_{24}$-P1 in PC3, **(F)** BMV-SM(PEG)$_{24}$-P2 in PC3. The nucleus is stained in blue (DAPI) and the cell membrane in green (WGA). The VNPs are in red and can be located with the white arrows. The scale bar represents 10 µm.

Chapter 5

Conclusion

The aim of this study was to modify an icosahedral plant virus, *Brome mosaic virus*, with a fluorescent molecule and a targeting peptide. This VNP was then assessed for its targeting efficiency in normal and cancerous prostate cell lines.

BMV was purified from infected *N. benthamiana* plants with excellent yield in order to proceed with the conjugation methods. The fluorescent labeling of Cy5 to the glutamic acid residues on the surface of the BMV coat protein was successful. A consistent number of 50 fluorescent molecules could be bound per conjugation. Both peptides, PKRGFQD-C and SNTRVAP-C, could be conjugated to the lysine residues using the $SM(PEG)_{24}$ crosslinker. This was confirmed with SDS-PAGE and MALDI-TOF MS analysis. $SM(PEG)_{24}$ was the only crosslinker that provided efficient binding of the peptide, as confirmed with SDS-PAGE. A problem arose when we initially attempted to first conjugate the fluorescent molecule, and then use the fluorescently-labeled BMV for the peptide conjugation. In this case the peptide conjugation was unsuccessful and upon examination of the amino acid composition on the coat protein, we concluded that there might be interference from the glutamic acids when the fluorescent molecule is bound.

We then proceeded to conjugate both the fluorescent molecules and peptides simultaneously to the lysine residues, and this was successful. In spite of competition for binding sites between fluorescent molecules and peptides for the same amino acid, there was still a high number of fluorescent molecules bound. This suggests that the 180 reactive amino acids that were identified (Wen *et al*., 2012a) is sufficient for conjugation of both a fluorescent molecule and a targeting peptide. This reaction was only performed twice and therefore a future prospect will be to repeat the experiments. We could not however analyze the samples using MALDI-TOF MS due to unforeseen technical issues which rendered the equipment unavailable at this time. Future experiments to quantitatively analyze whether the peptides are bound are planned.

The uptake using both peptides into the androgen-independent cell line, PC3, was very high. Peptide 1 had an uptake of 75% and Peptide 2 was 95%, which is better than expected. We expected the VNPs to be targeted to androgen-independent cell lines as the peptides are specific for the receptors (Mandelin *et al*., 2015). The uptake in the androgen-dependent cell

line, VCaP, was also high, but it was lower than the normal prostate cells, PNT2. The efficient uptake into the normal prostate cells are not ideal as we would like to limit the uptake to cancerous prostate cells. The normal prostate cells may also contain the receptors as this has not been evaluated before, which would explain the high internalization. The uptake into the PC3 cells was however significantly more than for PNT2, and we would hope that the VNPs will preferentially enter the cells with the targeted receptors on the surface. The specificity of the peptides to control cell lines other than sarcoma have not been investigated (Mandelin *et al*., 2015) and therefore a future prospect will be to assess the uptake in outgroup cell lines, both normal and other cancerous, to validate whether the uptake will be similar for all other cells or if it is just higher in prostate cells. This may allow us to limit the VNPs to only prostate cells.

Further future studies will include attaching a drug molecule, Doxorubicin, to the VNPs. This will be assessed with cell death assays to validate whether drug is successfully delivered to the cancer cell lines.

In conclusion, this study proved that BMV is a valuable candidate as a VNP for prostate cancer. It can be purified with ease from *N. benthamiana* with high yield and it can be modified with a fluorescent label and targeting peptides using the lysine residues. The uptake of the VNPs into androgen-independent cell lines is also remarkable.

References

Acharya, S., Dilnawaz, F., Sahoo, S.K., 2009. Targeted epidermal growth factor receptor nanoparticle bioconjugates for breast cancer therapy. Biomaterials 30, 5737–5750.

Ahlquist, P., Allison, R., Dejong, W., Janda, M., Kroner, P., Pacha, R., Traynor, P., 1990. Molecular biology of bromovirus replication and host specificity, in: Viral Genes and Plant Pathogenesis. Springer Verlag, New York, pp. 144–155.

Alexis, F., Pridgen, E., Molnar, L., Farokhzad, O., 2008. Factors affecting the clearance and biodistribution of polymeric nanoparticles. Molecular Pharmaceutics 5, 505–515.

Bamrungsap, S., Zhao, Z., Chen, T., Wang, L., Li, C., Fu, T., Tan, W., 2012. Nanotechnology in Therapeutics. Nanomedicine 7, 1253–1271.

Berthon, P., Cussenot, O., Hopwood, L., Leduc, A., Maitland, N., 1995. Functional expression of SV40 in normal human prostatic epithelial and fibroblastic cells - differentiation pattern of nontumorigenic cell-lines. International Journal of Oncology 6, 333–343.

Bockstahler, L.E., Kaesberg, P., 1962. The molecular weight and other biophysical properties of bromegrass mosaic virus. Biophysical journal 2, 1.

Bouwman, P., Jonkers, J., 2014. Therapeutic implications of dysregulated DNA damage signalling, in: World Cancer Report 2014. International Agency for Research on Cancer/World Health Organization, Lyon, France, p. 205.

Bregoli, L., Movia, D., Gavigan-Imedio, J.D., Lysaght, J., Reynolds, J., Prina-Mello, A., 2016. Nanomedicine applied to translational oncology: A future perspective on cancer treatment. Nanomedicine: Nanotechnology, Biology and Medicine 12, 81–103. doi:10.1016/j.nano.2015.08.006

Bruckman, M.A., Steinmetz, N.F., 2014. Chemical Modification of the Inner and Outer Surfaces of Tobacco Mosaic Virus (TMV), in: Lin, B., Ratna, B. (Eds.), Virus Hybrids as Nanomaterials. Humana Press, Totowa, NJ, pp. 173–185.

Bujarski, J.J., 1998. Bromovirus isolation and RNA extraction, in: Foster, G.D., Taylor, S.C. (Eds.), Plant Virology Protocols. Humana Press Inc., Totowa, NJ.

Carrillo-Tripp, M., Shepherd, C.M., Borelli, I.A., Venkataraman, S., Lander, G., Natarajan, P., Johnson, J.E., Brooks, C.L., Reddy, V.S., 2009. VIPERdb2: an enhanced and web API

enabled relational database for structural virology. Nucleic Acid Research 37, D436–D442. doi:10.1093/nar/gkn840

Chanock, S.J., 2014. Genome-wide association studies, in: World Cancer Report 2014. International Agency for Research on Cancer/World Health Organization, Lyon, France, pp. 193–202.

Chariou, P.L., Lee, K.L., Wen, A.M., Gulati, N.M., Stewart, P.L., Steinmetz, N.F., 2015. Detection and Imaging of Aggressive Cancer Cells Using an Epidermal Growth Factor Receptor (EGFR)-Targeted Filamentous Plant Virus-Based Nanoparticle. Bioconjugate Chemistry 26, 262–269. doi:10.1021/bc500545z

Chatterji, A., Ochoa, W., Shamieh, L., Salakian, S.P., Wong, S.M., Clinton, G., Ghosh, P., Lin, T., Johnson, J.E., 2004. Chemical Conjugation of Heterologous Proteins on the Surface of Cowpea Mosaic Virus. Bioconjugate Chemistry 15, 807–813. doi:10.1021/bc0402888

Colotta, F., Allavena, P., Sica, A., Garlanda, C., Mantovani, A., 2009. Cancer-related inflammation, the seventh hallmark of cancer: links to genetic instability. Carcinogenesis 30, 1073–1081. doi:10.1093/carcin/bgp127

COMA, 2007. Publicly Available Specification 136: Terminology for Nanomaterials. British Standards Institute, London.

Cooper, G.M., 2000. Endocytosis, in: The Cell: A Molecular Approach. Sinauer Associates, Sunderland (MA).

Culig, Z., Hobisch, A., Hittmair, A., Peterziel, H., Cato, A., Bartsch, G., 1998. Expression, structure and function of androgen receptor in advanced prostatic carcinoma. Prostate 35, 63–70.

Daniel, M.C., Tsvetkova, I.B., Quinkert, Z.T., Murali, A., De, M., Rotello, V.M., Kao, C.C., Dragnea, B., 2010. Role of surface charge density in nanoparticle-templated assembly of bromovirus protein cages. ACS nano 4, 3853–3860.

Das, M., Mohanty, C., Sahoo, S.K., 2009. Ligand-based targeted therapy for cancer tissue. Expert Opinion On Drug Delivery 6, 285–304.

Debes, J.D., Tindall, D.J., 2004. . The New England Journal of Medicine 351, 1488–1490.

Destito, G., Schneemann, A., Manchester, M., 2009. Biomedical nanotechnology using virus-based nanoparticles, in: Viruses and Nanotechnology. Springer, Berlin, pp. 95–122.

Dixit, S.K., Goicochea, N.L., Daniel, M.C., Murali, A., Bronstein, L., De, M., Stein, B., Rotello, V.M., Kao, C.C., Dragnea, B., 2006. Quantum dot encapsulation in viral capsids. Nano Letters 6, 1993–1999.

Fauquet, C.M., Mayo, M.A., Maniloff, J., Desselberger, U., Ball, L.A. (Eds.), 2005. Virus Taxonomy: Eighth Report of the International Committe on the Taxonomy of Viruses. Elsevier Academic Press, San Diego, California.

Ferlay, J., Soerjomataram, I., Ervik, M., Dikshit, R., Eser, S., Mathers, C., Rebelo, M., Parkin, D.M., Forman, D., Bray, F., 2013. GLOBOCAN 2012 v1.0, Cancer Incidence and Mortality Worldwide: IARC CancerBase No. 11.

FlowJo, 2016.

Forman, D., Ferlay, J., 2014. The global and regional burden of cancer, in: World Cancer Report 2014. International Agency for Research on Cancer/World Health Organization, Lyon, pp. 16–53.

Freitas, R.A., 1999. Nanomedicine, Volume I: Basic Capabilities. Landes Bioscience, Austin.

Futreal, P.A., Coin, L., Marshall, M., Down, T., Hubbard, T., Wooster, R., Rahman, N., Stratton, M.R., 2004. A census of human cancer genes. Nature Reviews Cancer 4, 177–183. doi:10.1038/nrc1299

Futreal, P.A., Kasprzyk, A., Birney, E., Mullikin, J.C., Wooster, R., Stratton, M.R., 2001. Cancer and genomics. Nature 409, 850–852.

GraphPad Prism, 2012. . GraphPad Software, La Jolla California USA.

Grivennikov, S.I., Greten, F.R., Karin, M., 2010. Immunity, Inflammation, and Cancer. Cell 140, 883–899. doi:10.1016/j.cell.2010.01.025

Hanahan, D., Weinberg, R.A., 2011. Hallmarks of Cancer: The Next Generation. Cell 144, 646–674. doi:10.1016/j.cell.2011.02.013

Hanahan, D., Weinberg, R.A., 2000. The hallmarks of cancer. Cell 100, 57–70.

Heidel, J.D., Davis, M.E., 2011. Clinical Developments in Nanotechnology for Cancer Therapy. Pharmaceutical Research 28, 187–199. doi:10.1007/s11095-010-0178-7

Henshall, S.M., Quinn, D.I., Lee, C.S., Head, D.R., Golovsky, D., Brenner, P.C., 2001. Altered expression of androgen receptor in the malignant epithelium and adjacent stroma is associated with early relapse in prostate cancer. Cancer Research 61, 423–427.

Huang, X., Bronstein, L.M., Retrum, J., Dufort, C., Tsvetkova, I., Aniagyei, S., Stein, B., Stucky, G., McKenna, B., Remmes, N., Baxter, D., Kao, C.C., Dragnea, B., 2007. Self-Assembled Virus-like Particles with Magnetic Cores. Nano Letters 7, 2407–2416. doi:10.1021/nl071083l

Huang, X., Stein, B.D., Cheng, H., Malyutin, A., Tsvetkova, I.B., Baxter, D.V., Remmes, N.B., Verchot, J., Kao, C., Bronstein, L.M., Dragnea, B., 2011. Magnetic Virus-like Nanoparticles in *N. benthamiana* Plants: A New Paradigm for Environmental and Agronomic Biotechnological Research. ACS Nano 5, 4037–4045. doi:10.1021/nn200629g

Hudson, T.J., 2014. Genomics, in: World Cancer Report 2014. International Agency for Research on Cancer/World Health Organization, Lyon, France, pp. 184–192.

Hudson, T.J., Anderson, W., Aretz, A., Barker, A.D., Bell, C., Spellman (Leader), P.T., Pearson, J.V., Puente, X.S., Quesada, V., Lichter (Leader), P., Eils (Leader), et al., 2010. International network of cancer genome projects. Nature 464, 993–998. doi:10.1038/nature08987

Hull, L.C., Farrell, D., Grodzinski, P., 2014. Highlights of recent developments and trends in cancer nanotechnology research—View from NCI Alliance for Nanotechnology in Cancer. Biotechnology Advances 32, 666–678. doi:10.1016/j.biotechadv.2013.08.003

Image Lab, 2014. . Bio-Rad Laboratories.

Jung, B., Rao, A.L.N., Anvari, B., 2011. Optical Nano-Constructs Composed of Genome-Depleted *Brome Mosaic Virus* Doped with a Near Infrared Chromophore for Potential Biomedical Applications. ACS Nano 5, 1243–1252. doi:10.1021/nn1028696

Kaighn, M.E., Narayan, K.S., Ohnuki, Y., Lechner, J.F., Jones, L.W., 1979. Establishment and characterization of a human prostatic carcinoma cell line (PC-3). Investigative urology 17, 16–23.

Kinoshita, H., Shi, Y., Sandefur, C., Meisner, L.F., Chang, C., Choon, A., 2000. Methylation of the androgen receptor minimal promoter silences transcription in human prostate cancer. Cancer Research 60, 3623–3630.

Korenchuk, S., Lehr, J.E., MClean, L., Lee, Y.G., Whitney, S., Vessella, R., Lin, D.L., Pienta, K.J., 2001. VCaP, a cell-based model system of human prostate cancer. In vivo 15, 163–168.

Kuulasma, T., 2000. Oligo Explorer.

Lane, L.C., 1974. The Bromoviruses. Advances in Virus Research 19.

Langley, R.R., 2014. Tumour microenvironment, in: World Cancer Report 2014. International Agency for Research on Cancer/World Health Organization, Lyon, France, pp. 236–243.

Lara, P.N., Meyers, F.J., 1999. Treatment options in androgen-independent prostate cancer. Cancer Investigation 17, 137–144.

Larson, S.B., Lucas, R.W., McPherson, A., 2005. Crystallographic Structure of the T=1 Particle of Brome Mosaic Virus. Journal of Molecular Biology 346, 815–831. doi:10.1016/j.jmb.2004.12.015

Laufer, M., Denmeade, S.R., Sinibaldi, V.J., Carbucci, M.A., Eisenberger, M.A., 2000. Complete androgen blockade for prostate cancer: What went wrong? Journal of Urology 164, 3–9.

Li, S., Huang, L., 2008. Pharmacokinetics and biodistribution of nanoparticles. Molecular Pharmaceutics 5, 496–504.

Lucas, R.W., Kuznetsov, Y.G., Larson, S.B., McPherson, A., 2001. Crystallization of Brome Mosaic Virus and T = 1 Brome Mosaic Virus Particles Following a Structural Transition. Virology 286, 290–303. doi:10.1006/viro.2000.0897

Lucas, R.W., Larson, S.B., McPherson, A., 2002. The crystallographic structure of brome mosaic virus. Journal of Molecular Biology 317, 95–108. doi:10.1006/jmbi.2001.5389

Manchester, M., Steinmetz, N.F. (Eds.), 2009. Viruses and Nanotechnology, Current Topics in Microbiology and Immunology. Springer Berlin Heidelberg, Berlin, Heidelberg.

Mandelin, J., Cardó-Vila, M., Driessen, W.H.P., Mathew, P., Navone, N.M., Lin, S.-H., Logothetis, C.J., Rietz, A.C., Dobroff, A.S., Proneth, B., Sidman, R.L., Pasqualini, R., Arap, W., 2015. Selection and identification of ligand peptides targeting a model of castrate-resistant osteogenic prostate cancer and their receptors. Proceedings of the National Academy of Sciences 201500128. doi:10.1073/pnas.1500128112

Michel, J.-P., Gingery, M., Lavelle, L., 2004. Efficient purification of bromoviruses by ultrafiltration. Journal of Virological Methods 122, 195–198. doi:10.1016/j.jviromet.2004.09.005

Misra, R., Acharya, S., Sahoo, S.K., 2010. Cancer nanotechnology: application of nanotechnology in cancer therapy. Drug Discovery Today 15, 842–850. doi:10.1016/j.drudis.2010.08.006

Parveen, S., Sahoo, S.K., 2008. Polymeric nanoparticles for cancer therapy. Journal of Drug Targeting 16, 108–123. doi:10.1080/10611860701794353

Parveen, S., Sahoo, S.K., 2006. Nanomedicine: Clinical applications of polyethylene glycol conjugated proteins and drugs. Clinical Pharmacokinetics 45, 965–988.

Paul, R., Breul, J., 2000. Antiandrogen withdrawal syndrome associated with prostate cancer therapies: Incidence and clinical significance. Drug Safety 23, 381–390.

Pettersen, E.F., Goddard, T.D., Huang, C.C., Couch, G.S., Greenblatt, D.M., Meng, E.C., Ferrin, T.E., 2004. UCSF Chimera - a visualization system for exploratory research and analysis. Journal of Computational Chemistry 25, 1605–1612.

Pfeiffer, P., Hirth, L., 1975. The effect of conformational changes in brome mosaic virus upon its sensitivity to trypsin, chymotrypsin and ribonuclease. FEBS letters 56, 144–148.

Rambeaud, J.J., 1999. Intermittent complete androgen blockade in metastatic prostate cancer. European Urology 35, 32–36.

Reichert, J., 2008. Development trends for new cancer therapeutics and vaccines. Drug Discovery Today 13, 30–37. doi:10.1016/j.drudis.2007.09.003

Samuel, N., Hudson, T.J., 2013. Translating Genomics to the Clinic: Implications of Cancer Heterogeneity. Clinical Chemistry 59, 127–137. doi:10.1373/clinchem.2012.184580

Scalbert, A., Romieu, I., 2014. Metabolic change and metabolomics, in: World Cancer Report 2014. International Agency for Research on Cancer/World Health Organization, Lyon, France, pp. 222–227.

Schreiber, R.D., Old, L.J., Smyth, M.J., 2011. Cancer immunoediting: integrating immunity's roles in cancer suppression and promotion. Science 331, 1565–1570.

Sciarra, A., Casale, P., Colella, D., Di Chiro, C., Di Silverio, F., 1999. Hormone-refractory prostate cancer? Anti-androgen withdrawal and intermittent hormone therapy. Scandinavian Journal of Urology and Nephrology 33, 211–216.

Singh, P., Gonzalez, M.J., Manchester, M., 2006. Viruses and their uses in nanotechnology. Drug Development Research 67, 23–41. doi:10.1002/ddr.20064

Singhal, S., Nie, S., Wang, M.D., 2010. Nanotechnology Applications in Surgical Oncology. Annual Review of Medicine 61, 359–373. doi:10.1146/annurev.med.60.052907.094936

Steinmetz, N.F., 2010. Viral nanoparticles as platforms for next-generation therapeutics and imaging devices. Nanomedicine: Nanotechnology, Biology and Medicine 6, 634–641. doi:10.1016/j.nano.2010.04.005

Steinmetz, N.F., Ablack, A.L., Hickey, J.L., Ablack, J., Manocha, B., Mymryk, J.S., Luyt, L.G., Lewis, J.D., 2011. Intravital Imaging of Human Prostate Cancer Using Viral Nanoparticles Targeted to Gastrin-Releasing Peptide Receptors. Small 7, 1664–1672. doi:10.1002/smll.201000435

Strable, E., Finn, M.G., 2009. Chemical Modification of Viruses and Virus-Like Particles, in: Viruses and Nanotechnology. Springer, Heidelberg, Germany, pp. 1–22.

Stratton, M.R., Campbell, P.J., Futreal, P.A., 2009. The cancer genome. Nature 458, 719–724. doi:10.1038/nature07943

Sun, J., DuFort, C., Daniel, M.C., Murali, A., Chen, C., Gopinath, K., Stein, B., De, M., Rotello, V.M., Holzenburg, A., Kao, C.C., Dragnea, B., 2007. Core-controlled polymorphism in virus-like particles. Proceedings of the National Academy of Sciences 104, 1354–1359.

Thermo Scientific, 2012. Crosslinking Technical Handbook.

Thiery, J.P., Acloque, H., Huang, R.Y.J., Nieto, M.A., 2009. Epithelial-Mesenchymal Transitions in Development and Disease. Cell 139, 871–890. doi:10.1016/j.cell.2009.11.007

Trinchieri, G., 2014. Immunology and immunotherapy, in: World Cancer Report 2014. International Agency for Research on Cancer/World Health Organization, Lyon, France, pp. 253–260.

Turley, S.J., Cremasco, V., Astarita, J.L., 2015. Immunological hallmarks of stromal cells in the tumour microenvironment. Nature Reviews Immunology 15, 669–682.

van Kan-Davelaar, H.E., van Hest, J.C.M., Cornelissen, J.J.L.M., Koay, M.S.T., 2014. Using viruses as nanomedicines: Using viruses as nanomedicines. British Journal of Pharmacology 171, 4001–4009. doi:10.1111/bph.12662

Wang, C., Uchida, T., 1997. Androgen receptor gene mutations in prostate cancer. The Japanese Journal of Urology 88, 550–556.

Wang, Q., Lin, T., Johnson, J.E., Finn, M.G., 2002. Natural supramolecular building blocks: cysteine-added mutants of cowpea mosaic virus. Chemistry & biology 9, 813–819.

Weis, S.M., Cheresh, D.A., 2011. Tumor angiogenesis: molecular pathways and therapeutic targets. Nature 17, 1359–1370.

Wen, A.M., Lee, K.L., Yildiz, I., Bruckman, M.A., Shukla, S., Steinmetz, N.F., 2012a. Viral Nanoparticles for In Vivo Tumor Imaging. Journal of Visualized Experiments. doi:10.3791/4352

Wen, A.M., Shukla, S., Saxena, P., Aljabali, A.A.A., Yildiz, I., Dey, S., Mealy, J.E., Yang, A.C., Evans, D.J., Lomonossoff, G.P., Steinmetz, N.F., 2012b. Interior Engineering of a Viral Nanoparticle and Its Tumor Homing Properties. Biomacromolecules 13, 3990–4001. doi:10.1021/bm301278f

Wen, A.M., Steinmetz, N.F., 2014. The Aspect Ratio of Nanoparticle Assemblies and the Spatial Arrangement of Ligands can be Optimized to Enhance the Targeting of Cancer Cells. Advanced Healthcare Materials 3, 1739–1744. doi:10.1002/adhm.201400141

White, E.J., Venter, M., Hiten, H.F., Burger, J.T., 2008. Modified Cetyltrimethylammonium bromide method improves robustness and versatility: The benchmark for plant RNA extraction. Biotechnology Journal 3, 1424–1428.

Yildiz, I., Shukla, S., Steinmetz, N.F., 2011. Applications of viral nanoparticles in medicine. Current Opinion in Biotechnology 22, 901–908. doi:10.1016/j.copbio.2011.04.020

Yildiz, I., Tsvetkova, I., Wen, A.M., Shukla, S., Masarapu, M.H., Dragnea, B., Steinmetz, N.F., 2012. Engineering of Brome mosaic virus for biomedical applications. RSC Advances 2, 3670. doi:10.1039/c2ra01376b

Zen 2.1 (black), 2015. . Carl Zeiss Miscroscopy GmbH.

Zou, W., 2005. Immunosuppressive networks in the tumour environment and their therapeutic relevance. Nature Reviews Cancer 5, 263–274. doi:10.1038/nrc1586